NAVAL POSTGRADUATE SCHOOL

Monterey, California

AD-A245 727

DTIC
ELECTE
JAN 29 1992
S B D

DISSERTATION

NONLINEAR TRANSFORMATION OF
DIRECTIONAL WAVE SPECTRA
IN SHALLOW WATER

by

Manuel A. Abreu

September, 1991

Dissertation Supervisor E. B. Thornton
Co-Advisor A. Larraza

Approved for public release; distribution is unlimited

92-02116

AD-A245727

PAGE
#58
MISSING FROM
DOCUMENT
AS RECEIVED
FROM THE
ORIGINATOR

UNCLASSIFIED

SECURITY CLASSIFICATION OF THIS PAGE

REPORT DOCUMENTATION PAGE

Form Approved
OMB No 0704-0188

1a REPORT SECURITY CLASSIFICATION UNCLASSIFIED	1b RESTRICTIVE MARKINGS
2a SECURITY CLASSIFICATION AUTHORITY	3 DISTRIBUTION / AVAILABILITY OF REPORT Approved for public release; distribution is unlimited
2b DECLASSIFICATION / DOWNGRADING SCHEDULE	
4 PERFORMING ORGANIZATION REPORT NUMBER(S)	5 MONITORING ORGANIZATION REPORT NUMBER(S)
6a NAME OF PERFORMING ORGANIZATION Naval Postgraduate School 6b OFFICE SYMBOL (If applicable)	7a NAME OF MONITORING ORGANIZATION Naval Postgraduate School
6c ADDRESS (City, State, and ZIP Code) Monterey, California 93943-5000	7b ADDRESS (City, State, and ZIP Code) Monterey, California 93943-5000
8a NAME OF FUNDING / SPONSORING ORGANIZATION 8b OFFICE SYMBOL (If applicable)	9 PROCUREMENT INSTRUMENT IDENTIFICATION NUMBER
8c ADDRESS (City, State, and ZIP Code)	10 SOURCE OF FUNDING NUMBERS PROGRAM ELEMENT NO / PROJECT NO / TASK NO / WORK UNIT ACCESSION NO

11 TITLE (Include Security Classification)
NONLINEAR TRANSFORMATION OF DIRECTIONAL WAVE SPECTRA IN SHALLOW WATER

12 PERSONAL AUTHOR(S)
Abreu, Manuel A.

13a TYPE OF REPORT	13b TIME COVERED	14 DATE OF REPORT (Year, Month, Day)	15 PAGE COUNT
Ph.D.	FROM _____ TO _____	1991, September	127

16 SUPPLEMENTARY NOTATION
The views expressed in this thesis are those of the author and do not reflect the official policy or position of the Department of Defense or the U.S. Government.

17 COSATI CODES			18 SUBJECT TERMS (Continue on reverse if necessary and identify by block number)
FIELD	GROUP	SUB-GROUP	Nonlinear Spectral Transformation; Shallow Water

19 ABSTRACT (Continue on reverse if necessary and identify by block number)

A shallow water, nonlinear spectral wave transformation model is developed for conditions of a mild sloping bottom ($\mu = \nabla h/kh < 1$) and small amplitude effects ($\epsilon = \eta/h < 1$). Nonlinearities and combined shoaling and refraction effects act on the same time and length scales. The evolution equation of the wave action is prescribed by the wave Boltzmann equation, whereby resonant collinear triad interactions transfer energy among Fourier components. Combined shoaling and refraction effects are taken into account through the geometrical optics approximation. A numerical solution of thre three wave collision integral is developed, and the steady state wave Boltzmann equation is integrated using a piecewise ray method. The model is tested using the high resolution frequency-directional wave spectrum of Freilich, Guza and Elgar

20 DISTRIBUTION / AVAILABILITY OF ABSTRACT	21 ABSTRACT SECURITY CLASSIFICATION
☒ UNCLASSIFIED/UNLIMITED ☐ SAME AS RPT ☐ DTIC USERS	Unclassified
22a NAME OF RESPONSIBLE INDIVIDUAL Dr. Edward B. Thornton	22b TELEPHONE (Include Area Code) (408) 646-2847 / 22c OFFICE SYMBOL Code OC/Tm

DD Form 1473, JUN 86 *Previous editions are obsolete* SECURITY CLASSIFICATION OF THIS PAGE

S/N 0102-LF-014-6603 UNCLASSIFIED

#19 - ABSTRACT - (CONTINUED)

(1990) that shows nonlinear transfers of energy between both harmonic and non-harmonic frequencies. A digitized version of the measured frequency-directional spectrum at 10 meter depth is evolved 246 meter shoreward over a bathymetry of straight and parallel bottom contours to 4 meter depth. The model predicts the prominent spectral features in the measured wave field. The model results are in general superior to estimates using linear, finite depth wave theory, and they compare well with the observations in the region of the spectrum dominated by nonlinear effects.

Approved for public release; distribution is unlimited.

Nonlinear Transformation of Directional Wave Spectra in Shallow Water

by

Manuel A. Abreu
Lieutenant, Portuguese Navy
B.S., Escola Naval, Portugal, 1983
M.S., Naval Postgraduate School, 1989

Submitted in partial fulfillment of the requirements for the degree of

DOCTOR OF PHILOSOPHY IN PHYSICAL OCEANOGRAPHY

from the

NAVAL POSTGRADUATE SCHOOL
September 1991

Author: _____
Manuel A. Abreu

Approved by: _____
Beny Neta, Professor of Mathematics

_____
Timothy P. Stanton
Adjunct Professor of Oceanography

_____
Roland W. Garwood
Professor of Oceanography

_____
Andrés Larraza
Adjunct Professor of Physics
Co-Advisor

_____
Edward B. Thornton
Professor of Oceanography
Dissertation Supervisor

_____
Curtis A. Collins
Chairman, Department of Oceanography

_____
Richard S. Elster
Dean of Instruction

ABSTRACT

A shallow water, nonlinear spectral wave transformation model is developed for conditions of a mild sloping bottom ($\mu = \nabla h/kh \ll 1$) (and small amplitude effects ($\epsilon = \eta/h \ll 1$). Nonlinearities and combined shoaling and refraction effects act on the same time and length scales. The evolution equation of the wave action is prescribed by the wave Boltzmann equation, whereby resonant collinear triad interactions transfer energy among Fourier components. Combined shoaling and refraction effects are taken into account through the geometrical optics approximation. A numerical solution of the three wave collision integral is developed, and the steady state wave Boltzmann equation is integrated using a piecewise ray method. The model is tested using the high resolution frequency-directional wave spectrum of Freilich, Guza and Elgar (1990) that shows nonlinear transfers of energy between both harmonic and non-harmonic frequencies. A digitized version of the measured frequency-directional spectrum at 10 meter depth is evolved 246 meter shoreward over a bathymetry of straight and parallel bottom contours to 4 meter depth. The model predicts the prominent spectral features in the measured wave field. The model results are in general superior to estimates using linear, finite depth wave theory, and they compare well with the

observations in the region of the spectrum dominated by nonlinear effects.

DTIC
COPY
INSPECTED
1

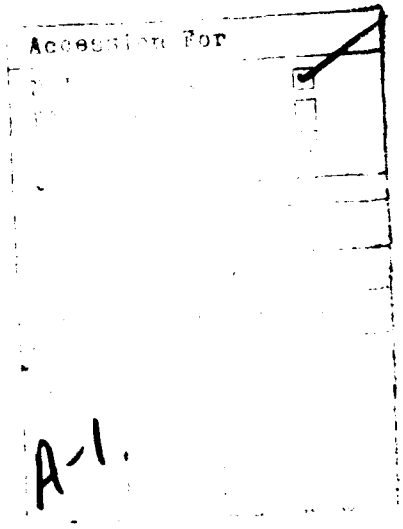

TABLE OF CONTENTS

ACKNOWLEDGMENTS

I wish to express my sincere gratitude to my advisors, Professor Edward Thornton and Professor Andrés Larraza. Without their commitment, guidance and friendship, this work would not have been finished.

I also wish to thank my entire doctoral committee for their support of my work, and also thank Dr. Alejandro Garcia for his fruitful ideas.

DEDICATION

To my wife, Margarida, and to my three sons Manuel, José and António.

To my father.

I. INTRODUCTION

Directional wave spectra give a complete description of the frequency and directional spreading of the ocean wave field. As surface gravity waves propagate shoreward in shoaling waters, linear and nonlinear processes act simultaneously to transform substantially their frequency and directional characteristics. The objective of this study is to derive a model for the spatial evolution of frequency-directional wave spectra in shallow water, accounting for nonlinear three-wave resonant interactions and combined shoaling and refraction effects. Unlike previous studies, energy transfers across the spectrum by triad resonant interactions are considered within a collision integral formulation. A numerical solution for the model equations is developed and the operational validity of the model is tested.

The changing bottom topography causes refraction and shoaling, that result in spatial variations in the amplitudes and directions of the wave field. Linear refraction theory has been extensively used to estimate the evolution of a shoaling wave field (Longuet-Higgins, 1957; Collins, 1972; LeMehaute and Wang, 1982; Pawka et al., 1984; Izumiya and Horikawa, 1987), with reasonable success in predicting the directional characteristics of the waves in shallow water. However, ocean surface gravity waves are essentially nonlinear, and the

evolution of ocean wave spectra in shallow water is determined to a considerable extent by the energy flux between spectral wave components, as shown by the observations of Freilich, Guza and Elgar (1990). In the shallow water regime three wave resonant interactions are possible. These nonlinearities, of lower order than the four wave processes, dominate the flux of energy across the spectrum. The consequences of the transfer of energy associated with resonant wave interactions are not only distortions of the frequency spectrum, but also alterations of the directional spreading of energy.

Considerable progress has been made in the last decade in the development of models based on nonlinear theories. Boussinesq equations have been used to establish evolution equations for the amplitudes and phases of waves propagating in one dimension over slowly varying topography, under the effects of harmonic generation (Freilich and Guza, 1984). Within the parabolic approximation method (Radder, 1979), the Boussinesq equations led to single harmonic models that, besides the harmonic generation, include refractive and diffractive effects (Liu, Yoon and Kirby, 1985). Alternatively, the radiative transfer equation was used to predict the evolution of directional wave spectra, by either including deep water four wave interaction processes (Young, 1988; Weber, 1988), or parametric finite depth extensions of the deep water formulations (WAMDI group, 1988).

The model equations are derived in Chapter II. The nonlinear three wave resonant interactions and combined shoaling and refraction effects are considered separately. Starting with the evolution equations for random surface gravity waves in shallow water, a three wave collision integral is derived. Energy redistribution is obtained by collinear resonant interactions. Combined shoaling and refraction effects are considered through the application of the geometrical optics approximation, and the linear evolution equation for the wave action is formally derived. Nonlinearities and linear shoaling and refraction effects are combined, in the form of a wave Boltzmann equation that constitutes the basic model equation. Because of validity conditions of the three wave collision integral, interactions are restricted to waves satisfying the shallow water wave criterion, but transfer of energy is allowed to spectral components beyond the shallow water regime.

Chapter III considers the solution for the model equations. The numerical solution of the three wave collision integral is based on a linear discretization formulation. The propagation of the spectral energy adopts a piecewise ray method to integrate the wave Boltzmann equation.

Chapter IV contains the model simulations with application to a synthetic data set representing observations at Torrey Pines Beach, California, by Freilich, et al. (1990). The model results are presented.

Conclusions and recommendations for future research constitute Chapter V. In the appendices, the conceptual application of the model to an arbitrary bottom topography is developed (Appendix A), and details of the model performance and a sensitivity analysis are presented (Appendix B).

II. FORMULATION OF THE PROBLEM

A. THE ENERGY OF A SYSTEM OF SHOALING SURFACE GRAVITY WAVES

The objective is to define the energy of a system of shoaling surface gravity waves. The problem is limited to oscillatory motion in a depth-limited ocean. The fluid is assumed homogeneous, incompressible and inviscid, and gravity is taken as constant. The bottom is a rigid and impermeable surface at $z = -h(\vec{x})$, where $\vec{x}$ and z are the horizontal and vertical coordinates. The unperturbed free surface coincides with the plane $z = 0$. The flow is assumed potential and surface tension effects are ignored.

Let $z = \eta(\vec{x}, t)$ be the dynamical free surface and $\phi(\vec{x}, z, t)$ the hydrodynamic velocity potential, with $\psi(\vec{x}, t) = \phi(\vec{x}, z, t)|_{z=\eta}$. The fluid flow is described by Laplace's equation

$$\nabla^2\phi + \frac{\partial^2\phi}{\partial z^2} = 0 \qquad -h(\vec{x}) \le z \le \eta(\vec{x}, t) , \tag{2.1}$$

with the bottom boundary condition

$$\frac{\partial\phi}{\partial z} + \nabla h \cdot \nabla\phi = 0 \qquad at \qquad z = -h(\vec{x}) , \tag{2.2}$$

and the two conditions at the free surface (Zakharov, 1968)

$$\frac{\partial \eta}{\partial t} = \frac{\delta H}{\delta \psi} \ , \qquad (2.3a)$$

and

$$\frac{\partial \psi}{\partial t} = -\frac{\delta H}{\delta \eta} \ . \qquad (2.3b)$$

where

$$H = \frac{1}{2}\int d\vec{x} \int_{-h}^{\eta} \left[(\nabla \phi)^2 + \left(\frac{\partial \phi}{\partial z} \right)^2 \right] dz + \frac{g}{2} \int \eta^2 d\vec{x} \quad , \qquad (2.4)$$

is the total energy of the fluid, ∇ is the two-dimensional gradient in the (x, y) plane, and δ denotes the functional derivative. Equation (2.3a) is the kinematic free surface boundary condition for Laplace's equation, while (2.3b) is the dynamical free surface boundary condition described by Bernoulli's integral at the free surface. Specifying the canonical variables η and ψ defines the fluid flow because the boundary value problem for Laplace's equation has a unique solution.

For the problem of shallow water (dispersionless), weakly nonlinear, shoaling waves over a mild sloping bottom, the Hamiltonian (2.4) reduces to

$$H = \frac{1}{2}\int d\vec{x} \{ (h+\eta)(\nabla \psi)^2 + g\eta^2 \} \ . \qquad (2.5)$$

By adding higher order dispersive terms ($\nabla^2\psi$, *etc.*) in (2.5), Hamilton's equations (2.3a) and (2.3b) yield the Boussinesq equations in Liu et al. (1985) (their equations (2.3) and (2.4)).

The Hamiltonian (2.5) includes both the effects of weak nonlinearity (vis the term $\eta(\nabla\psi)^2$) and the effects of a slowly varying bottom ($h = h(\vec{x})$) . To systematically examine weakly nonlinear random waves propagating over irregular bottom topography, the amplitude effects are identified by a small parameter ε ($\varepsilon = \eta/h$) , with higher powers of ε representing higher order nonlinearities. Small variations in topography (denoted by $\mu = \nabla h/kh$) affect the properties of the propagating waves introducing shoaling and refraction effects. Thus, for $\mu = 0$ and $0 < \varepsilon \ll 1$ (i.e., horizontal bottom), the evolution of a homogeneous sea of random waves is determined by nonlinear interactions. On the other hand, the ordering $\varepsilon^2 \ll \mu \ll \varepsilon$ describes the geometrical optics evolution of infinitesimal waves propagating over arbitrary bathymetry with the corresponding refraction effects. If both restrictions are replaced by $\varepsilon, \mu \ll 1$, the nonlinearities and refraction terms act on the same length and time scales, and the evolution of the wave action is prescribed by the wave Boltzmann equation or radiative transfer equation. Although this later scaling of the amplitude and topography effects is more appealing, it renders nonuniformities in the asymptotics that demand special care. Therefore, to separately examine

the consequences of nonlinear interaction and refraction the first two orderings are adopted. The combined effects of triad nonlinear interactions and refraction are then examined by relaxing the ordering such that $\varepsilon, \mu < 1$ for the final model.

B. THE COLLISION INTEGRAL ($\mu = 0, 0<\varepsilon<1$)

A homogeneous sea of random waves in shallow water is considered. Each wave evolves on a long time scale because of nonlinearity. The theory of such evolution has been developed by Benney and Saffman (1966) for the case of dispersive waves. Newell and Aucoin (1971), hereinafter referred as N&A, showed that nondispersive waves in two and higher dimensions possess a natural asymptotic closure. The general results of N&A are applied to the problem of shallow water gravity waves, but first the interaction coefficient must be evaluated, and some minor differences considered. For shallow water waves, the redistribution of energy within the spectrum is achieved by resonant interaction between collinear triads.

In order to consider the evolution of random surface gravity waves in shallow water, $\eta(\vec{x}, t)$ and $\psi(\vec{x}, t)$ are expressed as Fourier integrals

$$\eta = \frac{1}{2\pi}\int \hat{\eta}(k)\, e^{i\vec{k}\cdot\vec{x}} d\vec{k} \quad , \qquad (2.6a)$$

and

$$\psi = \frac{1}{2\pi}\int \Psi(k)\, e^{i\vec{k}\cdot\vec{x}} d\vec{k} \quad . \tag{2.6b}$$

In terms of the Fourier integral representations (2.6), the Hamiltonian (2.5) takes the form

$$\mathbf{H} = \frac{1}{2}\int (k^2 h \Psi_k \Psi_{-k} + g\hat{\eta}_k \hat{\eta}_{-k})\, d\vec{k} - \frac{1}{4\pi}\int \vec{k}\cdot\vec{k}_1 \Psi_0 \Psi_1 \hat{\eta}_2 \delta_{0+1+2}\, d012 \quad , \tag{2.7}$$

where use was made of the shorthand notation $\Psi_i = \Psi(\vec{k}_i)$, $d12\ldots = d\vec{k}_1 d\vec{k}_2 \ldots$, and $\delta_{0+1+\ldots} = \delta(\vec{k}+\vec{k}_1+\ldots)$, with corresponding to $\vec{k}$. The canonical transformation to the variables ia_k^* and a_k (Zakharov, 1968) is now considered to get

$$\Psi_k = -i\left(\frac{\omega_k}{2k^2 h}\right)^{\frac{1}{2}} (a_k - a_{-k}^*) \quad , \tag{2.8}$$

and

$$\hat{\eta}_k = \left(\frac{k^2 h}{2\omega_k}\right)^{\frac{1}{2}} (a_k + a_{-k}^*) \quad , \tag{2.9}$$

where $\omega_k = \sqrt{(gh)}\, k$ is the dispersion relation for infinitesimal amplitude, shallow water gravity waves. In

terms of the variables ia_k^* and a_k, Hamilton's equations become

$$\frac{\partial a_k}{\partial t} = -i\frac{\delta H}{\delta a_k^*} \quad , \tag{2.10}$$

where

$$H = \int \omega_k a_k a_k^* dk + \int V_{0,12}(a_0^* a_1 a_2 + a_0 a_1^* a_2^*)\delta_{0-1-2}\, d012, \tag{2.11}$$

with

$$V_{0,12} = \frac{1}{8\pi\sqrt{2}}\left(\frac{c}{h}\right)^{\frac{1}{2}}\left\{\left(\frac{k}{k_1 k_2}\right)^{\frac{1}{2}}\vec{k}_1\cdot\vec{k}_2 + \left(\frac{k_1}{k k_2}\right)^{\frac{1}{2}}\vec{k}\,.\,\vec{k}_2 + \left(\frac{k_2}{k k_1}\right)^{\frac{1}{2}}\vec{k}\,.\,\vec{k}_1\right\}. \tag{2.12}$$

$V_{0,12}$ is a symmetric function under exchange of its arguments, and $c = \sqrt{(gh)}$ is the phase speed of the shallow water gravity waves. Note that the Hamiltonian (2.11) includes only those terms that contribute to the resonant transfer of energy for the component a_k. From Hamilton's equation (2.10), and eliminating the familiar linear response by setting

$$a_k \rightarrow a_k e^{-i\omega_k t} \quad , \tag{2.13}$$

yields

$$\frac{\partial a_k}{\partial t} = -i\varepsilon \int d12 \left\{ V_{0,12} a_1 a_2 e^{iW_{0,12}t} \delta_{0-1-2} + 2 V_{1,02} a_1 a_2^* e^{-iW_{1,02}t} \delta_{0+2-1} \right\} \tag{2.14}$$

In equation (2.14), the bookkeeping parameter ε has been incorporated. It labels the amplitude and serves as an ordering parameter for the time scales and the asymptotics for the closure problem. Also, the shorthand notation $W_{0,12} = \omega_0 - \omega_1 - \omega_2$ has been used.

The evolution equations for the spectral cumulant hierarchy can be obtained from equation (2.14). N&A start with the evolution of the a-correlators, and give the arguments why the fourth order cumulants do not influence the evolution of the second order a-correlations as $t \to \infty$, such as the mean wave action of the random waves. This has the effect of introducing irreversibility into the scattering process. Defining the wave action n_k per unit mass density by

$$\langle a_k a_{k'}^* \rangle = 4\pi^2 n_k \delta(\vec{k} - \vec{k}') \quad , \tag{2.15}$$

and using the ordering appropriate to the problem of two dimensional dispersionless shallow water waves, gives

$$\frac{\partial n_k}{\partial t} = \frac{\pi^{\frac{5}{2}}}{h^{\frac{1}{2}}} k^{\frac{9}{2}} \left\{ \int_0^1 d\alpha [\alpha(1-\alpha)]^{\frac{3}{2}} \{ n_{\alpha k} n_{(1-\alpha)k} - n_k n_{\alpha k} - n_k n_{(1-\alpha)k} \} \right.$$

$$\left. + 2 \int_0^{\infty} d\gamma [\gamma(1+\gamma)]^{\frac{3}{2}} \{ n_{\gamma k} n_{(1+\gamma)k} + n_k n_{(1+\gamma)k} - n_k n_{\gamma k} \} \right\} , \quad (2.16)$$

where n_k changes according to the slow time scale $T = (2/3)\varepsilon^2 (c/h)^{\frac{1}{2}} t^{\frac{3}{2}}$.

According to equation (2.16), energy redistributes by collinear resonant interaction of waves. The most interesting feature at this time scale is that no angular (in k space) transfer of energy occurs. Randomization in angle can be brought about only by slower collision processes (of higher order in ε), whereby redistribution occurs by a local transfer between adjacent rays. However, when the energy transfer has reached those wavelengths for which the shallow water limit no longer applies, then further redistribution can take place by resonance of four waves over a much longer time. This mechanism can also lead to angle spreading of the spectrum. Energy then accumulates at certain scales. While not formally addressing this transition scale, energy transfers are allowed only for those wavelengths consistent with the shallow water approximation. Further comments about this point are made in Chapter IV.

C. SHOALING AND REFRACTION OF SHALLOW WATER WAVES: THE GEOMETRICAL-OPTICS APPROXIMATION ($\varepsilon^2 < \mu < \varepsilon$)

In the geometrical optics approximation, waves propagate along the rays defined by Fermat's principle. At each point on the surface, the propagation velocity of the waves is defined as that corresponding to flat bottom conditions with the local depth. The variation of the amplitude of the waves along a ray is determined using the principle of conservation of wave action. The purpose of this section is to obtain the evolution equation for the wave action of a sea of random waves.

The main difficulty in the analysis is that, if η and ψ are divided at $t = 0$ into Fourier modes, the wavenumber and frequency of each wave packet will change secularly as it traverses the fluid surface. A clear procedure to overcoming this obstacle has been presented by Soward (1975). At time $t = 0$ a particular realization of the system is

$$\eta = \frac{1}{2\pi} \int \hat{\eta}(\vec{k}_0 ; \vec{x}, 0)\, e^{i\vec{k}_0 \cdot \vec{x}} d\vec{k}_0 \quad , \tag{2.17}$$

and similarly for ψ . The explicit dependence on $\vec{x}$ emphasizes the fact that (2.17) provides a local decomposition of the canonical variables. The individual wave trains $\hat{\eta}(\vec{k}_0 ; \vec{x}, t) e^{i\vec{k}_0 \cdot \vec{x}} d\vec{k}_0$, comprising (2.17) evolve at time t into

$$\eta(\vec{k};\vec{x},t)e^{i\theta(\vec{k};\vec{x},t)}d\vec{k}_0 \quad , \tag{2.18}$$

where

$$\vec{k}(\vec{k}_0;\vec{x},t) = \nabla\theta \tag{2.19}$$

and

$$\omega(\vec{k}_0;\vec{x},t) = -\frac{\partial\theta}{\partial t} \quad , \tag{2.20}$$

and the infinitesimal $d\vec{k}_0$ is fixed. Also $\vec{k}(\vec{k}_0;\vec{x},0) = \vec{k}_0$. A local canonical transformation (2.8) yields the Hamiltonian

$$\mathrm{H} = \int \omega_k a_k a_k^* \, d\vec{k}_0 + O(\varepsilon^2\mu) \quad . \tag{2.21}$$

From Hamilton's equation to lowest order in $\varepsilon\mu$, the evolution for the correlator $\langle a_k a_{k+\kappa}^* \rangle = \nu(\vec{k},\vec{k}+\vec{\kappa})$ can be obtained,

$$\left[\frac{\partial}{\partial t} + i(\omega_k - \omega_{k+\kappa})\right]\nu(\vec{k},\vec{k}+\vec{\kappa}) = 0 \quad . \tag{2.22}$$

Because of the changing bottom topography, ν is nondiagonal in the wave vectors with the typical scale of spatial nonuniformity, $2\pi/\kappa$. For $\mu < 1$, slowly changing bottom topography, the condition $\kappa < k$ is satisfied. Expanding up

to first order in κ and making use of the half Fourier transform

$$n_k(\vec{x}, t) = \sigma(\vec{k}, \vec{x}, t)\int \nu\left(\vec{k} - \frac{\vec{\kappa}}{2}, \vec{k} + \frac{\vec{\kappa}}{2}\right) e^{i\vec{\kappa}\cdot\vec{x}} d\vec{\kappa} \quad , \qquad (2.23)$$

equation (2.22) gives

$$\frac{\partial n_k}{\partial t} + \frac{\partial \omega_k}{\partial \vec{k}} \cdot \frac{\partial n_k}{\partial \vec{x}} = 0 \quad . \qquad (2.24)$$

Because of the inconvenience of having to refer back repeatedly to the initial instant $t = 0$ and to k_0 space, (2.23) is written with the weighting factor

$$\sigma(\vec{k}, \vec{x}, t) = \frac{\partial(k_{01}, k_{02})}{\partial(k_1, k_2)} \quad , \qquad (2.25)$$

corresponding to the Jacobian of the transformation. Thus, whereas the half Fourier integral of ν refers to the wave train, the wave action refers to a unit volume in k space. Equation (2.24) shows that the wave action n_k is constant at points moving with the group velocity. The final step is to transform from the independent variables $(\vec{k}_0, \vec{x}, t)$ to $(\vec{k}, \vec{x}, t)$, yielding

$$\frac{\partial n_k}{\partial t} + \frac{\partial \omega_k}{\partial \vec{k}} \cdot \frac{\partial n_k}{\partial \vec{x}} - \frac{\partial \omega_k}{\partial \vec{x}} \cdot \frac{\partial n_k}{\partial \vec{k}} = 0 \quad . \qquad (2.26)$$

It should be noted that the result (2.26) is of great generality. It was obtained from the linear wave field Hamiltonian without further reference to the dispersion relation. Indeed, any linear wave field has a local Hamiltonian of the form given in (2.21). Thus, while the results of the previous section can be applied only to nonlinear dispersionless shallow water waves, (2.26) is applicable to linear shoaling waves of arbitrary depth in particular, and to any linear wave field in a slowly varying background in general.

D. THE MODEL: COMBINED EFFECTS OF REFRACTION AND TRIAD NONLINEAR INTERACTIONS ($\varepsilon, \mu \ll 1$)

When the restrictions made in the previous two sections, $\mu = 0$, and $0 \ll \varepsilon \ll 1$ for the collision integral and $\varepsilon^2 \ll \mu \ll \varepsilon$ for the geometrical optics approximation, are replaced by $\varepsilon, \mu \ll 1$, the nonlinearities add collision terms to equation (2.26) that may be formally as large (or larger) than the streaming terms shown. Therefore, (2.26) is replaced by the wave Boltzmann equation

$$\frac{\partial n_k}{\partial t} + \frac{\partial \omega_k}{\partial \vec{k}} \cdot \frac{\partial n_k}{\partial \vec{x}} - \frac{\partial \omega_k}{\partial \vec{x}} \cdot \frac{\partial n_k}{\partial \vec{k}} = I\{n_k\} \quad , \qquad (2.27)$$

where $I\{n_k\}$ is the collision integral defined by the right hand side of equation (2.16). Equation (2.27) is a statement of the conservation of the total energy of the system.

Conventional practice considers the directional frequency spectrum $S(f,\varphi)$ (measured in $cm^2/Hz/deg$) rather than the directional wavenumber spectrum. The wave action per unit mass density n_k is related to the directional frequency spectrum $S(f,\varphi)$ by

$$n(\vec{k},\vec{x},t) = \frac{gcc_g}{2\pi\omega^2} S(f,\varphi,\vec{x},t) \quad , \tag{2.28}$$

where c and c_g are the phase and group speeds respectively. In steady state, (2.27) and (2.28) yield

$$\frac{d(cc_gS)}{dl} = I\{S\} \quad , \tag{2.29}$$

where

$$I\{S\} = \frac{2^{\frac{3}{2}}\pi^4 g^{\frac{1}{4}}}{h^{\frac{5}{4}}} f^{\frac{5}{2}} \left\{ \int_0^1 d\alpha[\alpha(1-\alpha)]^{-\frac{1}{2}} \{S_{\alpha f}S_{(1-\alpha)f} - (1-\alpha)^2 S_f S_{(1-\alpha)f}\} \right.$$

$$\left. + 2\int_0^\infty d\gamma[\gamma(1+\gamma)]^{-\frac{1}{2}} \{S_{\gamma f}S_{(1+\gamma)f} + \gamma^2 S_f S_{(1+\gamma)f} - (1+\gamma)^2 S_f S_{\gamma f}\} \right\} \tag{2.30}$$

and the parameter l is related to the ray's path by

$$\frac{d\vec{x}}{dl} = \vec{t} \tag{2.31}$$

and

$$\frac{d\varphi}{dl} = -\vec{p}\cdot\frac{1}{c}\frac{\partial c}{\partial \vec{x}} \quad , \tag{2.32}$$

where $\vec{t}$ and $\vec{p}$ are unit vectors tangent and perpendicular to the ray.

Equations (2.29) to (2.32) constitute a model for weakly nonlinear shoaling surface gravity waves in shallow water. The left hand side of equation (2.29) is valid for waves of arbitrary depth, while the right hand side applies only to the dispersionless shallow water waves. Thus, for those frequencies that satisfy the shallow water wave criterion, nonlinear energy transfer as well as restitution of energy will be considered. On the other hand, while allowing energy transfer to higher frequencies, the restitution will be set equal to zero for waves beyond the shallow water regime. Those waves will therefore be considered bounded waves.

III. SOLUTION OF THE MODEL EQUATIONS

A. COLLISION INTEGRAL

The numerical solution of the collision integral (2.30) utilizes a linear discretization. The intent is thus to discretize frequency and spectral energy density at the values $f = f_0, 2f_0, \ldots, Nf_0$, where f_0 is the frequency resolution. For practical applications, the frequency range is bounded both above and below. In fact, ray theory does not account for reflection of wave energy, and the present formulation that allows transfer of energy by resonant three-wave interactions is valid only for frequencies within the shallow water approximation. The spectral energy density is thus neglected for frequencies outside a defined range. Details of the working frequency range will be discussed in Chapter IV.

In order to avoid interpolation of the spectral energy density in solving (2.30) it must be required that both α and γ conform to the relation $(\alpha,\gamma)\times f = (integer = i)\times f_0$. This condition, together with the form of the discretization, determines the values $\alpha = 0, \frac{1}{i}, \frac{2}{i}, \ldots, 1$ and $\gamma = 0, \frac{1}{i}, \frac{2}{i}, \ldots, \frac{(N+1)}{i}$, where Nf_0 is the highest frequency for which the transfer of spectral energy density is calculated. Applying the trapezoidal rule in composite form

$$\int_a^b f(x)\,dx \approx \sum_{j=1}^{k-1} \Delta x\, f(j) + \frac{1}{2}\,[\,f(a)+f(b)\,]\,, \qquad (3.1)$$

where $j=0$ and $j=k$ correspond to the limits of integration a and b, , and δx is the sampling interval, the discretized form of the collision integral (2.30) becomes

$$I\{S\}_i \approx \frac{2^{\frac{3}{2}} i^4 g^{\frac{1}{4}} f^{\frac{5}{2}}}{h^{\frac{5}{4}}} \left\{ 2\sum_{j=1}^{N-i} \left(\frac{1}{i}\right)^2 [(i+j)j]^{-\frac{1}{2}} \left[i^2 S_j S_{j+i} + j^2 S_i S_{j+i} - \right.\right.$$

$$\left.\left. -(j+i)^2 S_i S_j \right] + \sum_{j=1}^{i-1} \left(\frac{1}{i}\right)^2 [j(i-j)]^{-\frac{1}{2}} \left[i^2 S_j S_{i-j} - j^2 S_i S_{i-j} - (i-j)^2 S_i S_j \right] \right\}. \qquad (3.2)$$

The derivation of the discretized form (3.2) makes use of the concept of a limited working frequency range, not considering the computation of the collision integral at the endpoints (a and b in (3.1)), and not taking into account restitutions from frequencies above Nf_0.

The requirement of a limited range for the collisions and restitutions processes is imposed on (3.2) by restricting the possible values of the indexes of the spectral energy density terms. Designating the upper limit of the range of interactions by I_{max}, the conditions for each of the product terms inside the summations in (3.2) are:

i) Restitutions

$$S_j S_{j+i} \rightarrow j+j+i \leq I_{max} ,$$

$$S_i S_{j+i} \rightarrow i+j+i \leq I_{max} .$$

ii) Collisions

$$S_i S_j \rightarrow (i, j) \leq I_{max} ,$$

$$S_i S_{i-j} \rightarrow (i-j) \leq I_{max} ,$$

$$S_j S_{i-j} \rightarrow (j, i-j) \leq I_{max} .$$

B. SPATIAL PROPAGATION OF WAVE SPECTRAL ENERGY

The transformation of wave spectra under the combined effects of shoaling, refraction and triad interactions can be evaluated through the integration of the Boltzmann equation (2.29) along the rays defined by the refraction and shoaling laws (2.31) and (2.32). To solve numerically the integrated form of the steady state Boltzmann equation

$$cc_g S = c_0 c_{g0} S_0 + \int I\{S\} dl , \qquad (3.3)$$

a piecewise ray method (Sobey and Young, 1986) is adopted. This approach considers a grid of points across the domain of integration and computes all the rays reaching each of the nodes. The propagation is done in steps along the domain. In this way the rays are not decoupled, contrary to full ray methods (Collins, 1972). The full spectrum is always available at each grid point, and it is thus possible to

couple spectral components through mechanisms like triad interactions.

The propagation process consists of the computation of the ray path, the integration of the collision term along the ray and the evaluation of the transformed spectral energy distribution at the new position. The type of bathymetry under consideration greatly influences the details of the method.

1. **The Ray Path**

To compute the ray parameters, direction, arc length and extreme points, a cartesian coordinate system is considered. The x axis, perpendicular to the coastline, defines the origin for the directions of the incoming waves (Figure (3.1)).

A finite difference form of the shoaling and refraction laws (2.31) and (2.32) is

$$x_{k+1} = x_k + \Delta l \cos\bar{\varphi} \ , \qquad (3.4a)$$

$$y_{k+1} = y_k + \Delta l \sin\bar{\varphi} \ , \qquad (3.4b)$$

and

$$\varphi_{k+1} = \varphi_k + \ln\left(\frac{c_{k+1}}{c_k}\right)[\tan\bar{\varphi} - \cot\bar{\varphi}] \ . \qquad (3.4c)$$

The subscripts k and $k+1$ designate the extreme points of the ray, Δl is the arc length, and $\overline{\varphi}$ is the average direction of the ray (Figure (3.2)). The set of equations (3.4) is taken as the basis for an iterative procedure for the computation of the ray parameters.

The initial conditions are the coordinates of the starting point of the ray (k), the direction of the incoming waves at this point, and the abscissa of the target point ($k+1$). The computation of the ray parameters begins by solving (3.4) with $\overline{\varphi}$ given by the direction of the ray at k The iterations proceed by considering

$$\overline{\varphi} = \frac{\varphi_{k+1} + \varphi_k}{2} \quad . \tag{3.5}$$

The process is stopped when the difference between two consecutive iterations is less than a specified small value. For applications considering triad interactions, the stopping criterion is defined in accordance with the one adopted for the collinearity of the interacting components, and is always two orders of magnitude smaller than the latter.

Comparisons of the iterative method just presented with Dobson's (1967) method, for a bathymetry of straight and parallel bottom contours, consistently gives better agreement with the analytic solution (Snell's law). Also the propagation step of Dobson's method, defined in terms of arc

length, does not correspond to a defined discretization of the spatial domain as is the case with the present method. It should be noted that singularities exist in the solution of (3.4c) for waves at 0 and ±90 degrees. This is not a limitation of the method because a local rearrangement of the coordinate system can overcome this apparent difficulty.

2. **The Integration of the Collision Term**

The spatial integration of the collision integral in (3.3) has to account formally for the dependence on the integration path on both the depth and the spectral energy density. The integration of the spatial densities requires the reordering of terms in the discrete approximation of the collision integral (3.2). In order to avoid such difficulties, the spectral energy density is assumed constant for a full integration step of the collision integral, the value adopted being that at the last predicted level (Young, 1988; WAMDI group, 1988). Within this approximation, the discrete form of the integrated radiative transfer equation is

$$\int I(S)dl \approx 2^{\frac{3}{2}}\pi^4 g^{\frac{1}{4}} f^{\frac{5}{2}}\left[\int \alpha\,\&\,\gamma\right]\left\{\frac{\Delta l}{2}\left(h_k^{-\frac{5}{4}} + h_{k+1}^{-\frac{5}{4}}\right)\right\}, \qquad (3.6)$$

where $\left[\int \alpha\,\&\,\gamma\right]$ represents the terms inside the braces in (3.2), and the depth subscripts correspond to the initial and final positions in the propagation step. The estimation of the

error introduced in the solution by the assumption of a constant value for the spectral energy density will be considered in Appendix B. It should be noted that the propagation step must be sufficiently small to ensure the collinearity of the spectral component. Thus the error introduced is not expected to be significant.

3. Straight and Parallel Bottom Contours

Bathymetry with straight and parallel bottom contours greatly simplifies the application of a piecewise ray method. For propagation one only needs to consider a discretization line connecting the starting position to the target point (Figure (3.3)). Also, the depth along the propagation path is obtained by linear interpolation. For these bathymetric conditions, the proposed method of computing the ray path is advantageous. Unlike existing methods, there is no need for a backward propagation cycle, and only the directions of the rays at the target position need to be stored.

4. Arbitrary Bottom Topography

Two-dimensional bottom topography greatly complicates practical applications of the model. A full grid of points must be implemented, and interpolating both bathymetry and spectral density are required. Backward computation of the ray parameters becomes necessary. However, simplifications are possible. For instance, the domain of integration may be restricted to only positions that are possible origins for rays reaching a given target position. The possible

application of the model developed in Chapter II to an arbitrary bottom topography is demonstrated in Appendix A.

The integrated form of the Boltzmann equation (3.3), together with equations (3.4) and (3.6), constitutes the solution of the model formulated in Chapter II, that will be used in the simulations (Chapter IV). The applications will be restricted to a bathymetry having straight and parallel depth contours.

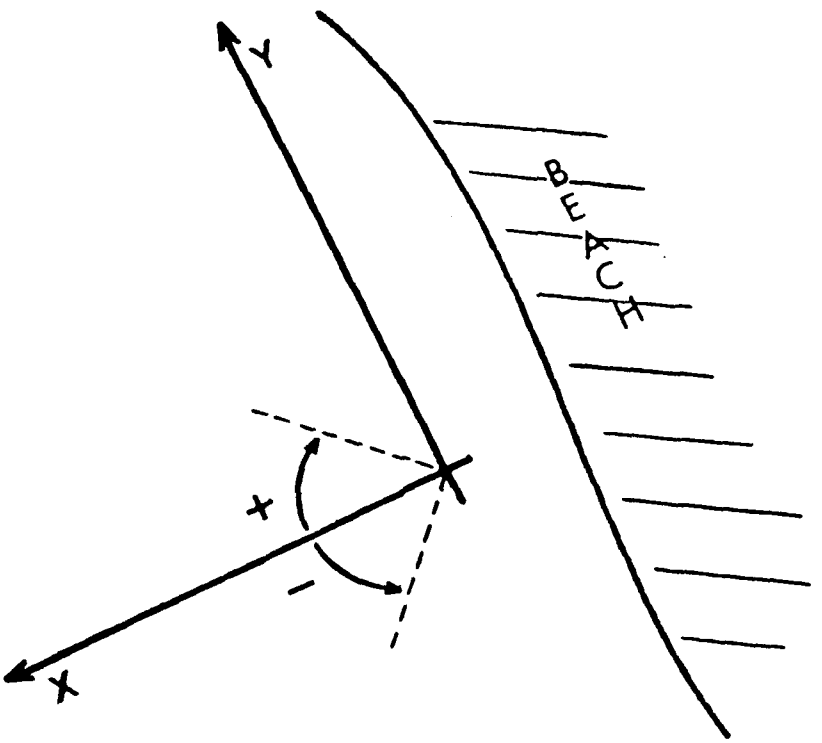

Figure 3.1 The Coordinate System. Directions are Referred to the Beach Normal Which is Made Coincident with the x-axis.

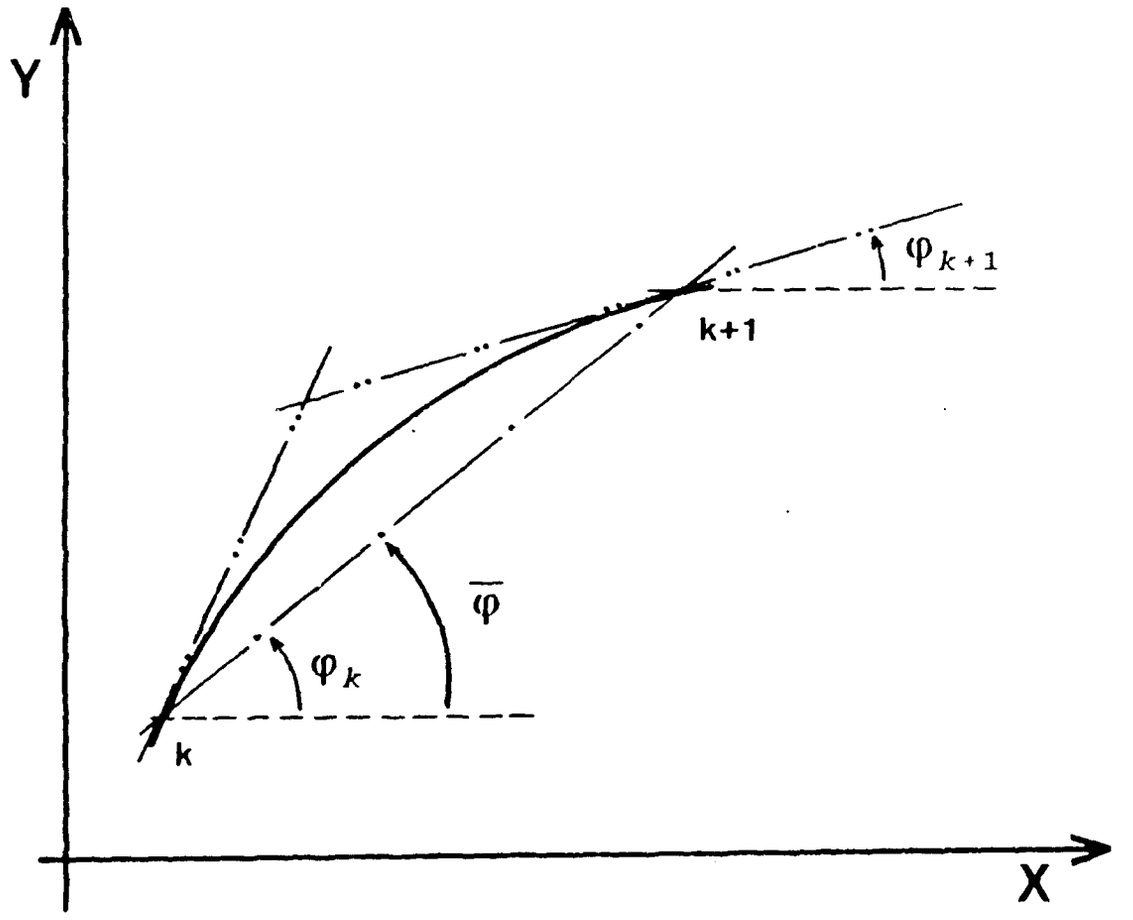

Figure 3.2 Ray Path. The Coordinates of the Initial (k) and of the Target Point (k+1) Together with the Directions (φ) at Those Two Points Define the Ray Path. The Average Direction of the Ray Between the Initial and Target Points is Represented by $\overline{\varphi}$.

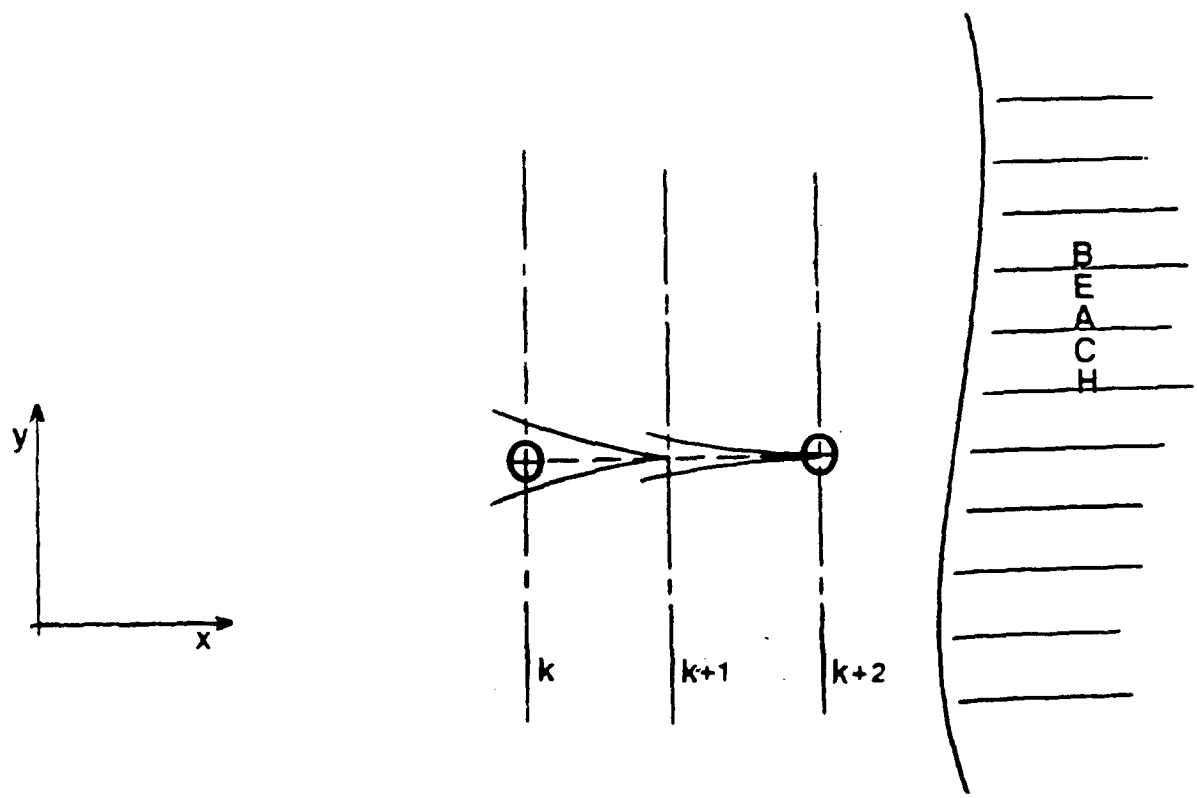

Figure 3.3 The Piecewise Ray Method for a Bathymetry of Straight and Parallel Bottom Contours is Done by Considering Only the Line Connecting the Initial to the Target Point.

IV. MODEL SIMULATIONS

A. INTRODUCTION

To test the wave spectral transformation model formulated in Chapter II (hereinafter WST model), high resolution frequency-directional spectra are required. The need for high resolution in the input data set is a direct consequence of the nonlinear effects under consideration--resonant three-wave interactions. Combined low frequency and directional resolution in the initial conditions can distort the simulated evolution of wave spectra by artificially introducing amplitude dispersion effects. The only known data set with adequate resolution for testing the performance of the WST model is that of Freilich, et al. (1990) (hereinafter FGE90). The FGE90 published data were digitized for use here. The resulting synthetic data set has limitations associated both with the limited extent of the information available, the errors inherent to a digitizing process and the numerical interpolation. Within such conditions, any quantitative evaluation of the model performance has questionable formal validity and one must be cautious of conclusions drawn. However, qualitative evaluation of the potential of the WST model is possible.

In the following development the bicoherence spectrum will be frequently referred as a measure of nonlinearities in the wave field and is briefly reviewed here for the reader. Bispectral analysis was introduced by Hasselman, et al. (1963) and has been used to study nonlinearities in a wide range of phenomena (Elgar and Guza, 1985 and references therein). The important estimator for discretely sampled data sets is the bispectrum (Haubrich, 1965; Kim and Powers, 1979), $B(\omega_k, \omega_j) = E[A_{\omega_k}, A_{\omega_j}, A^*_{\omega_k+\omega_j}]$ where A_ω are the complex Fourier coefficients of the series representation of a stationary random process and $E[\ ]$ is the average operator. The bispectrum is zero for independent modes (random phases relationship in a linear wave field). The bispectrum is generally represented in terms of its normalized phase and magnitude, this last being the bicoherence defined by Kim and Powers (1979) as

$$b^2(\omega_1, \omega_2) = \frac{|B(\omega_1, \omega_2)|^2}{E\left[|A_{\omega_1} A_{\omega_2}|^2\right] E\left[|A_{\omega_1+\omega_2}|^2\right]} \ . \qquad (4.1)$$

For a three-wave process, Kim and Powers (1979) showed that the bicoherence (4.1) corresponds to the fraction of power at frequency $\omega_i+\omega_j$ due to quadratic coupling of the modes ω_i, ω_j and $\omega_i+\omega_j$. This simple interpretation does not apply to broad band processes (e.g., ocean wave spectrum)

because a particular mode is simultaneously involved in many interactions (McComas and Briscoe, 1980); however, the bicoherence still indicates the degree of relative coupling between triads of waves. For the broad band case zero bicoherence ($b = 0$) corresponds to a random phase relationship (linear wave field) and unitary bicoherence ($b = 1$) to a maximum amount of coupling (Elgar and Guza, 1985).

In the following sections the observations of FGE90 and the synthetic data set are presented. Computational parameters are discussed and their implications for the model studied. An analysis of both linear and nonlinear simulations of the evolution of FGE90 observations concludes this chapter.

B. THE DATA

1. The Observations

FGE90 observations are presented in Figures (4.1) to (4.3) for frequency-directional spectra, directional spectra (seven selected frequencies) and frequency spectra. The observations are for a five hour period on 10 September 1980 at Torrey Pines Beach, California. Extensive detail of the observational conditions and experiment site are given in Freilich and Guza (1984).

The frequency-directional spectra were obtained using two alongshore linear arrays of six sensors (bottom mounted pressure sensors at 10.3 meter depth and wave staffs at 4.1

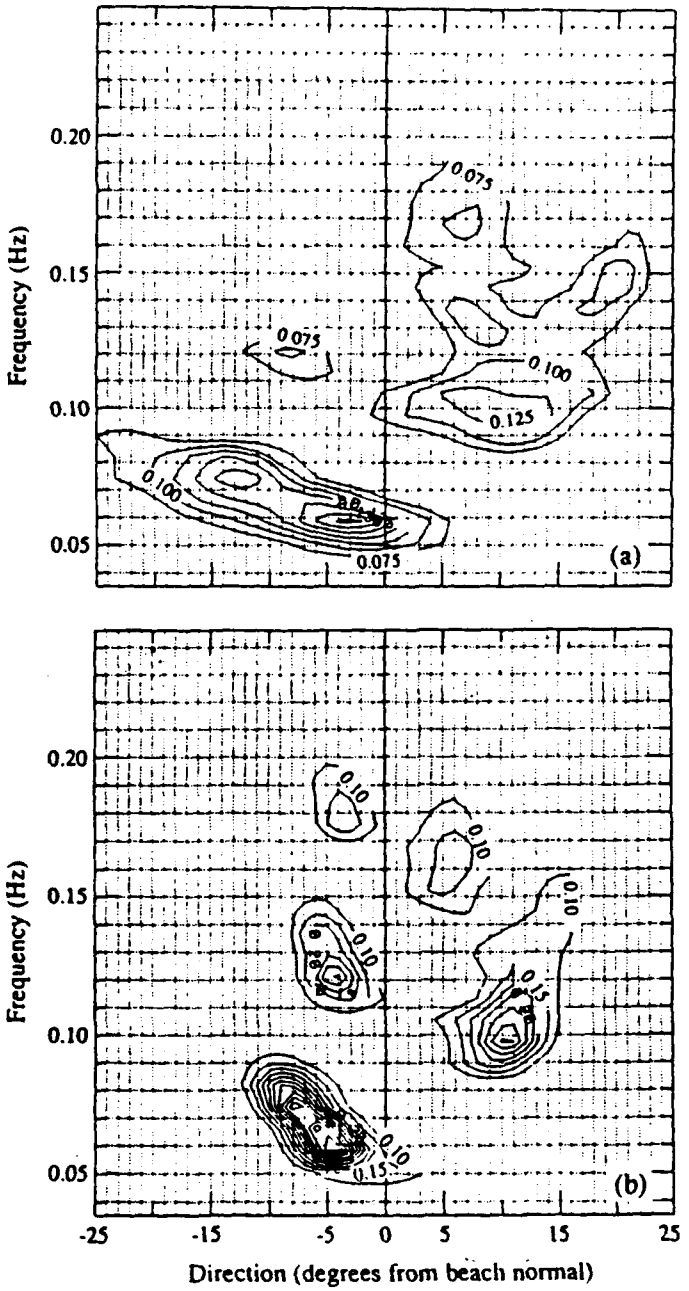

Figure 4.1 Measured Frequency Directional Wave Spectra at 10 Meter Depth (a) and 4 Meter Depth (b). At Each Frequency the Area Under the Curve is Proportional to the Spectral Energy Density at That Frequency. Nonlinearities for Waves Due North (Negative Directions) Result Mostly from Couplings of Harmonic Frequencies (.06, .12 Hz), While for Incoming Waves from the South, Interactions Between Non-harmonic Frequencies (.06, .10 Hz) are Dominant. (Adapted from FGE90.)

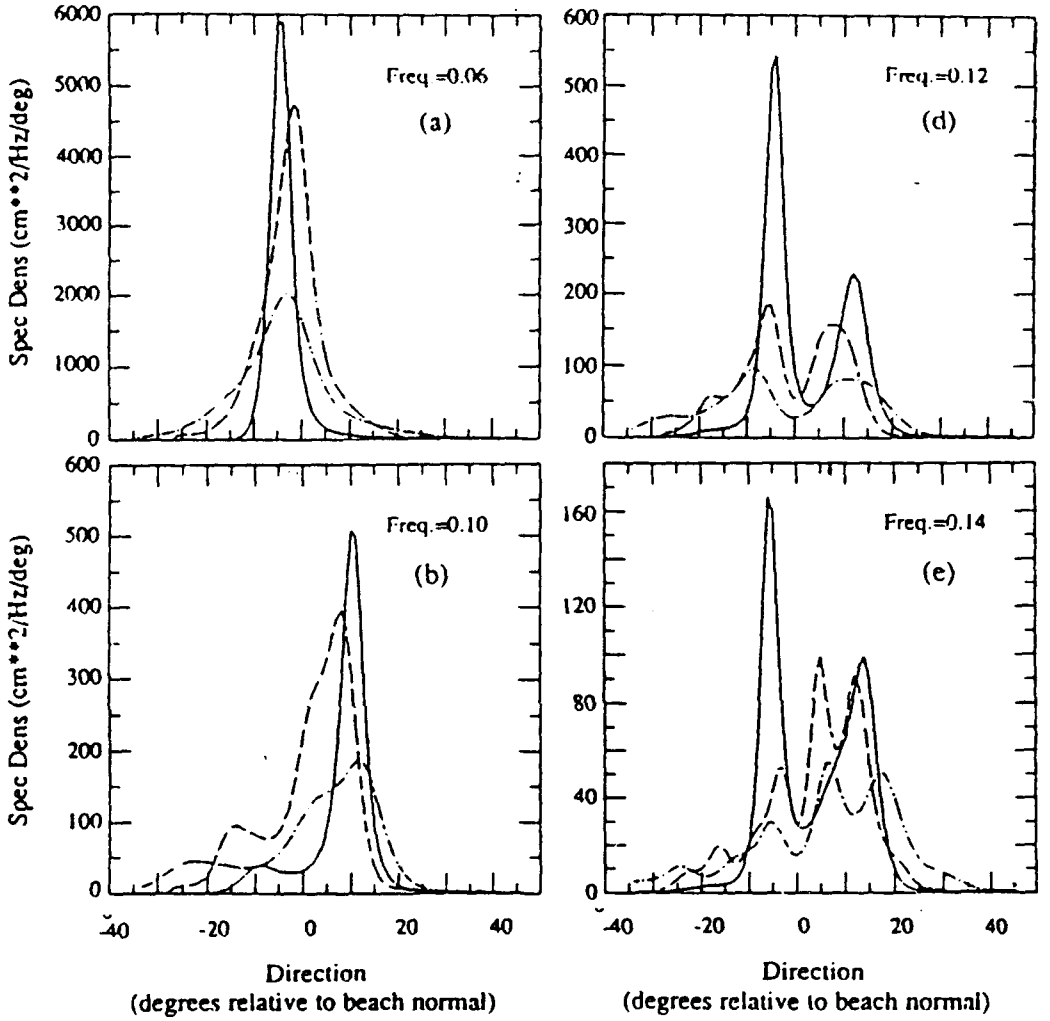

Figure 4.2 Measured Directional Wave Spectra of Selected Frequencies .06 (a), .10 (b), .12 (c) and .14 Hz (d) at 10 Meter Depth (Dash-dot Line), and 4 Meter Depth (Solid Line), and Linearly Predicted Directional Wave Spectra at 4 Meter Depth (Dashed Line) Using for Input the 10 Meter Depth Observed Frequency Directional Wave Spectra. Nonlinearly Generated Peaks of Energy are Evident at Frequency Bands .12 and .14 Hz. (Adapted from FGE90.)

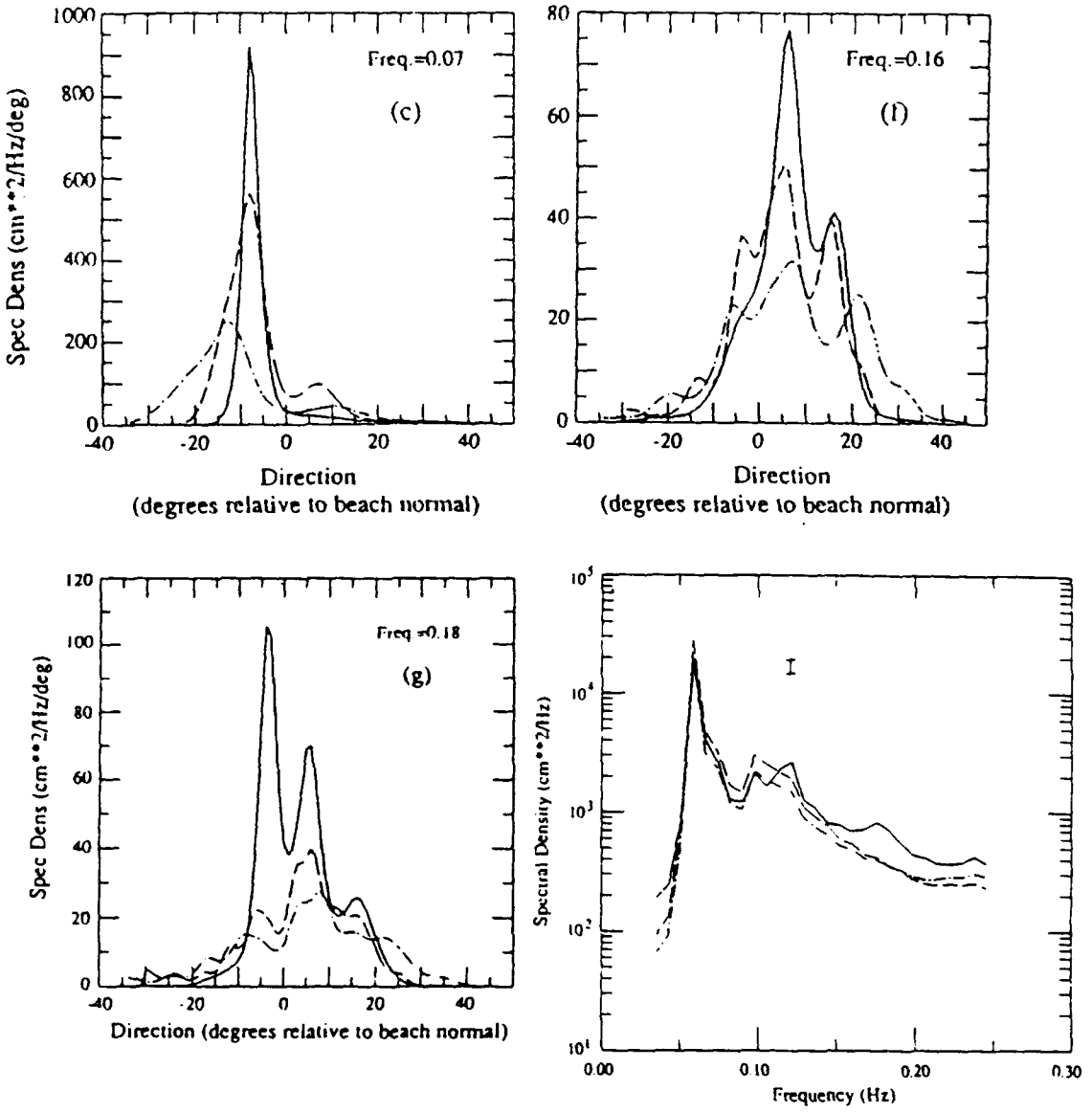

Figure 4.3 Directional Wave Spectra of Three Selected Frequency Bands (e), (f) and (g). The Frequency Directional Spectra of Sea Surface Elevation is Given in (h). Shown are Observations at 10 Meter Depth (Dash-dot Line) and 4 Meter Depth (Solid Line), and the Linearly Predicted Spectra at 4 Meter Depth (Dash Line) Using for Input the Observed Frequency Directional Spectra at 10 Meter Depth. Nonlinearly Generated Peaks of Energy are Evident in the Directional Wave Spectra of .16 and .18 Hz, and in the Frequency Spectra Increased Energy Centered at .12 and .18 Hz can be Noticed. (Adapted from FGE90.)

meter depth). The distance between the two arrays of sensors was 246 meters. The aliasing frequency, corresponding to the spatial resolution of the arrays, was 0.2 Hz. The directional resolution obtained for estimates of frequency-directional wave spectra depends on the estimation method used. When using maximum likelihood estimation techniques, the resolution obtained was about 8 degrees for wave trains at a frequency of .067 Hz (FGE90). Iterative maximum likelihood techniques (Pawka, 1982 and 1983; Oltman-Shay and Guza, 1984) used in FGE90 allowed for significant increase of the directional resolution. Although not stated in FGE90, the directional spectra of the seven selected frequencies presented suggests a final resolution of 0.5 degrees. It is noted that the iterative maximum likelihood estimator does converge upon a possible true spectrum. Confidence bounds for the resulting estimation are not known. The determination of these bounds is not a straightforward task and has involved considerable effort in the past two decades. The important point to note in the relation between the resolving power of the two arrays is that two wave trains that differed only slightly in direction could be resolved by the two arrays assuming that the beach had parallel bottom contours and that linear refraction theory was valid (FGE90).

The bathymetry of the experiment site (Figure (4.4)), is nearly planar and when approximated by a linear least squares fit of the tide-corrected soundings, the resulting

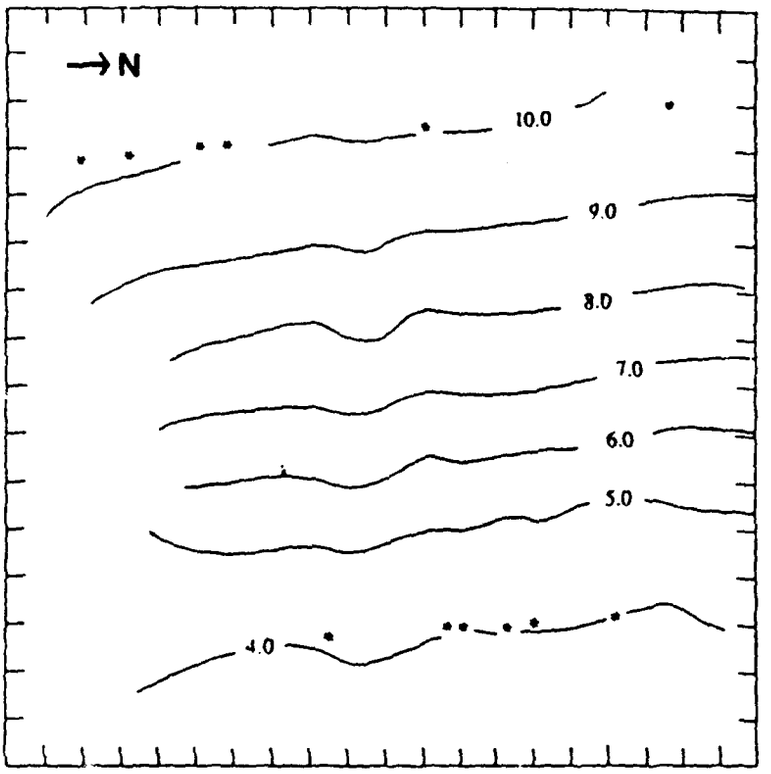

Figure 4.4 The Nearly Planar Bathmetry of the Experiment Site at Torrey Pines Beach, California, on 9 September 1980. Contours are 1 Meter Apart and Asterisks Represent the Locations of the Wave Sensors. Tick Interval (Axes) Correspond to 25 Meter. (Adapted from FGE90.)

plane has a mean slope of 0.025 and a beach normal oriented at 264 degrees true.

2. The Synthetic Data Set (SDS)

The directional spectra of the seven selected frequency bands (Figures (4.2) and (4.3)) are used to recreate the frequency-directional wave spectra presented in FGE90. The choice of the frequency resolution for the interpolation process was made considering both the evolution of the wave spectra from 10 to 4 meter depth in FGE90 observations and the measured bicoherence spectra (FGE90).

Reviewing the measured frequency-directional wave spectra (Figure (4.1)), two distinct areas can be noticed: waves approaching from the southern quadrant (negative angles) are dominated by interactions between harmonic frequencies (.06, .12 Hz), and waves coming from the northern quadrant show coupling of non-harmonic frequencies (.06, .10 Hz). The measured bicoherence spectrum (Figure (4.13b)) at 4 meter depth suggests that waves at .06 Hz are significantly coupled to waves at all other frequencies within the energetic band. To ensure that the suggested important nonlinear couplings are modeled, a .01 Hz frequency resolution was adopted (FGE90 frequency resolution is .0078 Hz). The frequency range chosen for the synthetic data set was from .05 to .19 Hz.

The directional resolution chosen was 1 degree, reducing artificial directional amplitude dispersion in the

model results. The linear distribution of variance between resolved directions used by FGE90 allows a simple interpolation to a 1 degree directional resolution.

a. The Digitizing and Interpolation Processes

Each of the seven selected directional spectra in FGE90 (.06, .07, .10, .12, .14, .16 and .18 Hz) (Figures (4.2) and (4.3)) was digitized at 2.5 degrees in the range -35 to 40 degrees. To minimize distortions of the observed wave field in the interpolation process, peaks and turning points were added to the basic discretization. Several numerical interpolation techniques were tested, without significant differences. The interpolation method adopted was a cubic spline with a "not a knot" endpoint condition. First, the directional spectrum at each of the selected frequencies was interpolated to a 1 degree resolution. Then, the directional spectra at intermediate frequencies in the range .06 to .18 Hz were obtained by interpolation across the frequency range. The definition of the directional spectra at the frequency bands .05 and .19 Hz used a linear extrapolation conditioned by a few points obtained from the corresponding contours of the FGE90 frequency-directional spectrum.

b. The Spectra

The frequency-directional wave spectrum of the SDS compares well with FGE90, with the total band variances differing by no more than 5 percent and peak directions by no

more than 1 degree for the selected frequencies (Table (4.1)). Similar to FGE90, the frequency-directional spectrum (Figure (4.5)) at each frequency was normalized by the total energy in that band. Uncertainties in the SDS may be expected at the interpolated frequency bands. The good agreement between the frequency spectra (Figure (4.7h)) suggests reasonable representation of the variance of the interpolated bands. However, for a model such as the WST that considers exclusively collinear interactions, it must be emphasized that, even small directional errors of the spectral components can have considerable effect on the results (Appendix B).

C. THE SPATIAL EVOLUTION OF SDS

1. The Computer Parameters

The WST model was installed in a user partition of the Naval Postgraduate School mainframe system (AMDAHL 5990-500 with VM/CMS operating system, and +300 MFLOPS). Each user partition has 3 megabytes of virtual memory (RAM) and a storage capacity limited to 2.4 megabytes. The simulations used machine double precision (64 bits).

To predict the evolution of the frequency-directional wave spectrum, the model uses a cycle of three steps: the computation of the ray path, the evaluation of the collision integral, and the transformation of the spectra by combined shoaling and refraction effects. Besides the propagation step, the user defines criteria for the calculation of the ray

TABLE 4.1

THE SYNTHETIC DATA SET. TOTAL BAND VARIANCES AND PEAK DIRECTIONS FOR THE DIRECTIONAL WAVE SPECTRA OBSERVED AT 10 METER DEPTH BY FGE90 AND FOR THE SYNTHETIC DATA SET (SDS). ALSO TABULATED IS THE RELATIVE ERROR BETWEEN THE SDS AND FGE90 OBSERVATIONS.

FREQ (Hz)	VARIANCES (cm^2)			PEAK DIRECTION	
	FGE90	SDS	% DIF	FGE90	SDS
.06	18684.	18650.	.2	-4	-4
.07	2283.	2386.	5.	-13	-13
.10	2203.	2251.	2.	+12	+12
.12	1501.	1566.	4.	-8	-8
				+11	+10
.14	750.	743.	1.	-5	-5
				+7	+8
				+17	+17
.16	480.	477.	1.	-6	-5
				+7	+7
				+21	+20
.18	387.	406.	5.	-8	-8
				+8	+7
				+15	+15

parameters (Section II.B.1), and the range of frequencies allowed to interact nonlinearly (to be discussed in Section IV.C.3.2).

Using a directional resolution of 1 degree (76 directions in the range -35 to 40 degrees) and a .01 Hz

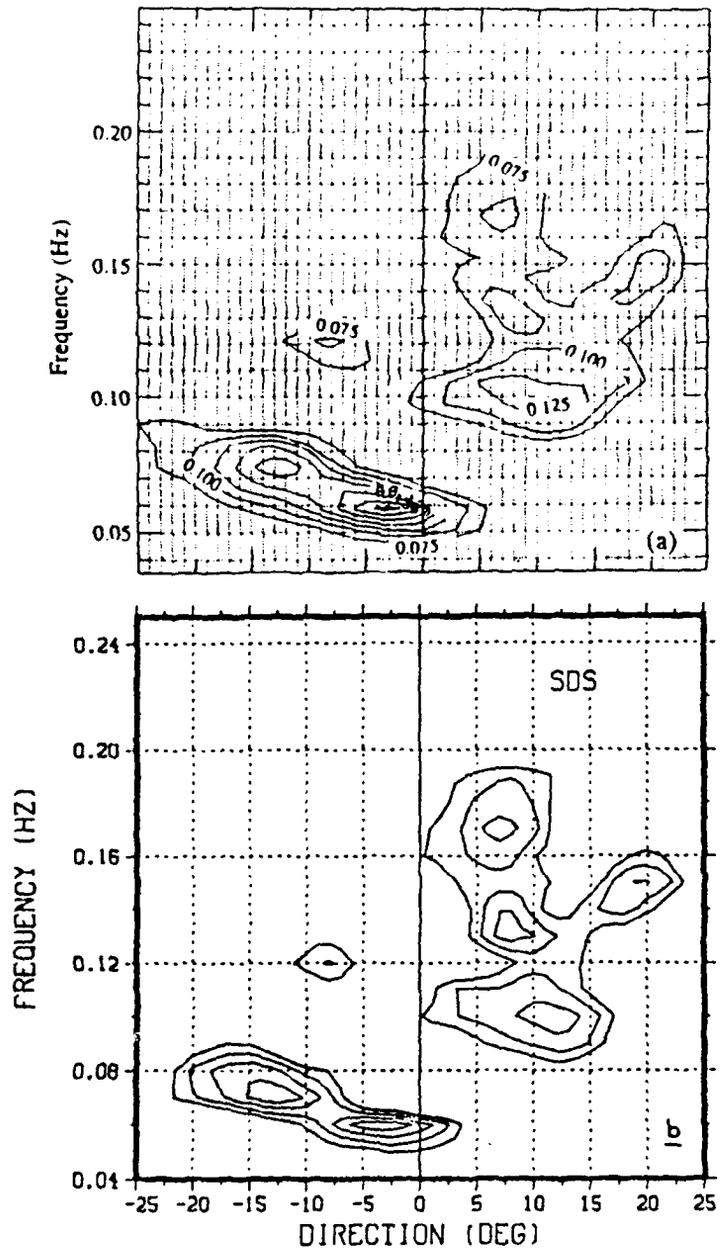

Figure 4.5 The Synthetic Data Set Frequency-directional Wave Spectra (Plot (b)) Reasonably Represents the Observations at 10 Meter Depth (Plot (a)). At Each Frequency the Area Under the Curve is Proportional to the Spectral Energy Density at That Frequency. For the Synthetic Data Set, the Exterior Contour Has a Value of .9, with the Contours .2 Units Apart. Directions are Relative to the Beach Normal.

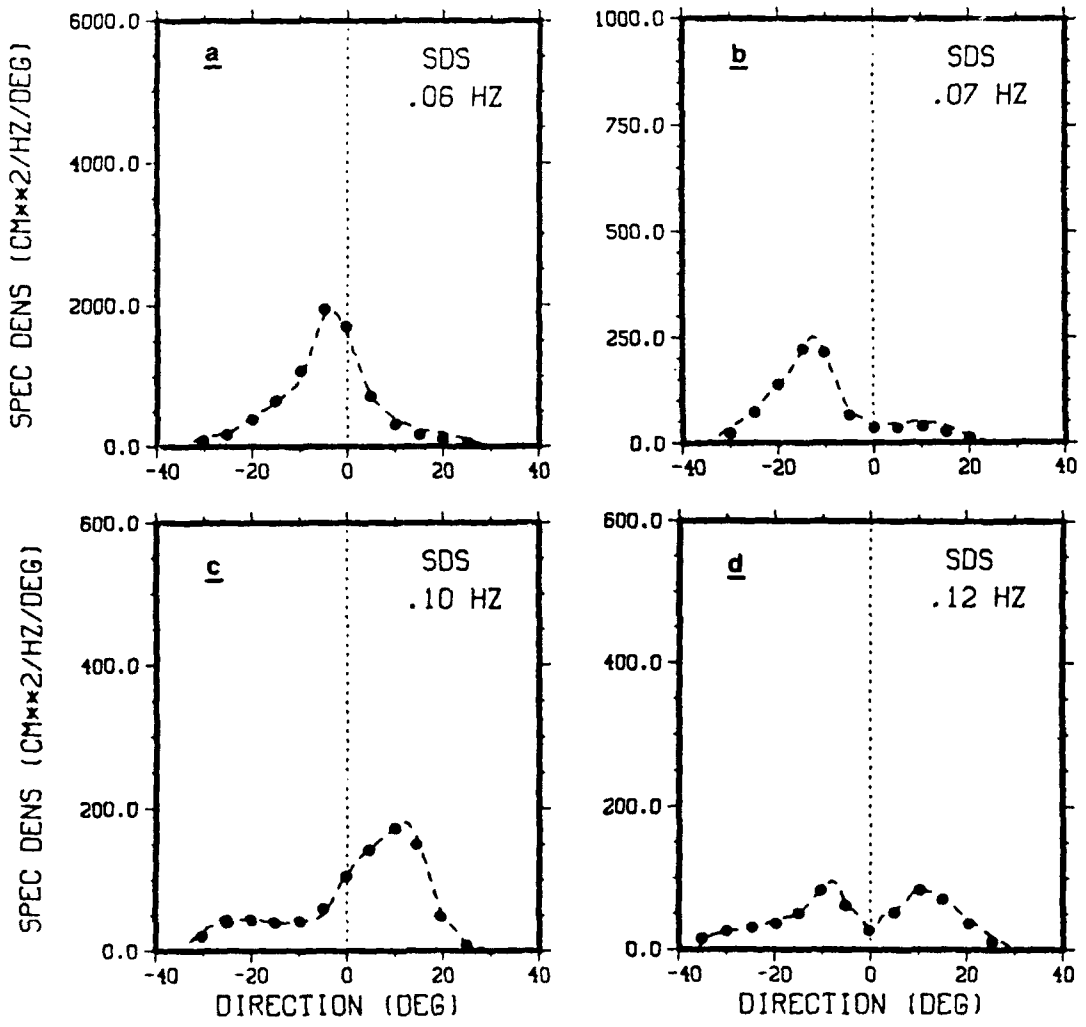

Figure 4.6 Synthetic Data Set Directional Spectra of Four Selected Frequency Bands of the Synthetic Data Set (Dash Line) is in Good Agreement with the Observations at 10 Meter Depth (Dots). Directions are Relative to the Beach Normal.

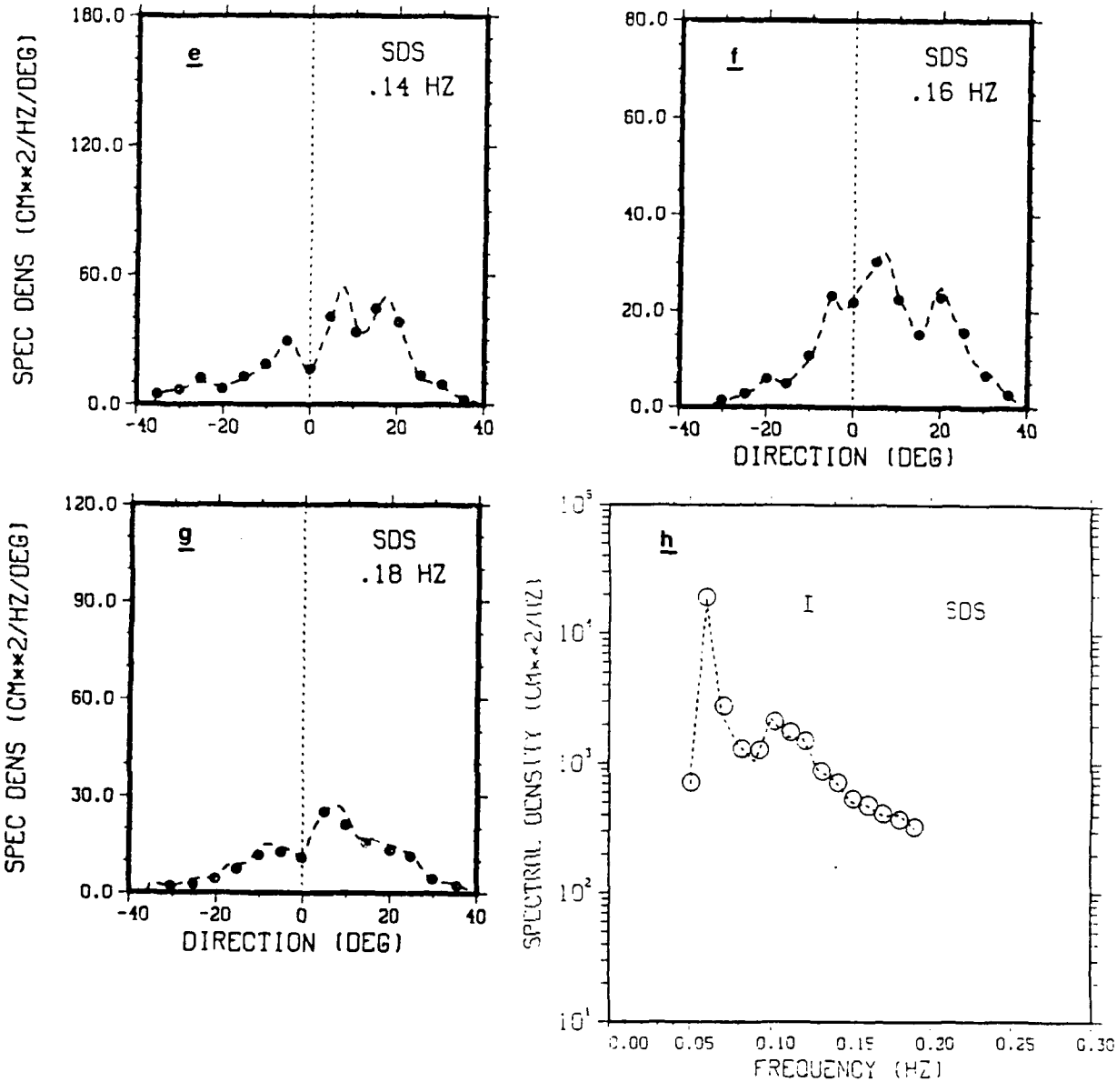

Figure 4.7 The Directional Wave Spectra of Three Selected Frequencies of the Synthetic Data Set (e), (f) and (g) (Dash Line) Show a Good Agreement with the Observations at 10 Meter Depth (Dots). The Frequency Spectrum (Plot (h)) of the Synthetic Data Set (Dash Line) Closely Follows the Measured Spectra at 10 Meter Depth (Circles). Diameter of the Circles in Plot (h) Equals the 95% Confidence Interval. Directions Relative to the Beach Normal.

frequency resolution (24 frequencies in the range .01 to .24 Hz), requires 1824 harmonics in each propagation cycle. Both the linear and nonlinear simulations adopted a propagation step of 1 meter. The iteration criteria for the calculation of the directions and coordinates along the ray (ray parameters) was 10^{-7} for both. For this computational set up, the model requires about 380 cpu seconds for the more demanding nonlinear simulations.

2. The Linear Evolution of SDS

The wave field during the experiment (Freilich and Guza, 1984) satisfies the linear finite depth wave theory conditions of small bottom slope, no significant input of energy by atmospheric forcing, and negligible dissipation processes (bottom friction and breaking). However, nonlinear wave interaction processes are observed (Figure 4.1)). Thus, it is expected that simulations of the evolution of SDS using a linear model will lack the effects of the transfer of energy between Fourier components and of directional distortions of the wave field caused by nonlinear wave interactions.

For the linear simulations the LeMehaute and Wang (1982) model and the linear version of WST are used. The objectives of these simulation are to further evaluate the quality of SDS, and test the performance of the piecewise ray method developed.

The linear model of LeMehaute and Wang has the form

$$S(f,\varphi) = \frac{k c_{g0}}{k_0 c_g} S_0(f,\varphi)\left\{f, \sin^{-1}\left[\frac{k}{k_0}\sin\varphi\right]\right\} \qquad (4.2)$$

where φ defines the angle of the wavenumber vector k with the beach normal, c_g is the group speed and f the frequency. The subscripted variables refer to values at the initial location. The linear dispersion relation for surface gravity waves

$$\omega = (gk\tanh(kh))^{1/2} \qquad (4.3)$$

provides the link between the variables involved.

The linear evolution of SDS predicted by LeMehaute's and Wang model and by the WST model (linear version) (Figures (4.9) and (4.10), and Table (4.2)), show good agreement that further verifies the propagation scheme. Also, the linear evolution of SDS (WST model) and FGE90 linear predictions (Figures (4.8), (4.9) and (4,10), and Table (4.2)) compare well; there is a similar distribution of energy both in frequency and in direction that suggest SDS is an accurate approximation of the FGE90 spectra.

The performance of the linear finite depth wave theory as an estimator for the evolution of frequency-directional spectra is extensively analyzed in FGE90. The two main points to recall are: (i) the inadequacy of the linear theory in

predicting both frequency and directional distributions of energy in regions of the wave spectra dominated by nonlinear effects (frequencies .12 Hz and above in Figures (4.2) and (4.3) and Table (4.2)); and (ii) that linear wave theory overpredicts the observed energy in the low frequency range (.06 to .10 Hz in Table (4.2)). Overprediction of energy by linear wave theory was not referred to by Freilich and Guza (1984) for simulations on other days during the experiment although reference is made to the energy of the observed spectral peak on 11 September 1980).

3. Nonlinear Simulation

a. Computational Parameters

Before proceeding with the analysis of the WST model results for the nonlinear propagation of SDS, the importance of the propagation step adopted (1 meter) and the criterion used for the definition of the frequency range of interacting spectral components is examined.

(1) The Propagation Step. The definition of the propagation step has three basic implications. The first refers to the propagation distances of the different spectral components. The second is related to collinearity between nonlinearly interacting waves, and the last is concerned with the assumption of a constant value for the spectral energy density in the spatial integration of the collision term (Section III.B.2). Only the first two of these are considered

TABLE 4.2

THE LINEAR EVOLUTION (4 METER DEPTH). TOTAL BAND VARIANCES AND PEAK DIRECTIONS OF THE DIRECTIONAL WAVE SPECTRA AT 4 METER DEPTH OF THE FGE90 OBSERVATIONS, LEMEHAUTE'S AND WANG (1982) (MW) LINEAR MODEL PREDICTIONS OF THE EVOLUTION OF THE SDS AND FGE90 OBSERVATIONS, AND THE EVOLUTION OF SDS PREDICTED BY THE LINEAR LIMIT OF THE WST MODEL.

FREQ (Hz)	VARIANCES (cm^2)				PEAK DIRECTION			
	SDS		FGE90		SDS		FGE90	
	MW	WST	MW	OBS.	MW	WST	MW	OBS.
.06	27884	27902	27969	19568	-2	-2	-2	-4
.07	3473	3477	3285	2667	-8	-8	-8	-8
.10	3083	3086	3030	2122	+8	+8	+8	+10
.12	2011	2083	1921	2621	-5	-5	-5	-4
					+8	+8	+7	+12
.14	894	895	912	1001	-3	-3	-3	-6
					+5	+5	+5	---
					+12	+12	+12	+14
.16	535	535	540	689	-4	-4	-4	---
					+5	+5	+5	+6
					+14	+14	+15	+16
.18	421	422	415	821	-6	-6	-6	-4
					+5	+5	+6	+6
					+16	+16	+16	+16

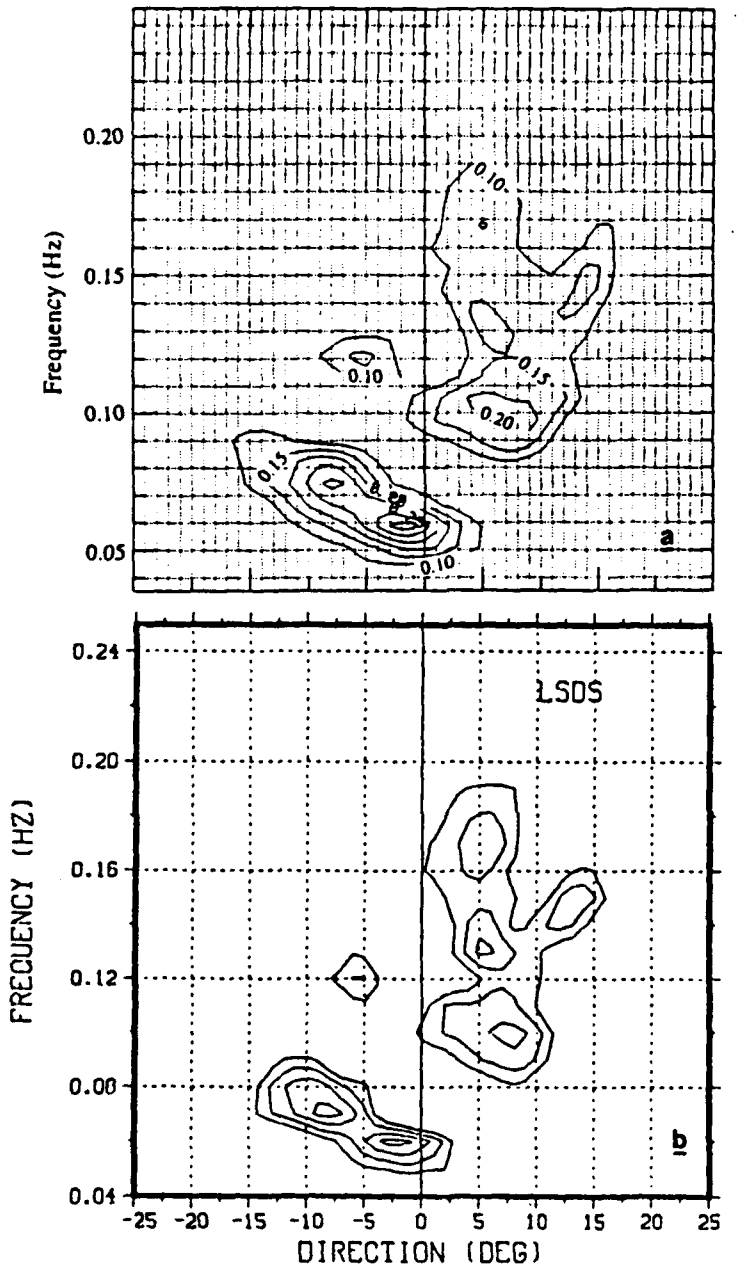

Figure 4.8 The Evolution of the Synthetic Data Set Frequency-Directional Wave Spectra from 10 to 4 Meter Depth Predicted by the Linear Limit of the WST Model (Plot (b)) is in Good Qualitative Agreement with the Linear Prediction of LeMehaute's and Wang (1982) Model (Plot (a)) Using the Observations at 10 Meter as Input. Directions are Relative to the Beach Normal.

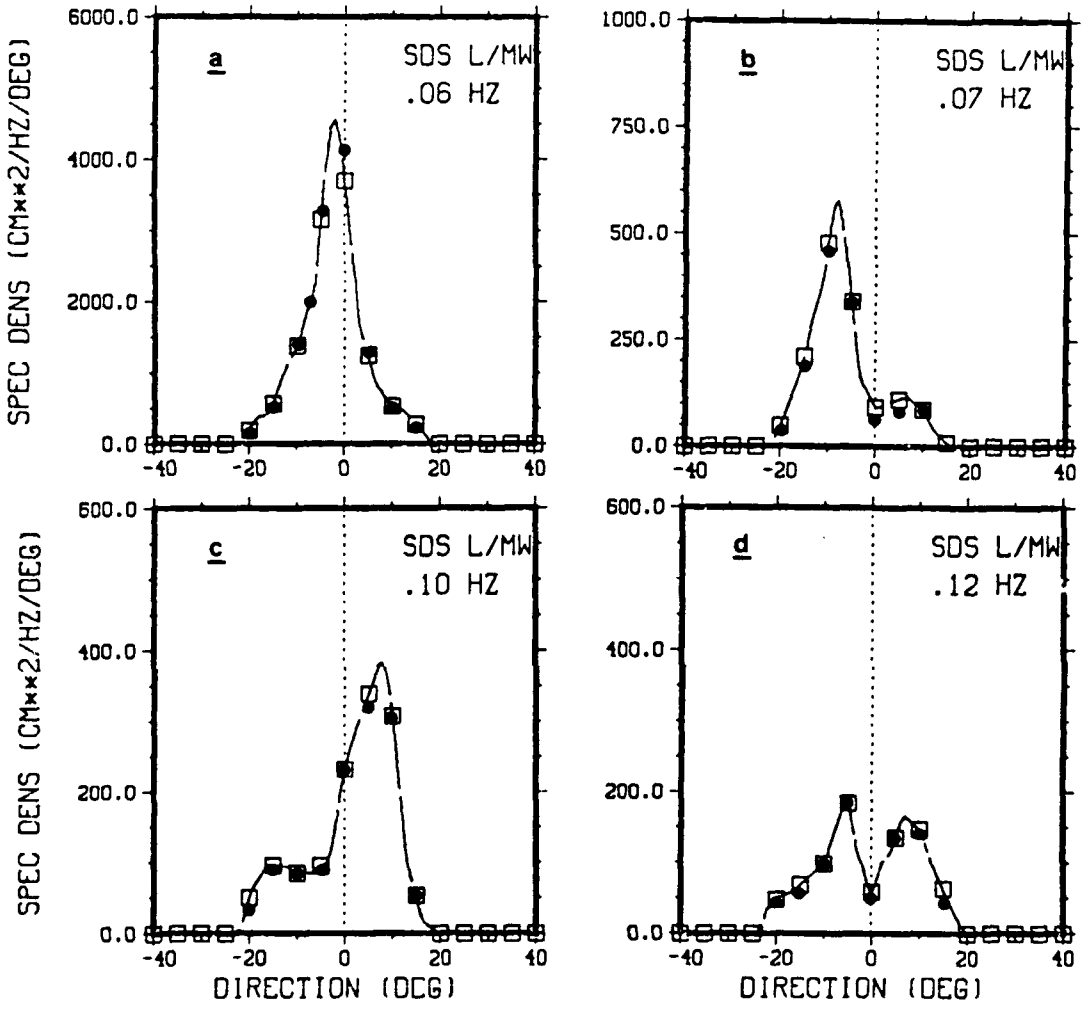

Figure 4.9 The Predicted Evolution of the Synthetic Data Set Directional Wave Spectra at 4 Meter Depth by the Linear Limit of the WST Model (Chaindash Line), and LeMehaute's and Wang Linear Model (Squares) are in Close Agreement, and Compare Well to the Linear Predictions of FGE90 (Dots) Using the Latter Model Initialized with the Observations of Frequency Directional Spectra at 10 Meter Depth. Directions are Relative to the Beach Normal.

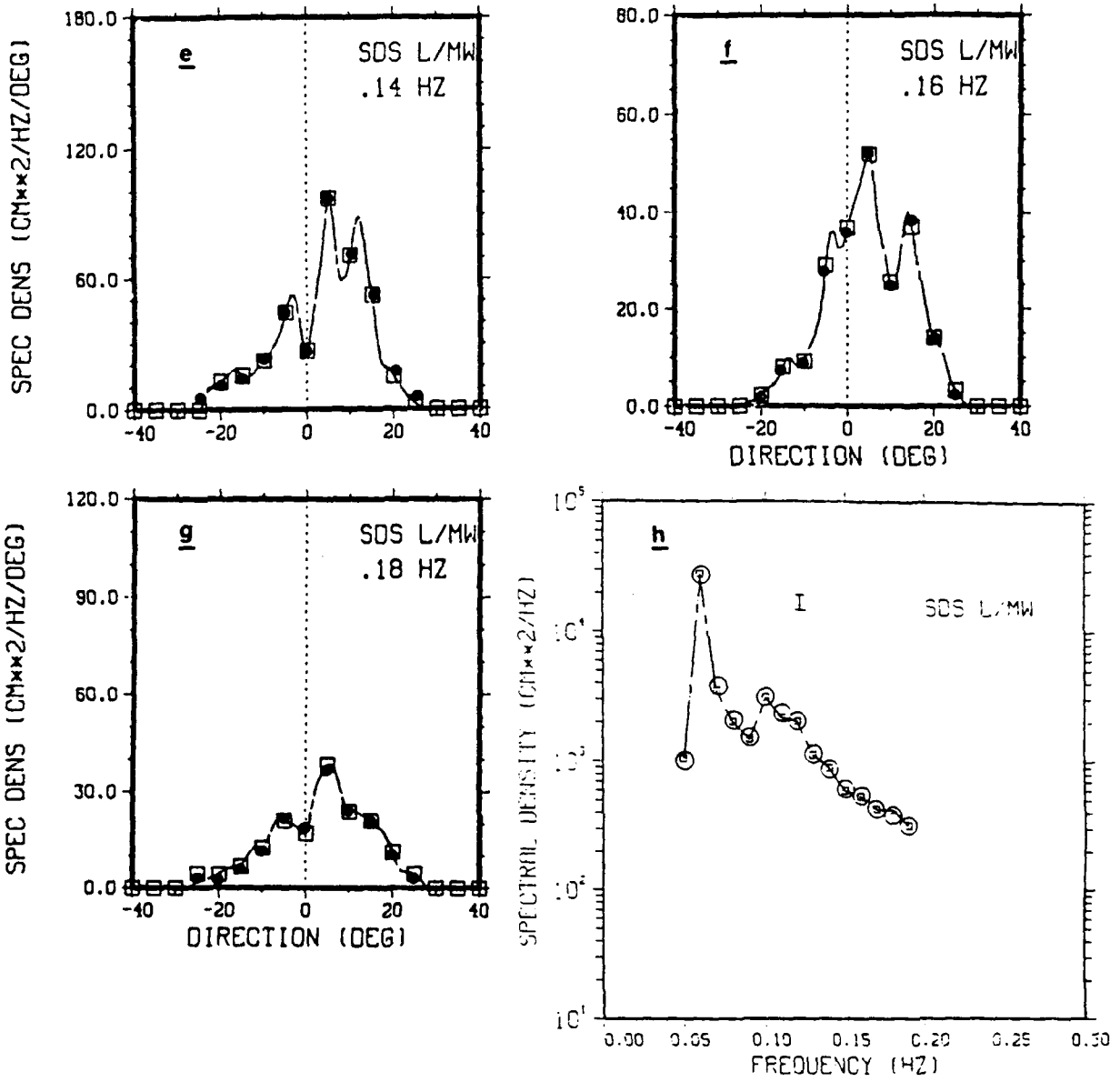

Figure 4.10 The Linear Evolution of Directional and Frequency Wave Spectra from 10 to 4 Meter Depth of the Directional Wave Spectra (Plots (e), (f) and (g)) and of Frequency Spectra (Plot (h)) of the Synthetic Data Set, Computed with the Linear Limit of the WST Model (Chaindash Line) and LeMehaute's and Wang Linear Model (Squares) Compare Well with the Predictions of FGE90 (Dots in (e), (f) and (g); Circles in (h)) Using the Latter Model and the 10 Meter Depth Observations of Frequency Directional Wave Spectra. The Diameter of the Circles in Plot (h) Equals the 95 Percent Confidence Interval. Directions are Relative to the Beach Normal.

in this section. The third is studied in the sensitivity analysis of the model results (Appendix B), where it is concluded that there are no significant differences in the model results for propagation steps of 1, 3 and 6 meter. In the following discussion, it should be noted that computational requirements are not a constraint in the selection of the propagation step.

The problem of the total distance of propagation and interaction can be divided in two parts: the validity of the ray theory of wave propagation, and the rigor of the method used to compute the ray parameters. For the first part, the success of the ray theory and its recognition as a rational framework within the applicability conditions (Chapter II) is assumed a reasonable safeguard. Relative to the calculation of the ray parameters, the piecewise ray method developed performed well in comparison both with Dobson's method and with Snell's law (Section III.B.1).

Regarding the collinearity of nonlinearly interacting spectral components, the propagation step must be chosen properly because it directly determines the per-step change in direction of the waves by refraction. Smaller propagation steps correspond to smaller differences in the directions of two initially collinear components at the end of the propagation cycle. The 1 meter propagation step closely simulates collinearity of interacting components. It gives rise to a maximum change in the direction of the coupled

components of $2.5*10^{-4}$ radian per step. The Fourier components are thus taken as collinear if their directions do not differ by more than .02 degrees, that is, by no more than 2 percent of the directional resolution adopted. The significance of these small numbers can be estimated by computing the wavenumber product of an interaction both at zero angle and at .02 degrees. To compute the relative error of wavenumbers corresponding to interactions at .02 degrees (k_φ) and to collinear interactions (k_{col}), the relation

$$\rho_\varphi = \frac{k_{col} - k_\varphi}{k_{col}} \quad , \qquad (4.4)$$

is used. The distribution of the relative error as a function of the frequency of the coupled components for 10 meter depth is shown in Figure (4.11). The interacting wavenumbers are calculated using the shallow water linear dispersion relation. Distributions of the relative error given by (4.3) for other depth values in the range 4 to 9 meter are similar to the 10 meter depth case. As can be concluded from Figure (4.11), the propagation step yields negligible departure from the exact kinematic resonant conditions, and the collinearity condition is verified.

(2) The Collision Range. The objective is to establish a criterion that ensures conditions of three wave kinematic resonance for spectral components undergoing

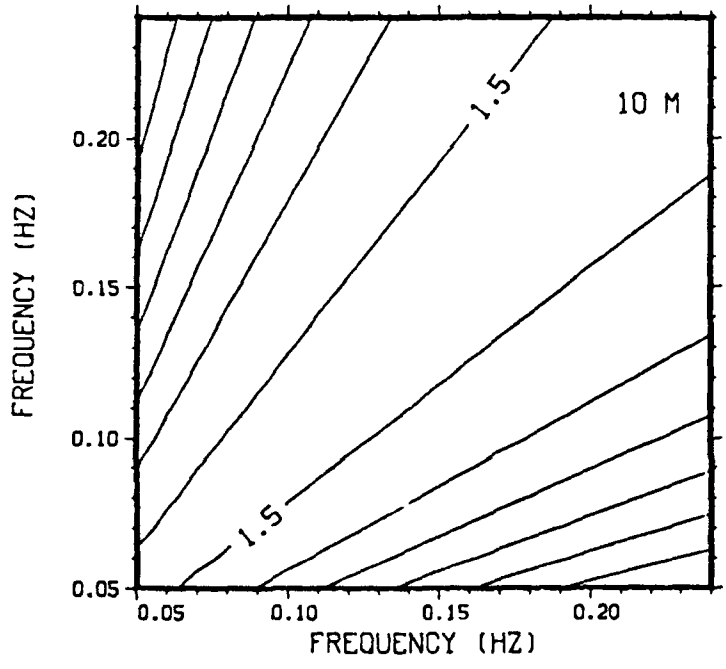

Figure 4.11 The Percent Mismatch in the Computed Wavenumber as a Result of Nonlinear Interactions ($\bar{K}_3 = \bar{K}_2 + \bar{K}_1$) Between Components at an angle (.02 Degrees) and Collinear Components. Contour Values Correspond to Scaled Percentages of Mismatch (Contour Value = % Mismatch*10^6). The Contour Interval is .1, with Decreasing Values Outward from the 1.5 Labelled Contours.

nonlinear interactions. In the shallow water regime, the existence of triad interactions is a direct consequence of the nondispersive form of the linear dispersion relation.

Classical finite depth linear wave theory adopts the value $kh < \pi/10$ as a limit for the shallow water regime, which corresponds to errors in the approximation of the dispersion relation of at most 1 percent. The error of wavenumbers computed with the linear shallow water approximation (k_s) relative to wavenumbers calculated with the surface gravity wave linear dispersion relation (k_c) is given by

$$\rho = \frac{k_c - k_s}{k_c} \qquad (4.5)$$

and is shown in Figure (4.12) for frequencies in the range .06 to .21 Hz (at .03 Hz interval) and depths from 4 to 10 meter. It can be concluded from Figure (4.12) that frequencies less than .05 Hz meet the $kh < \pi/10$ criterion in the range of depths considered, and that .06 Hz verifies the criterion close to 4 meter depth. The adoption of a criterion based on a value of $kh < \pi/10$ negates the feasibility of the nonlinear evolution observed by FGE90 resulting from nonlinear triad resonant interactions.

On the other hand, the measured bicoherence spectra (FGE90) reproduced in Figure (4.13), show that .06 Hz

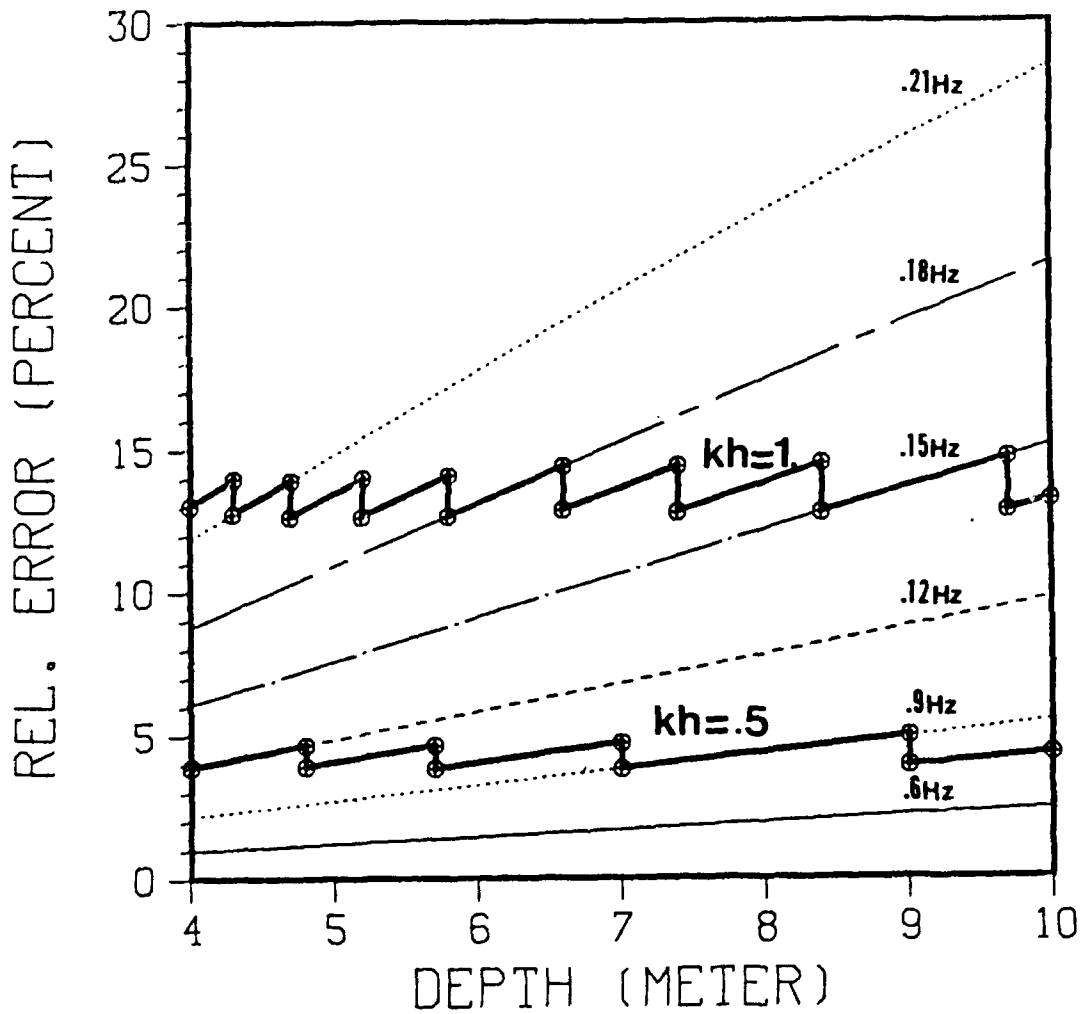

Figure 4.12 Relative Error of the Wavenumber Computed with the Surface Gravity Waves Linear Dispersion Relation and with the Shallow Water Dispersion Relation, for Six Frequency Bands (.06 to .21 Hz at .3 Hz Interval) and the Range of Depth of the Experiment Site. The Solid Lines Correspond to the Values kh = 1 and kh = .5 with the Wavenumber Computed Using the Surface Gravity Waves Linear Dispersion Relation.

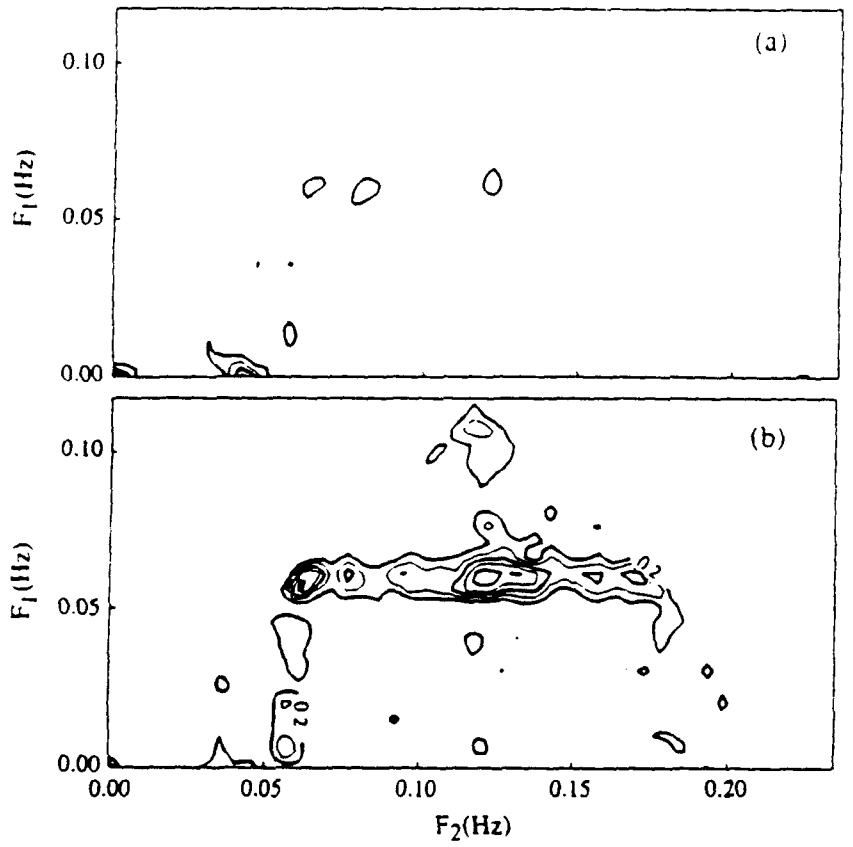

Figure 4.13 Measured Bicoherence Spectra at 10 Meter Depth (a) and at 4 Meter Depth (b). Only Significant Bicoherences are Shown with the Bold Lines Corresponding to Significance Levels Above 90 Percent (Contour Interval is .1). Insignificant Levels of Bicoherence at the Deeper Location Suggest Little Nonlinear Coupling Between Spectral Components. The Measured Bicoherence at 4 Meter Depth Suggests that Waves at .06 Hz are Significantly Coupled to Waves at All Other Frequencies. (Adapted from FGE90.)

computed with the linear dispersion relation and the shallow water approximation. The error in satisfying the wavenumber resonance condition (4.7) is shown in Figures (4.14a, b) for interacting frequencies up to .24 Hz and depth values of 4, 6, 8 and 10 meter, with the convention that $f_3 = f_1 + f_2$. The areas enclosed by the dotted lines correspond to the values of $kh = .5$ and $kh = 1$.

Using the information in Figures (4.14a, b), the limit for the interacting spectral components was chosen as $kh < .5$. This value corresponds to a mismatch in the wavenumber resonance condition (4.7) of 5 percent at most. It represents a small departure from the strict conditions of applicability of the WST model and is a compromise between the classical shallow water criterion and the range of strong interactions suggested by the measured bicoherence spectra. For the criterion adopted, $kh < .5$, the collision range in the observational conditions in FGE90 extends up to the frequency .12 Hz.

4. Results

In this section, the evolution of SDS predicted by the WST model is analyzed by comparing the model results for frequency, frequency-directional and directional spectra with FGE90 observations. As noted earlier, only a qualitative analysis is possible because of the synthesis of the SDS data set.

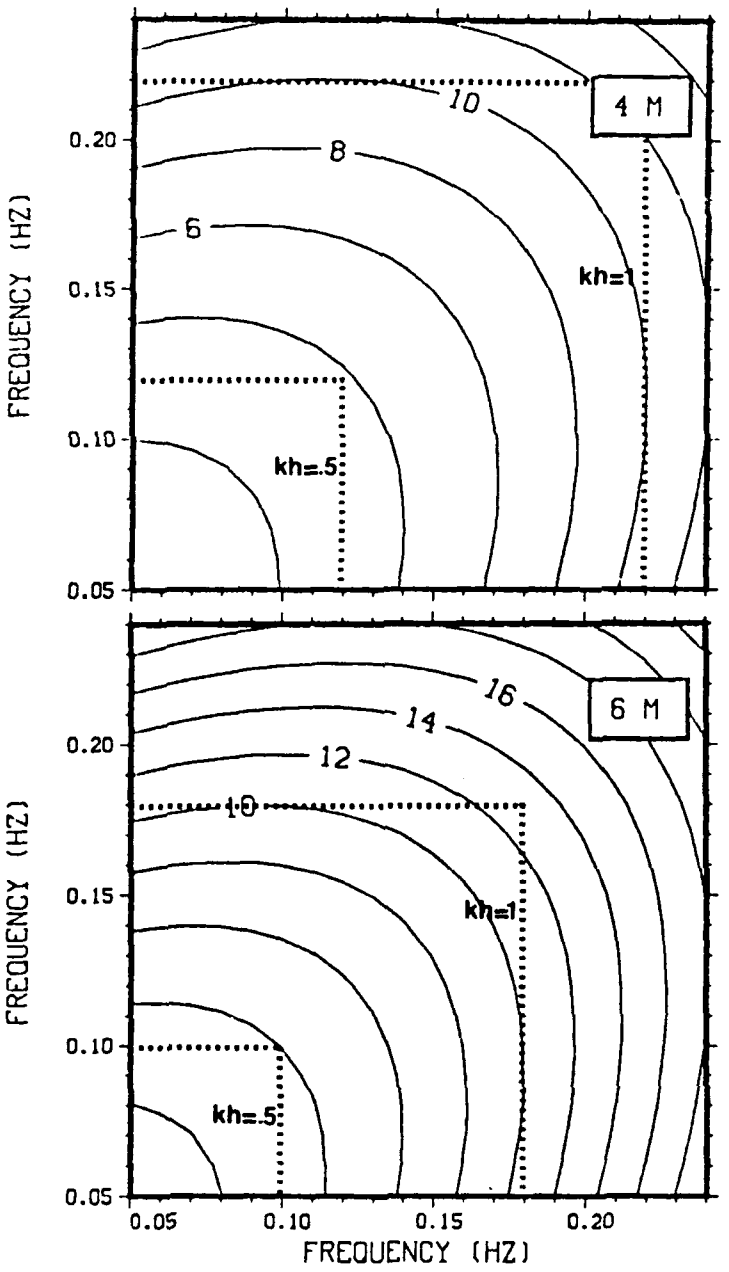

Figure 4.14a Percent Mismatch in the Wavenumber Calculation of a Collinear Interaction ($k_3 = k_2 + k_1$), When the Coupled Wavenumbers are Computed with the Surface Gravity Waves Linear Dispersion Relation Compared with the Shallow Water Dispersion Relation, for the Depths of 4, 6. Dotted Lines Correspond to the Values of kh = 1 and kh = .5.

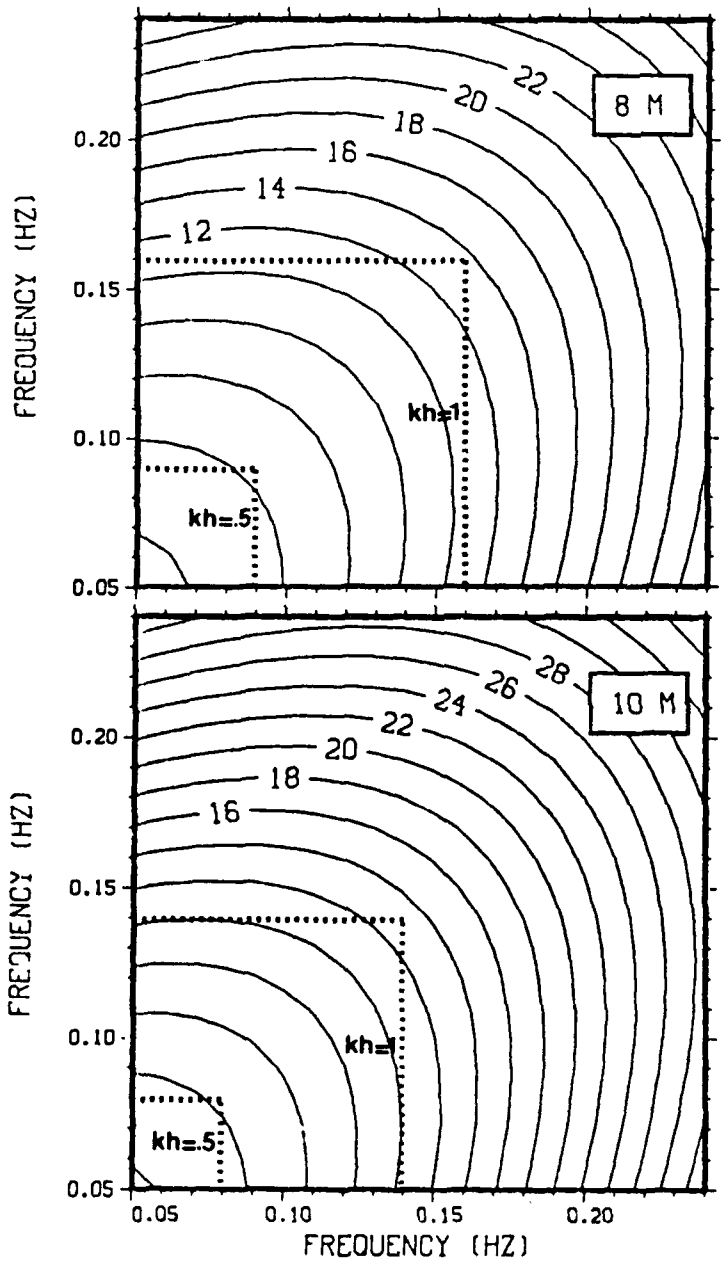

Figure 4.14b Same as 4.14a for 8 and 10 Meter.

a. Frequency Spectra (Figure (4.16a))

Comparing the simulations and the observations at 4 meter depth, it is observed that the model results for the frequency spectrum are not statistically different from the observations for most of the frequency range (95 percent confidence level for the spectral estimates based on 320 degrees of freedom (FGE90)). The simulations (Figure (4.16a) and Table (4.3)) show a considerable transfer of energy to frequencies .12 Hz and above. This range of frequencies corresponds to the region of the spectrum where linear wave theory is inadequate (Figure (4.3g) and Table (4.3)). All the prominent peaks of energy due to nonlinear wave interactions (at .12, .16 and .18 Hz in Figure (4.3)) are predicted by the WST model (Figure (4.16a)). Contrary to what is suggested by Figure (4.16a) the peak of energy at .12 Hz is not statistically different from the observations. This apparent discrepancy is due to the differences between the resolved frequencies of the WST model and FGE90.

The total band variances (Table (4.3)) are overpredicted by the WST model. The excess energy predicted by linear wave theory for the low frequency range, .06 to .10 Hz (Table (4.3)), is reduced with the introduction of the nonlinearities. However, the nonlinear wave interactions do not explain all the difference. In fact, the excess energy in the frequencies from .06 to .10 Hz is larger than the total energy in the observations (4 meter depth) for frequencies .12

Hz and above. Within the WST model formulation, overprediction of energy in the low frequency range results in an increased transfer of energy by triad interactions to the higher frequencies. The validity of the predicted transfer of energy by nonlinear wave coupling is analyzed in the Appendix B, where a simulation is done with the linear shoaling and refraction effects artificially reduced. It is observed that for levels of energy in the range .06 to .10 Hz close to those observed by FGE90 at 4 meter depth, the total band variances for frequencies .12 Hz and above compare better with FGE90 observations. The reasons for the energy discrepancies in the low frequency range could possibly be associated with the simplified bathymetry used or neglecting dissipative processes.

b. Frequency-directional Spectrum (Figure (4.15))

The frequency-directional spectrum at 4 meter depth (Figure (4.15b)) shows that the major features of the nonlinear evolution of the wave field in FGE90 are reproduced. Compared with the linear wave theory simulations (Figure (4.8)), the most obvious nonlinear effects that can be noticed in the observations of FGE90 at 4 meter depth (Figure (4.15a)) are the peaks of energy centered at .16 Hz, +6 degrees (coupling of .06 with .10 Hz), and at .18 Hz, -4 degrees (coupling of .06 with .12 Hz). Also, an enhancement of the peak of energy centered at .12 Hz, -4 degrees (self-coupling

of.06 Hz) can be observed with differences in the directional distribution of the energy. The apparent prediction of the peak of energy centered at .16 Hz by the linear version of the WST model (Figure (4.8b)) is an artifice of the value adopted for the least energetic contour.

Comparing the model simulations with FGE90 observations at 4 meter depth (Figure (4.15)), it can be concluded that: for the waves approaching the beach from the southern quadrant (negative angles), both the peak of energy at .18 Hz, the enhancement of energy at .12 Hz, and the general distribution of energy with direction compare well; for waves from the northern quadrant (positive angles), the peak of energy at .16 Hz is predicted but in a direction close to the beach normal. Also a peak of energy is evident in the simulations centered at .14 Hz, +5 degrees (this peak is discussed in the analysis of the directional spectra).

c. <u>Directional Spectra (Figures 4.16b, c and d, and Figure 4.17)</u>

The following discussion of the directional spectrum at 4 meter depth subdivides the frequency range (.05 to .19 Hz) into bands, .06-.10 Hz and .12 Hz-.19 Hz. This division is motivated by the dominance of the nonlinear effects for frequencies .12 Hz and above.

The model results for the selected frequencies .06, .07 and .10 Hz are in qualitative agreement with FGE90 observations (Figures 4.16b, c and d and Table 4.3). The

TABLE 4.3

THE NONLINEAR EVOLUTION (4 METER DEPTH). TOTAL BAND VARIANCES AND PEAK DIRECTIONS OF THE DIRECTIONAL WAVE SPECTRA AT 4 METER DEPTH, FOR FGE90 OBSERVATIONS, AND WST NONLINEAR AND LINEAR PREDICTIONS OF THE EVOLUTION OF THE SDS.

FREQ(Hz)	VARIANCES (cm^2)			PEAK DIRECTION		
	FGE90	WST	LINEAR	FGE90	WST	LINEAR
.06	19568	25257	27902	-4	-2	-2
.07	2667	3157	3477	-8	-8	-8
.10	2122	2713	3086	+10	+8	+8
.12	2621	3911	2022	-4	-3	-5
				+12	+8	+8
.14	1001	1217	895	-6	-4/-9	-3
				---	+5	+5
				+14	+12	+12
.16	689	1010	535	---	---	-4
				+6	+1/+5	+5
				+16	+14	+14
.18	821	918	422	-4	-3	-6
				+6	+6	+5
				+16	---	+16

predicted directions for the peaks of energy (Table 4.3) differ by at most 2 degrees from the observations, and are coincident with the linear predictions. The shapes of the directional spectra predicted by the model are not

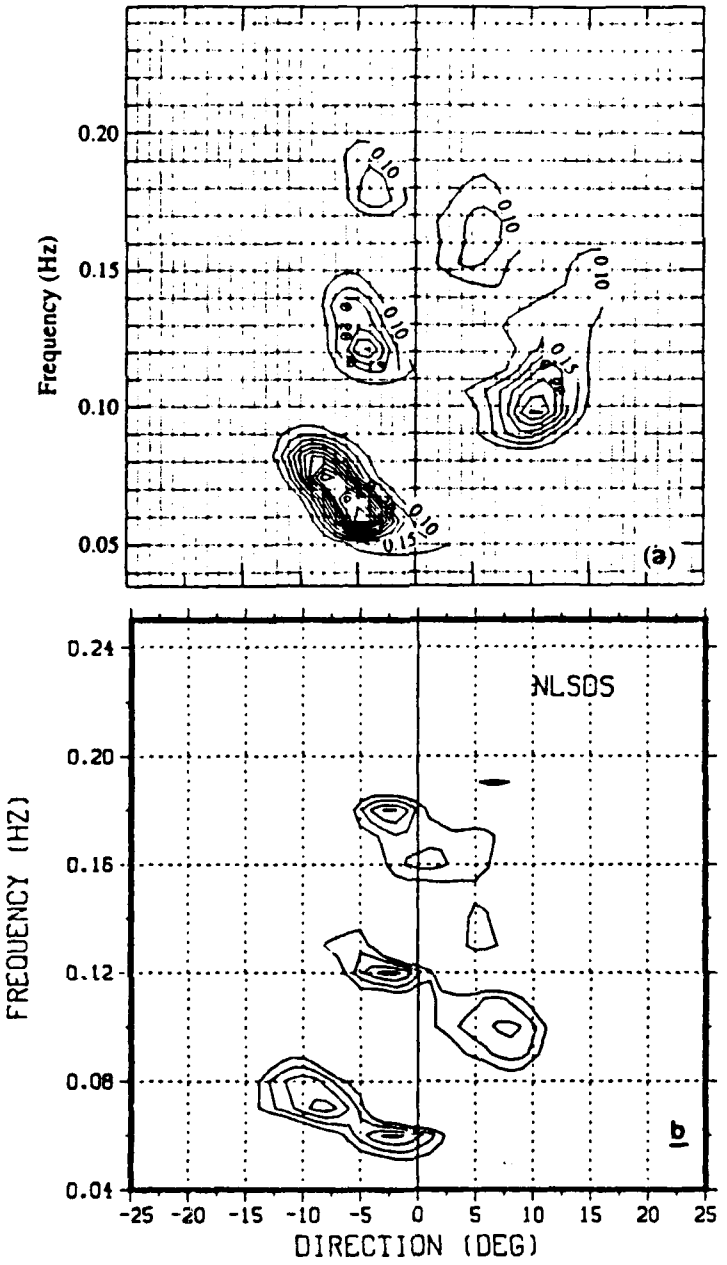

Figure 4.15 The Nonlinear Evolution of SDS Frequency-Directional From 10 to 4 Meter Depth Computed with the WST Model (b) Showing That the Major Features of the Observed Nonlinear Evolution (a) are Predicted. The Simulated Evolution of Waves Incoming from the North are Dominated by Nonlinear Interactions Between Harmonic Frequencies (.06, .12 Hz), While for Waves from the South the Most Evident Nonlinear Effect is the Peak of Energy Centered at .16 Hz. At each Frequency (Both in (a) and (b)) the Area Under the Curve is Proportional to the Autospectral Density at That Frequency. Directions are Relative to the Beach Normal. Exterior Contour for (b) Has a Value of 1.4, and the Contour Interval is .2.

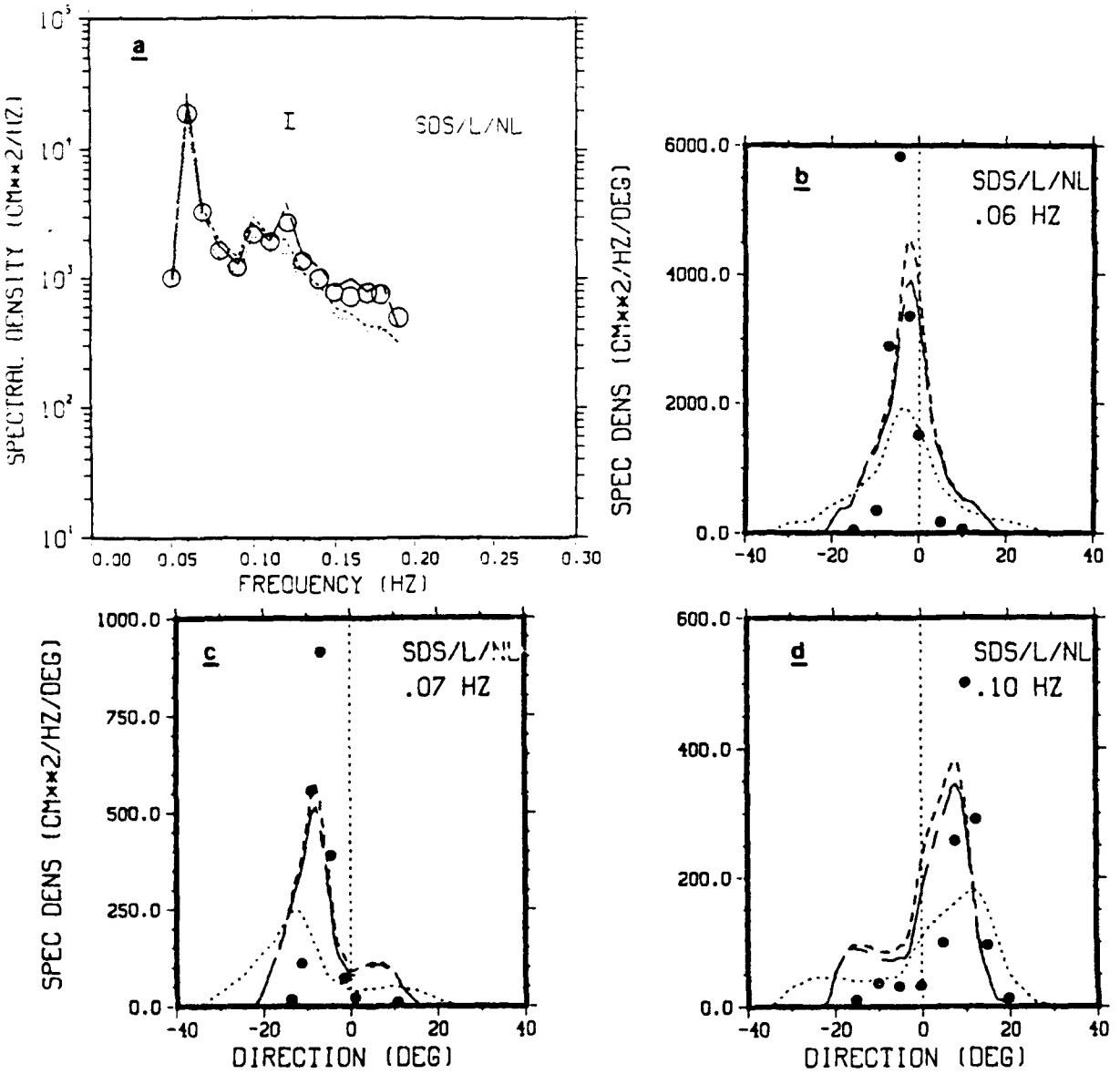

Figure 4.16 Frequency Spectrum (a) and Directional Wave Spectra (b), (c) and (d) of the SDS (Dot Line) Nonlinear (Chaindash Line) and Linear (Dash Line) Evolutions from 10 to 4 Meter Depth Predicted by the WST Model. Also Plotted are the Observations at 4 Meter Depth Dots and Circles (Diameter Equal to the 95 Percent Confidence Interval). The Nonlinear Predictions of the WST Model for the Frequency Spectra are Statistically Significant (Except for .16 Hz) When Compared with the Observations. Directions are Relative to the Beach Normal.

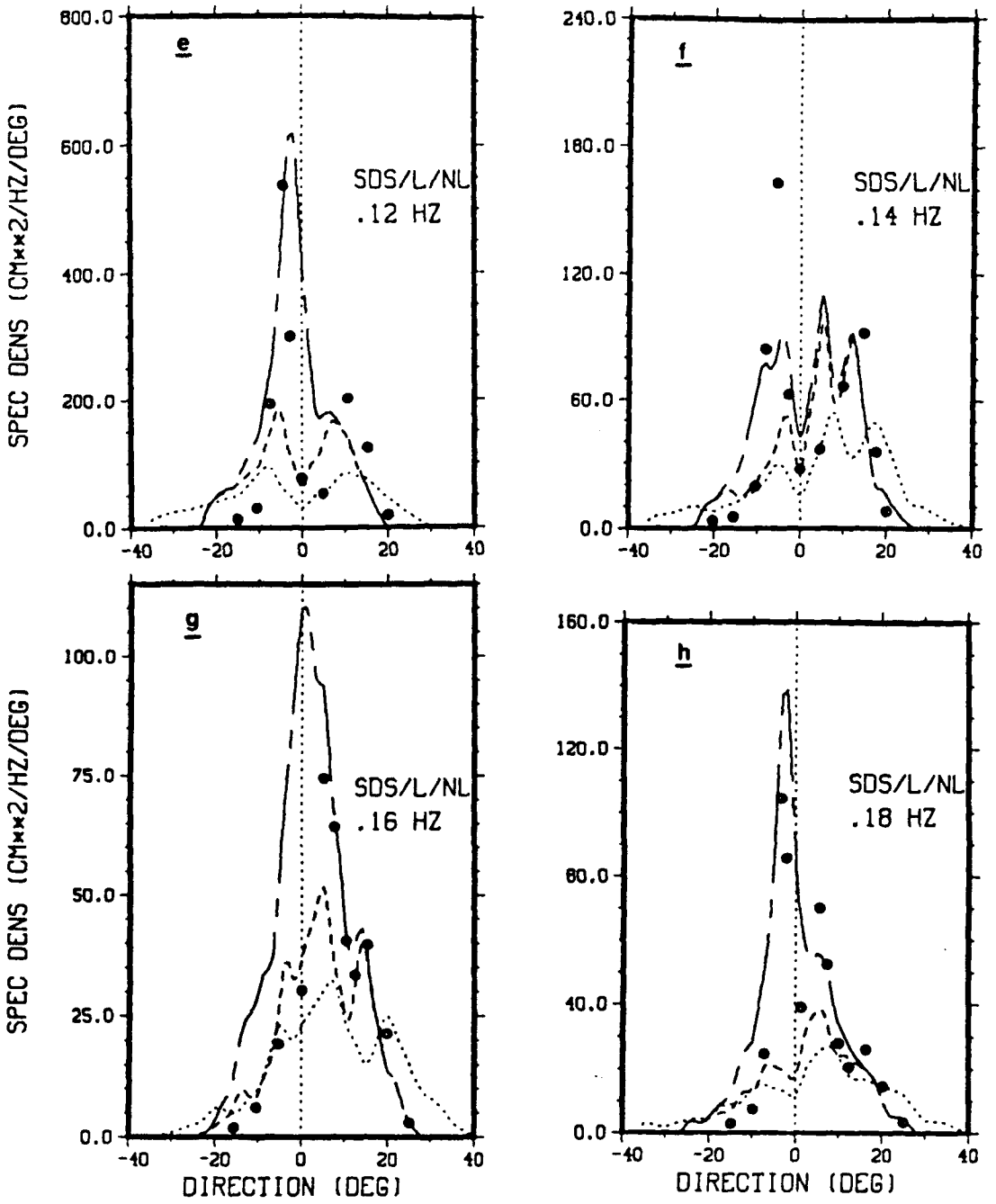

Figure 4.17 The WST Model Predictions of the Nonlinear Evolution of the SDS Directional Spectra (Chaindash Line) of Four Selected Frequencies Show That All the Observed (Dots) Peaks of Energy are Predicted (Except for .14 Hz) and in Their Approximated Directions. Also Shown are the SDS (Dot Line) and the WST Linearly Predicted Evolution of the SDS at 4 Meter (Dash Line). Directions are Relative to the Beach Normal.

significantly different from the observations (Figures 4.16b, c and d), and are close to that predicted by linear wave theory. A decreased energy content relative to the linear simulations is observed (Figures 4.16b, c and d and Table 4.3), which is consistent with the transfer of energy to higher frequencies by nonlinear interactions.

The predicted directional spectra for the frequency bands .12, .16 and .18 Hz (Figure 4.17) are also in qualitative agreement with the observations (.14 Hz will be considered later). Figure (4.17) and Table (4.3) show that the linear wave theory is inadequate to predict the directional distribution of shoaled waves whose evolution is determined by nonlinear effects. In fact, the linearly predicted directional spectrum for the bands .12, .16 and .18 Hz (Figure (4.17a, c and d)) have not only less energy than the observations, but also have different shapes. The WST model results (Figure (4.17a, c and d) and Table 4.3) show that all significant peaks of energy in FGE90 observations are predicted (the peak at .18 Hz, +16 degrees is not statistically significant). The directions of the peaks (.12, .16 and .18 Hz in Table 4.3) differ from the observations by not more than 1 degree for waves in the southern quadrant (negative angles); for waves in the northern quadrant, the directions differ from those observed in FGE90 by up to 5 degrees for the largest peak at .16 Hz. The shape of the directional spectra (Figure 4.17a, c and d) for the frequency

bands .12, .16 and .18 Hz is not significantly different from the observations in FGE90.

Contrary to the analysis of FGE90, which suggests that the reason for the increased energy at .16 Hz is the coupling of waves at ($.06\ Hz, -4^\circ$) with waves at ($.10\ Hz, +10^\circ$) via near-resonant interactions, the WST model results show that collinear interactions can explain the observed increase of energy. Recalling the observations at 10 meter depth (Figure (4.2)), there is considerable overlapping of energy at .06 and .10 Hz in the range 0 to +15 degrees. The linear predictions at 4 meter depth also overlap (Figure (4.2)). Therefore it is concluded that there are conditions for collinear coupling between .06 and .10 Hz for the full extent of the evolution between the two arrays. On the other hand, the vector wavenumber condition (equation (4.7)) can not be used to recast the direction of a peak of energy from observations at a single point. It is noted that the arrangement of the relative directions of the waves is a dynamic system in constant evolution. As an example, the application of the vector resonance condition to the coupling of the peaks of .06 and .12 Hz at 10 meter depth (Table 4.1), referred by FGE90 as having significant bicoherence (Figure 4.13), does not suggest the final collinearity of the peaks .06, .12 and .18 Hz observed in FGE90. It would be expected that the increase of energy at .16 Hz would be more probably due to resonant interactions of less energetic collinear

components as shown by the WST model results, than due to non-resonant interactions. In scaled laboratory experiments of the observational conditions in FGE90, but with a bathymetry of straight and parallel bottom contours, (Elgar et al., 1991) observed a .16 Hz directional spectrum in close agreement with the WST model predictions for shape and peak direction (Figure 4.18).

The evolution of the frequency band .14 Hz (Figure 4.17b) is the most questionable result of the model. It is observed that an extra peak is predicted in the northern quadrant (+5 degrees) relative to the observations. The .14 Hz directional spectrum at 10 meter depth (Figure (4.2)) is trimodal, evolving into a bimodal distribution of energy at 4 meter depth (Figure (4.2)). The vanishing of the peak at +5 degrees in the observations at 4 meter depth is not understood. The expected evolution of this peak is an increase of energy by transfer from .07 Hz (Figure 4.2). Alsc, the measured bicoherence (Figure (4.13)) does not suggest significant nonlinear interactions of .14 Hz that can lead to the observed loss of energy. The WST model results are, at least in principle, closer to what would be expected. In fact, they show (Figure (4.17)) the expected bimodal structure in the northern quadrant and an increase of energy by self-interactions of .07 Hz. Deficiencies of the maximum likelihood estimator in resolving a trimodal directional spectrum with two close peaks are a possible explanation for

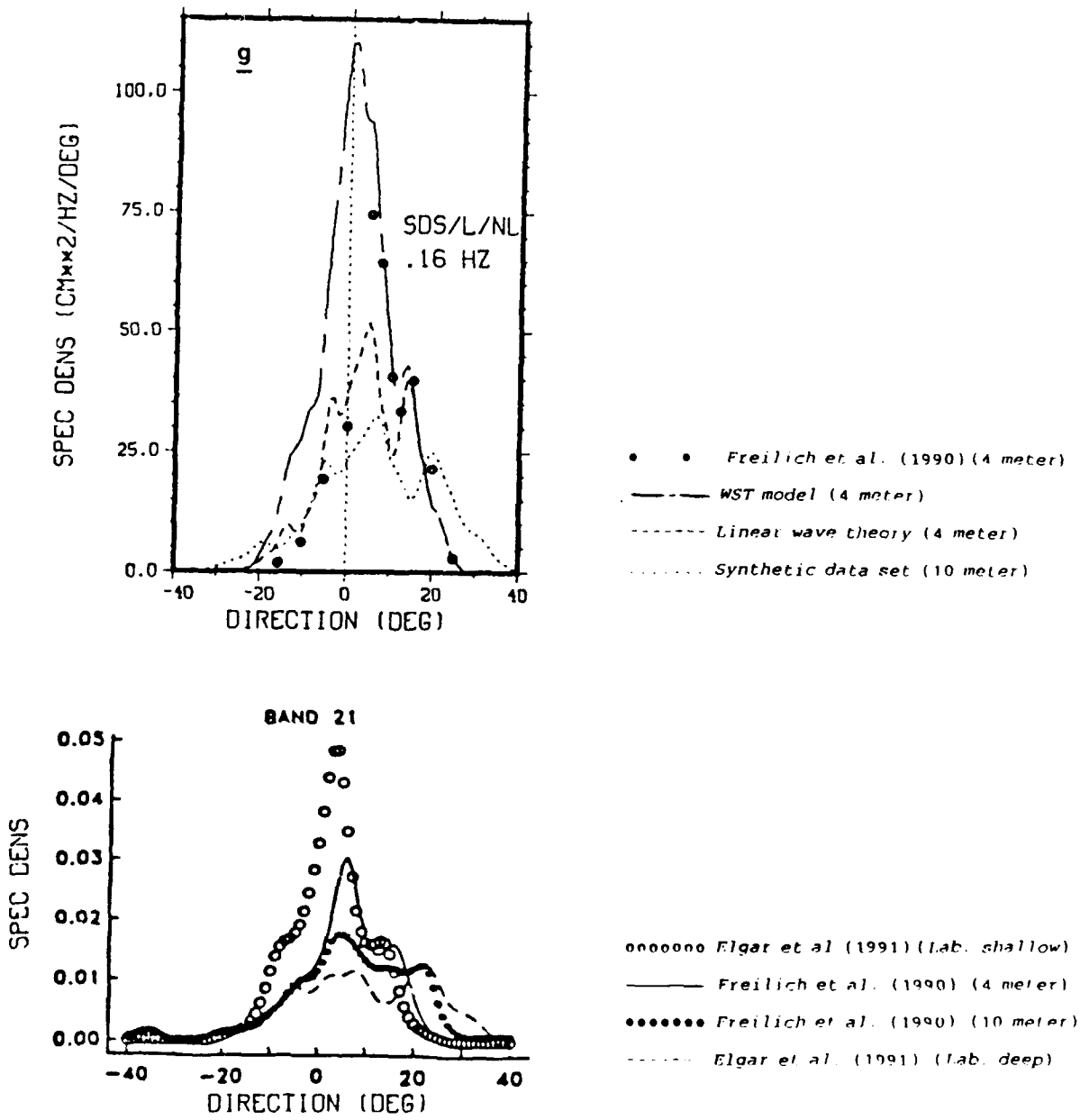

Figure 4.18 The Nonlinear Evolution of the .16 Hz Frequency Band Predicted by the WST Model (Plot (a)) is in Close Agreement with the Laboratory Observations of Elgar et al. (1991) (Plot (b)), Both for Shape and Peak Direction.

the observations in FGE90. Relative to the south quadrant (Figure 4.17), the shape of the peak of energy at -6 degrees is analyzed in detail in Appendix B. It is concluded that a directional error in the interpolated band of .08 Hz at 10 meter depth (SDS) is the reason for the predicted bimodal structure of the peak at -6 degrees.

The nonlinear simulations suggest that the WST model is, at least qualitatively, successful in predicting the nonlinear evolution of the wave field observed by FGE90. A detailed sensitivity analysis (Appendix B) concludes that the results obtained are not a consequence of fortuitous coincidences. In particular, it is noted that the nonlinear evolution of the selected frequencies is almost independent of the interpolated frequency bands (exception is .14 Hz), which further validates the agreement between model predictions and observations.

V. DISCUSSION AND CONCLUSIONS

A model was developed for the evolution of ocean frequency-directional spectra for waves propagating shoreward in shoaling waters. The model was solved numerically and tested against observations. A Hamiltonian formalism was used to derive the wave spectral transformation model (WST) to obtain a consistent approach for the problem of shallow water, weakly nonlinear, shoaling waves over mild sloping bottom. The WST model, which includes the physics of triad resonant interactions and combined linear refraction and shoaling, provides good qualitative agreement with field measurements by FGE90. Unlike existing shallow water model formulations, a random wave field collision integral formulation is used.

The criterion adopted for the definition of the collision range, $kh < .5$, is within the classic linear wave theory shallow water regime consistent with the so-called near-resonant interactions. However, the WST model is formulated in terms of the exact three-wave kinematic resonant conditions, yet the model results are in agreement with the observations.

Sensitivity analyses were conducted on the errors in the synthetic data set used to simulate the observations, on the increase in the amount of energy in the collision range, and on the assumption of a constant spectral energy density

content for a full propagation step; no significant consequences for the model results were found.

Several extensions of the model can be considered. The Boltzmann wave equation has been used in wave propagation models in the form (e.g., WAMDI group, 1988)

$$\frac{dS(f,\varphi)}{dt} = \sum Q_i(f,\varphi) \qquad (5.1)$$

The summation on the r.h.s. of (5.1) can represent separate influences, which transfer energy to, from or within the wave spectra, including atmospheric forcing, nonlinear wave interactions, bottom friction and breaking wave dissipation. Within the approximation (5.1), it is possible to include in the WST model these additional physical processes, taking advantage of existing formulations. Four-wave interactions could be possibly included by an ad-hoc formulation similar to the one used in the finite depth extension of the WAM model (WAMDI group, 1988). The immediate next step in the development of the WST model is, perhaps, the inclusion of an irregular bottom topography, for which the formulation described in Appendix A can be used.

In conclusion, the nonlinear directional wave spectral transformation model developed in this dissertation is not only operationally valid and computationally efficient, but also allows for future extensions.

APPENDIX A

ARBITRARY BOTTOM TOPOGRAPHY

Application of a piecewise ray method for propagating directional spectra over arbitrary bottom topography is developed. It is assumed that the bathymetry is described by a regular grid of soundings, and that the objective is to predict wave spectra at a single target point (Figure (A.1)). To take into account the effects of the changing bottom topography in the evolution of the wave spectra, the set of all points that are possible origins for rays reaching the final target point must be considered. This set of points, the domain of dependence, is defined using the grid of soundings to compute the limiting rays that are able to reach the target position (Figure (A.1)).

Once the domain of dependence is defined, a finer propagation grid is established with the discretization lines separated by a chosen propagation step (Figure (A.1)). The ray path in-between discretization lines is calculated by backward refraction from the grid points at line $k+1$ (k is the last known level of directional wave spectra). The method developed in Section (III.B.1) is used to compute the ray parameters. The local depth is obtained by interpolation of the original coarse grid of soundings (described below).

In most cases, the origin of the ray (level k in Figure (A.1)) is located at positions where the wave spectra are not known. Interpolation between nearby points of known wave spectra determines the wave energy to be propagated. The propagation cycle ends with the integration of the radiative transfer equation (3.3) along the calculated ray path.

The bathymetry can be interpolated by a bidimensional, cubic least squares fit. This type of approximating surface is inadequate to match a full surface, but when used in a mosaic it can give good results. The approximating surface has the form

$$\begin{aligned} P_3(xy) &= a_1 + a_2 x + a_3 y + a_4 x^2 + a_5 xy \\ &\quad + a_6 y^2 + a_7 x^3 + a_8 x^2 y + a_9 xy^2 + a_{10} y^3 \ , \end{aligned} \tag{A.1}$$

with the error at each point given by

$$\varepsilon_{ij} = h_{ij} - P_3(xy) \ . \tag{A.2}$$

Variables x and y represent the cartesian coordinates of the data points. In (A.2) h_{ij} is the observed depth. Adopting a 2-norm, the minimization of the error in a least squares sense requires that

$$\frac{\partial \varepsilon_{ij}}{\partial a_i} = 0 \ , \quad i = 1, \ldots, N_c \ . \tag{A.3}$$

where N_c represents the order of the coefficients. The set of conditions (A.3) leads to a system of equations that takes the form

$$[XY].[A] = [HXY] \ . \tag{A.4}$$

The matrix [XY] has the first row defined as

$$[N \ \sum x \ \sum y \ \sum x^2 \ \sum xy \ \sum y^2 \ \sum x^3 \ \sum x^2y \ \sum xy^2 \ \sum y^3] \tag{A.5}$$

and the following ones as

$$COEF_i \otimes [N \ \sum x \ \sum y \ \sum x^2 \ \sum xy \ \sum y^2 \ \sum x^3 \ \sum x^2y \ \sum xy^2 \ \sum y^3] \tag{A.6}$$

The operation $\otimes$ is defined as $COEF_i \otimes \sum a = \sum (a \times COEF_i)$ and $COEF$ takes by rows (r_i) the form

$$\begin{array}{lll} r_2 \rightarrow x & r_5 \rightarrow xy & r_8 \rightarrow x^2y \\ r_3 \rightarrow y & r_6 \rightarrow y^2 & r_9 \rightarrow xy^2 \\ r_4 \rightarrow x^2 & r_7 \rightarrow x^3 & r_{10} \rightarrow y^3 \end{array} \tag{A.7}$$

The column vector $[HXY]$ is given by rows as $[HXY] = COEF \otimes \sum h$. For this vector $COEF$ is for row one unitary, and for the other rows defined as in (A.7). The column vector $[A]$ contains the a_i coefficients of $P_3(xy)$ (equation (A.1)).

The important point to note is that the coefficient matrix $[XY]$ can be made constant for the entire domain of integration if a local system of coordinates is adopted. This reduces the computational effort for interpolating the bathymetry, because a decomposition of $[XY]$ to solve (A.4) needs to be calculated only once.

The interpolation of the wave spectral energy at each level does not pose difficulties. The separation of grid points is necessarily small and the bottom is mild sloping. The wave spectra at nearby points are not expected to vary significantly. A linear interpolation can be considered, which is consistent with the concept of the domain of dependence. It is noted that, contrary to existing methods (deep water applications), there is no need for interpolating the wave spectra also in direction, which is a significant advantage.

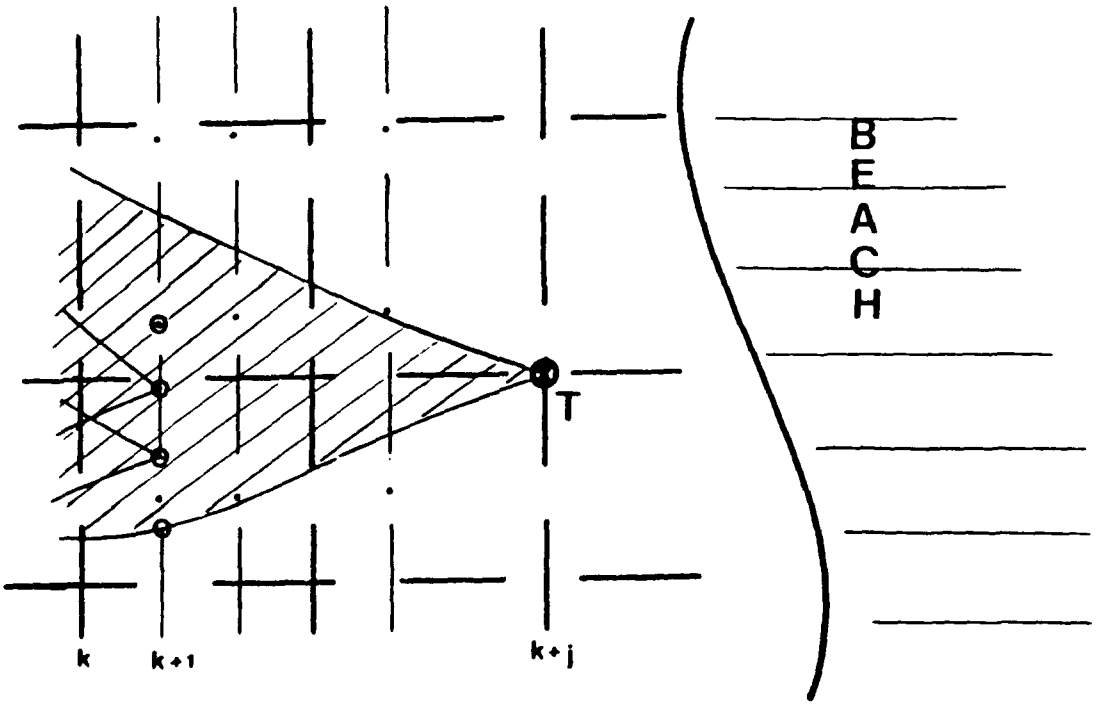

Figure A.1 The Grid of Soundings (Longdash Line) is Used to Determine the Domain of Dependence (Shaded Area) Enclosed by the Limiting Rays (Solid Line). The Limiting Rays are Computed by Backward Refraction from the Target Point (T). The Stepwise Ray Path (Dash Line) is Computed in a Finer Propagation Grid (Dashdot Line).

APPENDIX B

SENSITIVITY ANALYSIS

The sensitivity analysis is divided in two parts. The first serves to clarify performance characteristics of the WST model through simulations with simple initial conditions; the second analyzes the dependence of the simulated evolution of FGE90 wave field (Section IV.C.4) on approximations adopted in the WST model formulation, on errors in the synthetic data set, and on the simplified bathymetry. Within the collision integral formulation for the triad resonant interactions in an anisotropic spectra, quantification of errors is not possible. An alternative is to estimate the importance of errors through model simulations.

A. PERFORMANCE CHARACTERISTICS OF THE WST MODEL

The simulations in these section use the WST model to evolve simplified directional wave spectra over FGE90 bathymetry of straight and parallel bottom contours, for 246 meter from 10 to 4 meter depth.

1. Linear Refraction and Triad Resonant Interactions (Figures (B.1) and (B.2))

The objective is to appreciate the importance of linear refraction on the nonlinear transfer of energy by collinear triad interactions, and how nonlinear transfer of energy can distort the evolution of the wave field. To study

the importance of refraction for triad resonant interactions, two peaks of energy corresponding to waves at frequencies .06 Hz and .10 Hz are used to initialize the WST model (Figure (B.1, Plot 4A)). Because there is no overlapping of the directional wave spectra of the bands .06 and .10 Hz at 10 meter depth (Figure (B.1)), the first impression is that no transfer of energy by collinear triad interactions will occur. However, increased refraction effects for .06 Hz lead to the overlapping of the two directional wave spectra (.06 and .10 Hz) somewhere along the propagation from 10 to 4 meter depth. Collinear triad interactions become possible, and nonlinear transfer of energy occurs by the time the waves reach 4 meter depth (Figure (B.1, Plot 4RA)).

On the other hand, nonlinear transfer of energy by triad resonant interactions can cause apparent negative refraction. To simulate this effect of energy refracted away from the beach normal, the WST model is initialized with three peaks of energy at .06, .10 and .16 Hz (Figure (B.2, Plot 3A)). Linear shoaling and refraction of band .16 Hz directional spectrum initially centered on beach normal results in a modification of the spectral variance, but still centered on beach normal (Figure (B2, Plot 3LA)). The effects of combined linear refraction and shoaling with collinear triad interactions (coupling (.06, .10 Hz)) (Figure (B.2, Plot 3NA)) is to modify the direction of the peak of energy at .16

Hz (4 meter depth), which in case 3NA (Figure (B.2)) contradicts the expected effects of refraction.

It is concluded that the nonlinear evolution of the ocean wave spectra by refraction and collinear triad interactions has to be thought in terms of their combined effects along a propagation path, and that single point observations can not be used to estimate the nonlinear evolution of the wave field.

2. **Errors in the Direction of a Peak of Energy (Figure (B.3))**

The sensitivity of the WST model results to errors in the direction of a peak of energy involved in triad resonant interactions is considered. Two different relative orientations of peaks of energy at frequencies, .06 and .08 Hz are used to initialize the WST model (Figure (B.3, Plots 1A and 1B)). The directional spectra for .14 Hz (resultant of the coupling (.06, .08 Hz)) is initially set to zero. The effect of shifting the less energetic peak (.08 Hz) by 3 degrees (Figure (B.2, Plots 1A and 1B)) results in a significant change in the amount of nonlinearly transferred energy and direction of the peak. It is noted that interchanging the frequencies of the two initial peaks reduces the resulting change both in energy and direction. The WST model is sensitive to errors in the direction of peaks of energy because collinear triad resonant interactions are considered.

3. Errors in the Peakedness of the Directional Spectra (Figure (B.4))

The dependence of the nonlinearly transferred energy by collinear triad interactions on the peakedness of interacting components is analyzed. Two initial spectral conditions (Figure (B.3, Plots 2A and 2B)), differing in the peakedness of one of the interacting spectral components (.08 Hz) by about 30 percent, are considered. Normal incidence is used to negate refraction in order to isolate the nonlinear effects. The directional spectra of the nonlinearly transferred energy by the coupling (.06, .08 Hz) (Figure (B.3, Plots 2AA and 2BB)) show a significant increase in the total variance for the condition of initial increased peakedness (Figure (B.3, Plot 2B)). About 20 percent more energy is transferred for the more-peaked spectrum. It is noted that for components initialy at normal incidence to the beach, as in Figure (B.3), there is no significant difference in the 4 meter wave spectra if the frequency of the interacting spectral components is interchanged. However, for waves incident at an angle to the beach, the amount and direction of the nonlinearly transferred energy is strongly dependent on the relative frequencies of the coupled components (recall Section A.1, for the first case study).

B. ERRORS IN THE PREDICTED EVOLUTION OF FGE90 WAVE FIELD

1. Errors in the Synthetic Data Set

To investigate the errors in using the synthetic data set to initialize the WST model, it is assumed that the seven selected frequencies of FGE90 were correctly duplicated in the digitizing process. Within this assumption, the importance of errors in the directional spectra of the interpolated frequencies can be examined by initializing the WST model with a reduced wave spectrum comprised only of the selected frequency bands presented in FGE90. In the following analysis, reference to the full spectrum (FSPEC), corresponds to the SDS, and the reduced spectrum (RSPEC) refers to the frequency directional spectrum described by setting to zero the energy content of the interpolated frequency bands (.05, .08, .09, .11, .13, .15, .17 and .19 Hz).

The WST model predictions of the directional spectra at 4 meter depth, using as input the FSPEC are shown in Figures (B.5) and (B.6). In Table (B.1), total band variances for the selected frequencies are listed. It is concluded from Figures (B.5) and (B.6) and Table (B.1), that the largest error in the nonlinear evolution of SDS due to the interpolated frequency bands can occur at .14 Hz. In fact, for this frequency band, the RSPEC simulation is close to the FSPEC linear prediction, with about 85 percent of the energy nonlinearly transferred to .14 Hz resulting from coupling of interpolated frequencies (Table (B.1)). For the other selected

TABLE B.1

ERRORS IN THE SYNTHETIC DATA SET. TOTAL BAND VARIANCES OF THE DIRECTIONAL WAVE SPECTRA AT 4 METER DEPTH PREDICTED BY THE WST MODEL USING AS INPUT THE SDS (FSPEC), ONLY THE SELECTED FREQUENCIES OF FGE90 (RSPEC), THE SELECTED FREQUENCIES ADDED WITH THE INTERPOLATED BAND .08 HZ (RSPEC+.08), AND THE SELECTED FREQUENCIES TOGETHER WITH THE INTERPOLATED FREQUENCY BANDS OF .05 AND .09 (RSPEC+.05&.09). THE PERCENTAGES (% NL TRSF) CORRESPOND TO THE CHANGE OF NONLINEARLY TRANSFERRED ENERGY IN REDUCED SPECTRA SIMULATIONS (RSPEC+...) RELATIVELY TO THE SDS (FSPEC) SIMULATIONS.

FREQ (Hz)	VARIANCES (cm^2)				PEAK DIRECTION			
	FSPEC	RSPEC	+.08	+.05 &.09	FSPEC	RSPEC	+.08	+.05 &.09
.06	25257	25519	25432	25410	---	10	7	6
.07	3157	3201	3181	3185	---	16	7	9
.10	2713	2766	2751	2743	---	17	10	7
.12	3911	3953	3938	3942	---	2	1	2
.14	1217	943	1211	950	---	85	2	83
.16	1010	958	974	986	---	12	8	5
.18	918	844	878	853	---	17	8	15

frequency bands, the differences between the RSPEC and FSPEC simulations are minor. The main conclusion of the RSPEC simulation is that, with the exception of .14 Hz, more than 80 percent of the nonlinear evolution of the selected frequency

AD-A245 727 NONLINEAR TRANSFORMATION OF DIRECTIONAL WAVE SPECTRA IN SHALLOW WATER(U) NAVAL POSTGRADUATE SCHOOL MONTEREY CA M A ABREU SEP 91 2/2

UNCLASSIFIED NL

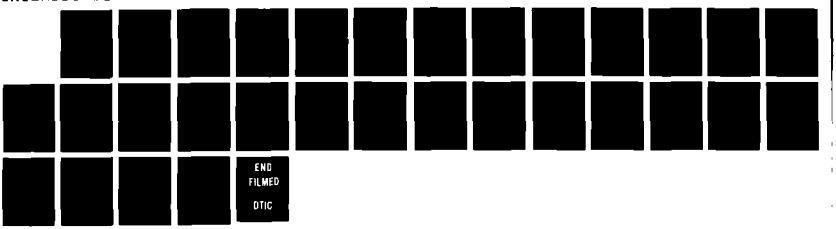

The anomalous result of the predicted evolution of the frequency band .14 Hz (SDS) is reexamined here in terms of the errors considered in Section A. As concluded from the reduced spectral simulations, where only selected frequencies are taken as input for the WST model, the band .14 Hz has a nonlinear evolution dominated by the coupling (.06, .08 Hz). To recreate a possible error in the directional distribution of energy at the interpolated band .08 Hz, the directional spectra at this frequency was shifted 4 degrees to the north, and a simulation was performed. As can be observed (Figure (B.11)), the peak of energy in the south sector (at about -4 degrees) has increased in energy relative to the original simulation (about 15 percent extra energy), with the direction of the main peak unchanged. Recalling the effects of an error in the peakedness of the energy distribution (Figure (B.4)), it is possible that a further correction in the spreading of energy in the .08 Hz band would make the results closer to FGE90 observations. Relative to the south sector of .14 Hz, several tests were performed, and no reasonable hypothesis was found to justify the differences in observations and/or the predictions.

2. The Increased Energy in the Collision Range

The nonlinear evolution of SDS predicted by the WST model (Table (4.3)), results in an excess of energy in the selected frequency bands. Under the conditions of the present study, besides resonant triad interactions only, the combined

effects of shoaling and refraction can be a possible source of the energy increase. It is recalled that the collision integral, while promoting the transfer of energy among Fourier components, conserves the energy of the system. To get an appreciation of what can be expected if the energy in the frequency bands comprising the collision range were lowered, a reducing parameter of the combined effects of shoaling and refraction was introduced into the model formulation; the direction of the spectral components due to refraction are, however, unchanged.

To establish the dependence of the reducing parameter on frequency, the percent increase of energy by shoaling and refraction for each of the seven selected bands was calculated (Figure (B.12)). The variation of energy with frequency is almost linear, and therefore, linear dependence on frequency is adopted for the reducing parameter.

Assuming that the combined effects of shoaling (k_s) and refraction (k_r) are constant ($(k_s k_r)^2 = const.$) across the full domain of propagation, it can be deduced that the total energy content of a frequency band (S) after m propagation steps is given by

$$S = S_0 (1 - (K_s K_r)^2 (\alpha - 1)^m), \qquad (B.1)$$

where S_0 represents the energy at the input and α is the per-step reducing parameter. Taking into consideration the amount of energy at the frequency band .06 Hz, both for a

linear and nonlinear simulations, it is concluded that a value of 0.3 for the reducing parameter (α) results in a total band variance for .06 Hz after propagation close to that measured by FGE90. The two points ($\alpha = .3, f = .06$) and ($\alpha = .0, f = .19$ Hz) define the line containing the values for the reducing parameter (not shown).

The consideration of a reducing parameter for the combined effects of refraction and shoaling, as explained above, represents an "ad-hoc" method to appreciate the dependence of the nonlinearly transferred energy on the amount of energy within the collision range. The results of this simulation should not be quantitatively compared to FGE90 observations.

The simulations corresponding to reduced linear and nonlinear effects are contained in Table (B.2), together with the original nonlinear simulation and FGE90 observations. A significant decrease in the nonlinearly transferred energy to the high frequency range occurs as a result of the reduced variance in the collision range for the WST model. However, the observed reduction does not result in the invalidation of the model simulations. The obtained levels of energy for the high frequency range (.12 Hz and above) are not unreasonable and still represent a significant transfer of energy by triad resonant interactions. The directional spectra of the seven selected frequencies, for the simulations with reduced and

TABLE B.2

THE INCREASED ENERGY IN THE COLLISION RANGE. TOTAL BAND VARIANCES OF THE DIRECTIONAL WAVE SPECTRA AT 4 METER DEPTH FOR THE FGE90 OBSERVATIONS, AND WST MODEL PREDICTIONS FULLY ACCOUNTING FOR THE SHOALING AND REFRACTION EFFECTS (WSTLF FOR LINEAR EVOLUTION AND WSTNLF FOR NONLINEAR) AND WITH PARAMETRICALLY REDUCED SHOALING AND REFRACTION EFFECTS (WSTLR FOR LINEAR EVOLUTION AND WSTNLR FOR NONLINEAR).

FREQ (Hz)	VARIANCES (cm^2)				
	FGE90	WST	WST(RED)	LINEAR	LINEAR(RED)
.06	19658	25257	19801	27902	21576
.07	2667	3157	2537	3477	2758
.10	2122	2713	2366	3086	2640
.12	2621	3911	3171	2023	1813
.14	1001	1217	1075	895	836
.16	689	1010	872	535	517
.18	821	918	743	422	417

theoretical linear effects (not shown), only differ in the amount of energy at corresponding directional bins.

3. The Constant Spectral Energy Density Approximation

The spatial integration of the collision term (Section II.B.2) assumes that the spectral energy density content of interacting components has a constant value during the propagation step. As previously stated, the propagation step is necessarily small because of requirements of collinearity between nonlinearly interacting spectral components. However,

the smallness of the propagation step does not mean that the error introduced by the constant spectral energy density content assumption is also small. An estimate of the influence of the approximation can be obtained from simulations using different propagation steps. The smaller the propagation step adopted in the simulation, the closer the model approximates a the constant change in the spectral energy density of the components. The grid steps adopted for this study are 3 and 6 meters, besides the basic 1 meter. Collinearity between nonlinearly coupled components is not compromised for the 6 meter propagation step.

The results of the nonlinear simulations at different propagation steps are contained in Table (B.3). As can be concluded, the variations of energy nonlinearly transferred are minor, a maximum difference between the grid steps 1 and 6 meter occurs at .18 Hz and is about 5 percent. It must be noted that a change in the grid step results in a variation in the amount of energy nonlinearly transferred, because it determines a change in the interaction distance of the spectral components. As will be observed in the next section, this effect has significant consequences for the results of the simulations.

4. The Bathymetry

Nonlinear simulations of the spatial evolution of frequency-directional wave spectra are considerably dependent on the bathymetry. First-order effects of shoaling and

TABLE B.3

CONSTANT SPECTRAL ENERGY DENSITY APPROXIMATION. TOTAL BAND VARIANCES OF THE PREDICTED DIRECTIONAL WAVE SPECTRA OF THE SDS AT 4 METER DEPTH (WST MODEL) FOR GRID STEP SIZES OF 1, 3 AND 6 METER.

FREQ (Hz)	VARIANCES (cm^2)		
	1 METER	3 METER	6 METER
.06	25257	25274	25298
.07	3157	3158	3160
.10	2713	2716	2715
.12	3911	3911	3894
.14	1217	1214	1211
.16	1010	1005	1006
.18	918	898	889

refraction are only dependent on the bathymetric conditions adopted, and can lead to significant errors in the energy content and in the direction of the spectral components. The definition of the collision range (Section (IV.C.3.a.2)) is based on the local depth and determines the interaction distance of coupled components, an important factor in the amount of nonlinearly transferred energy.

The present study considered the actual bathymetry approximated by a linear least squares fit of the tide-reduced soundings (FGE90) (Figure (4.28)). To study the dependence of the model results on the bathymetry adopted, variations of the basic linear least squares approximation was considered.

These alternative conditions correspond to accounting for the different spacing between the bathymetrics (Figure (4.4)), and to rotations of the beach normal.

The interest in including different spacing between bathymetrics is to estimate the amount of energy transferred as a function of the interaction distance of nonlinearly coupled components. To simulate the different spacing between the bathymetrics of the experimental site, seven discretization lines were considered. The distances between two consecutive intersecting points of the discretization lines with the bathymetrics was calculated, and their average was taken as representative of the actual spacing. The resulting bathymetry (BT2) (Figure (B.13)), closely follows the linear least squares fit of FGE90 (BT1). In fact, as can be concluded from the variances band listed in Table (B.4), the linear evolution of SDS using this alternative bathymetry (BT2) and the originally adopted bathymetry (BT1) are similar. The most evident difference in the nonlinear simulation for the alternative bathymetry (BT2) relative to the original results (BT1) is the increased energy at .18 Hz (Table (B.4)). This variation is a consequence of the increased interaction distance for the pair (.06, .12 Hz) (35 meter for (BT2) and 25 meter for (BT1)). For the other frequency bands there are no significant changes in the interaction distance. Directional spectra of the selected frequency bands for the (BT2) conditions (not shown) are not different from the directional

spectra obtained with FGE90 linear least squares fit of the bathymetry, except for the increase of energy at .18 Hz.

To simulate an error in the orientation of the beach normal, the directional spectra of all frequency bands of SDS (.05 to .19 Hz) were rotated 4 degrees to the south, that is, the zero of the original spectra is assigned to -4 degrees. The spatial dependence of the depth is maintained as defined in FGE90. The bathymetric conditions (BT3) with a different direction of the beach normal provides insight into refractive effects on the nonlinear evolution of the SDS. The different relative directions of the spectral components can change the pairs of interacting components, and lead either to a decrease or to an increase of the transfer of energy. The total band variances for the (BT3) nonlinear simulation (Table (B.4)) show that the model results are not sensitive to the changes introduced. A small reduction of the total band variances can be observed. It is noted that the working range of the directions extends from -35 to +40 degrees, and that the rotation of the wave field 4 degrees to south suppresses the energy in the original bins from -35 to -32 degrees. This artificial reduction of energy affects all bands of frequencies except .16 Hz. The consequences of the rotation of the beach normal are more evident in the directional spectra of the selected frequencies (Figure (B.14)). It can be observed, that the peaks of energy have a different orientation (maximum differences of 2 degrees), and also small

changes in the energy levels (increases at the peaks of .12, .16 and .18 Hz). It is noted that the directions of the (BT3) simulations (rotated beach normal) in Figure (B.14) are referenced to the original beach normal of FGE90. The small changes in the energy levels are a consequence of different couplings relatively to the original simulation ((BT1) bathymetry), imposed by different refraction of the spectral components.

TABLE B.4

BATHYMETRY EFFECTS. TOTAL BAND VARIANCES OF THE PREDICTED DIRECTIONAL WAVE SPECTRA OF THE SDS AT 4 METER DEPTH (WST MODEL LINEAR AND NONLINEAR) FOR THE PLANAR BATHYMETRY OF FGE90 (B1), FOR THE BATHYMETRY WITH VARIABLE SPACING BETWEEN THE BATHYMETRICS (B2), AND FOR A REORIENTED BEACH NORMAL (B3).

FREQ(Hz)	VARIANCES (cm^2)					
	NONLINEAR			LINEAR		
	(BT1)	(BT2)	(BT3)	(BT1)	(BT2)	(BT3)
.06	25257	25085	25053	27902	27905	27685
.07	3157	3137	3102	3477	3478	3419
.10	2713	2687	2695	3086	3087	3069
.12	3911	3913	3858	2023	2023	1978
.14	1217	1234	1205	895	895	885
.16	1010	1038	1012	535	535	537
.18	918	1054	911	422	422	417

The results obtained with the two alternative bathymetries, with changed spacing between the bathymetrics (BT2) and with a reoriented beach normal (BT3), show that the WST model results are more sensitive to variations in the interaction distance of coupled spectral components than to changes in the refraction effects, a conclusion at least valid for this study. However, for experimental conditions involving wave spectra with increased peakedness, the refractive effects would be of increased importance.

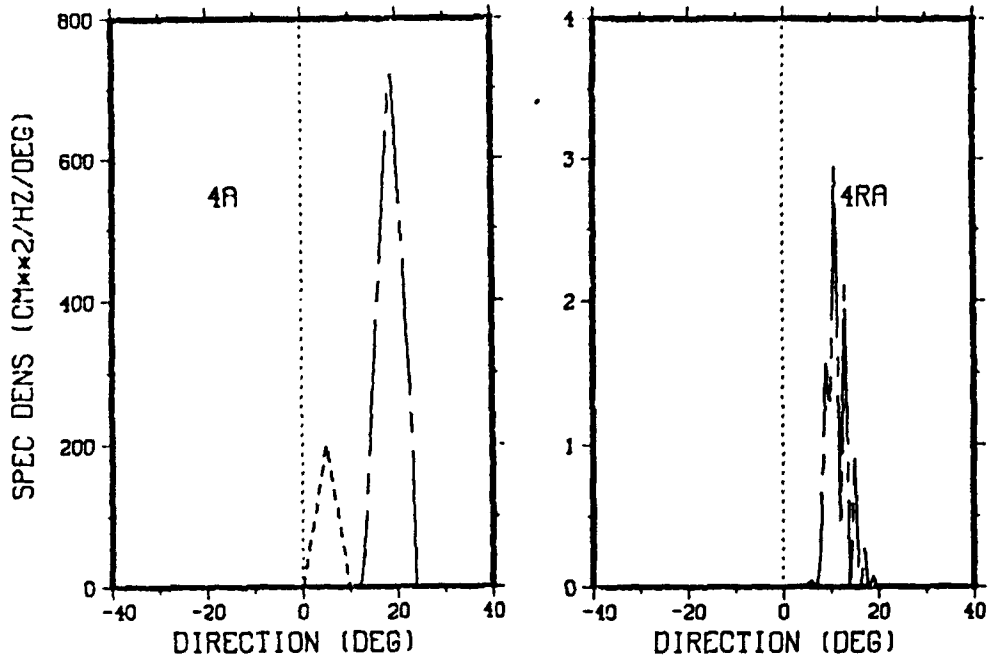

Figure B.1 The Propagation of Nonoverlapping Directional Wave Spectra (Plot (4a) for .06 Hz (Chaindash Line) and .10 Hz (Dash Line)) Under the Effects of Linear Refraction Can Lead to Unexpected Transfers of Energy by Collinear Triad Interactions.

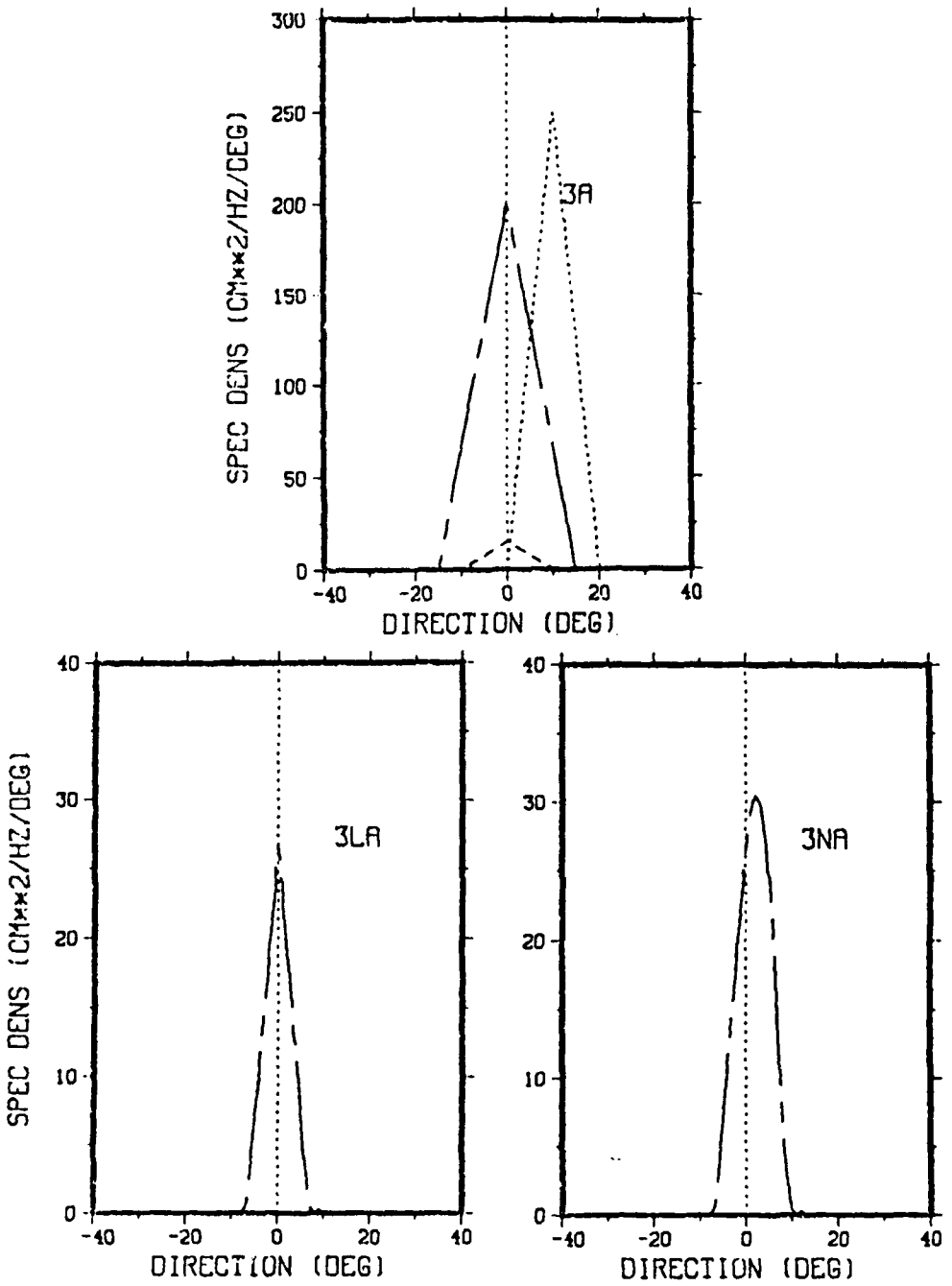

Figure B.2 Nonlinear Transfer of Energy by Collinear Triad Interactions (.06 (Dot Line), .10 (Chaindash Line) and .16 Hz (Dash Line), Plot 3A) Can Induce Effects of Negative Refraction with Energy Refracted Away From the Beach Normal. Plot 3LA Represents the Linear Evolution of .16 Hz and Plot 3NA the Nonlinear Evolution.

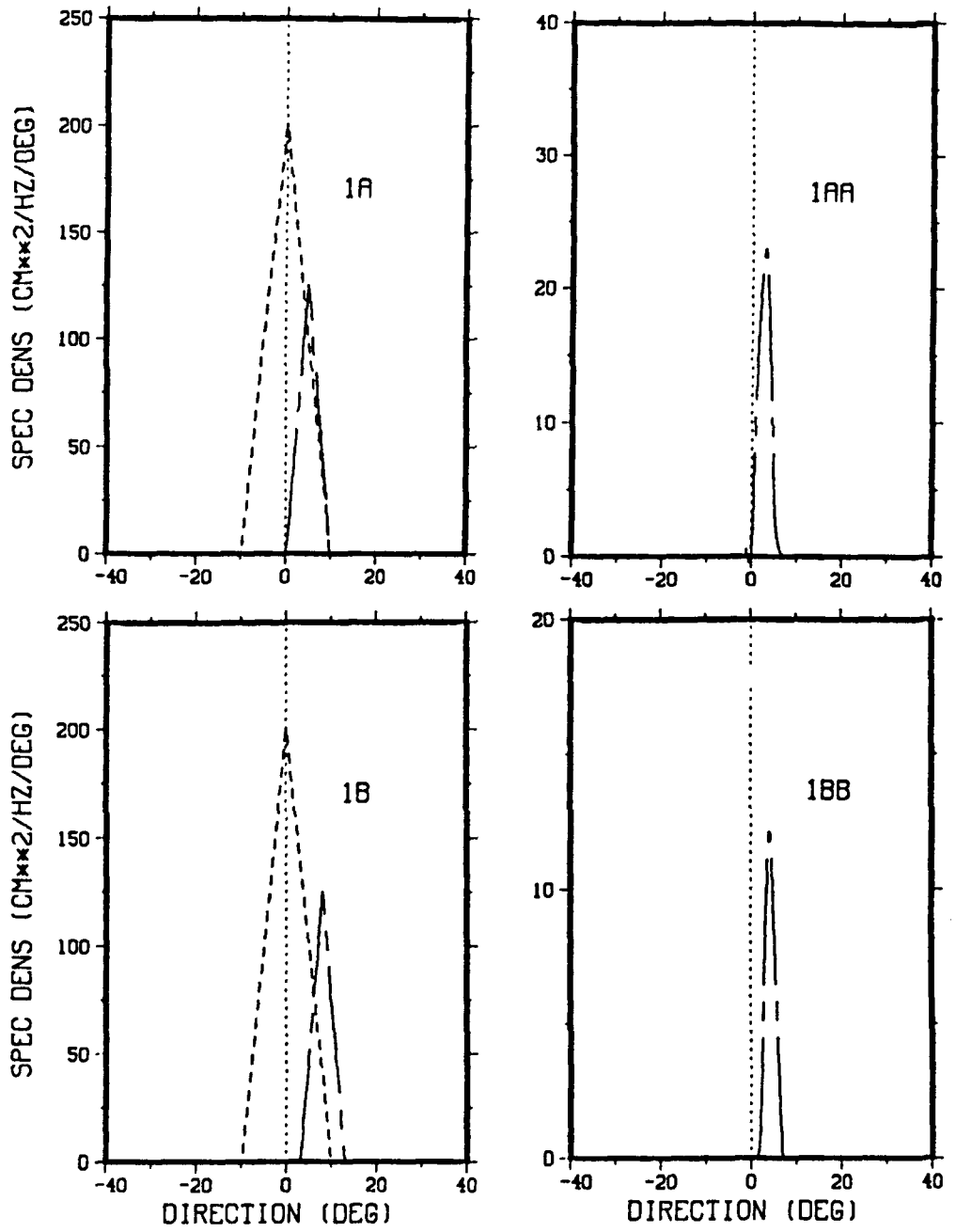

Figure B.3 For a Fixed Distribution of Energy at Two Interacting Frequency Bands, an Error in the Peak Direction at the Input (Plot 1A and 1B) Can Result in a Considerable Change in the Direction and Amount of Nonlinearly Transferred Energy (Plots 1AA and 1BB).

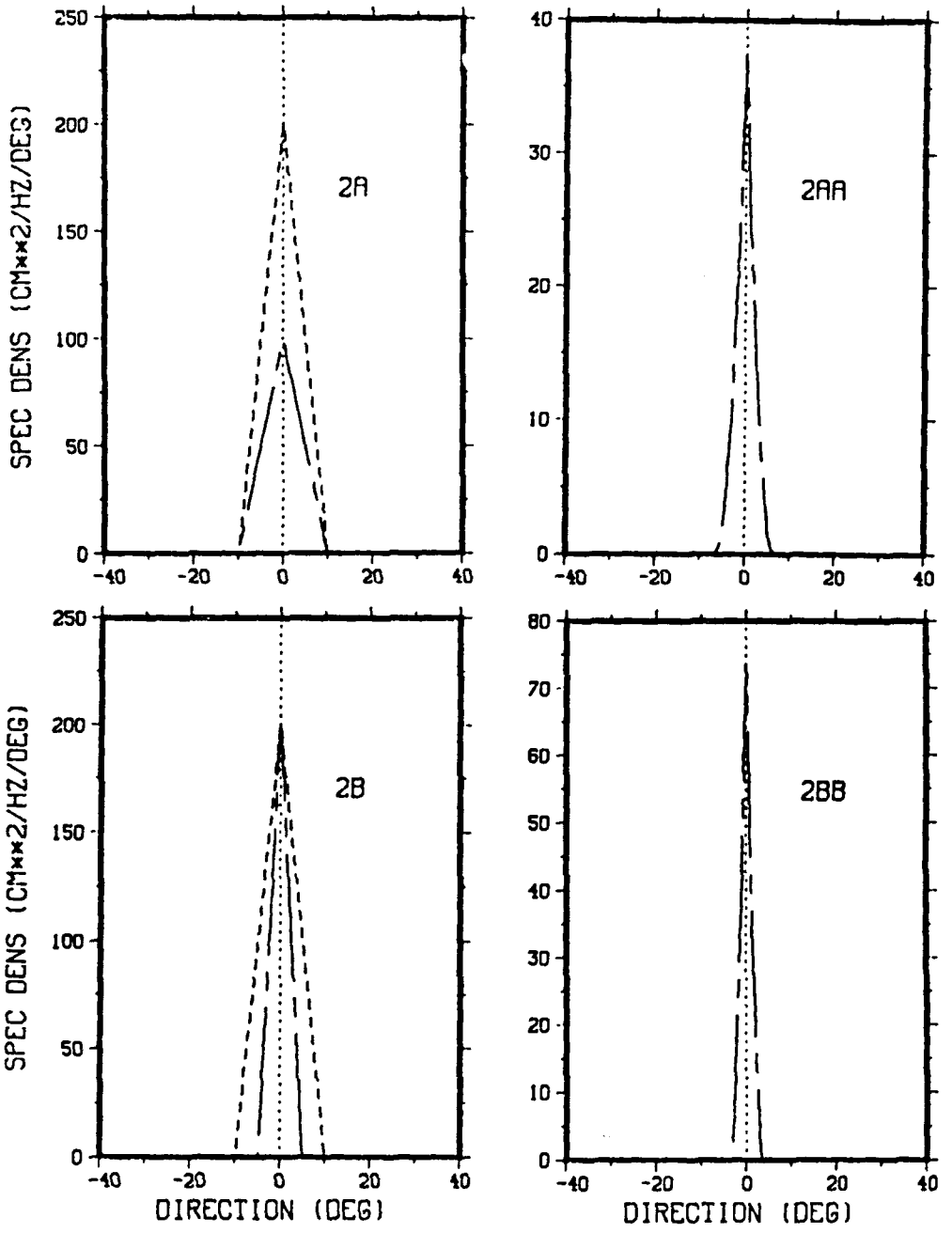

Figure B.4 An Error in the Peakedness of the Distribution of a Fixed Amount of Energy at the Input of the WST Model (Plots 2A and 2B), Can Result in a Significant Change in the Amount and Peakedness of the Nonlinearly Transferred Energy.

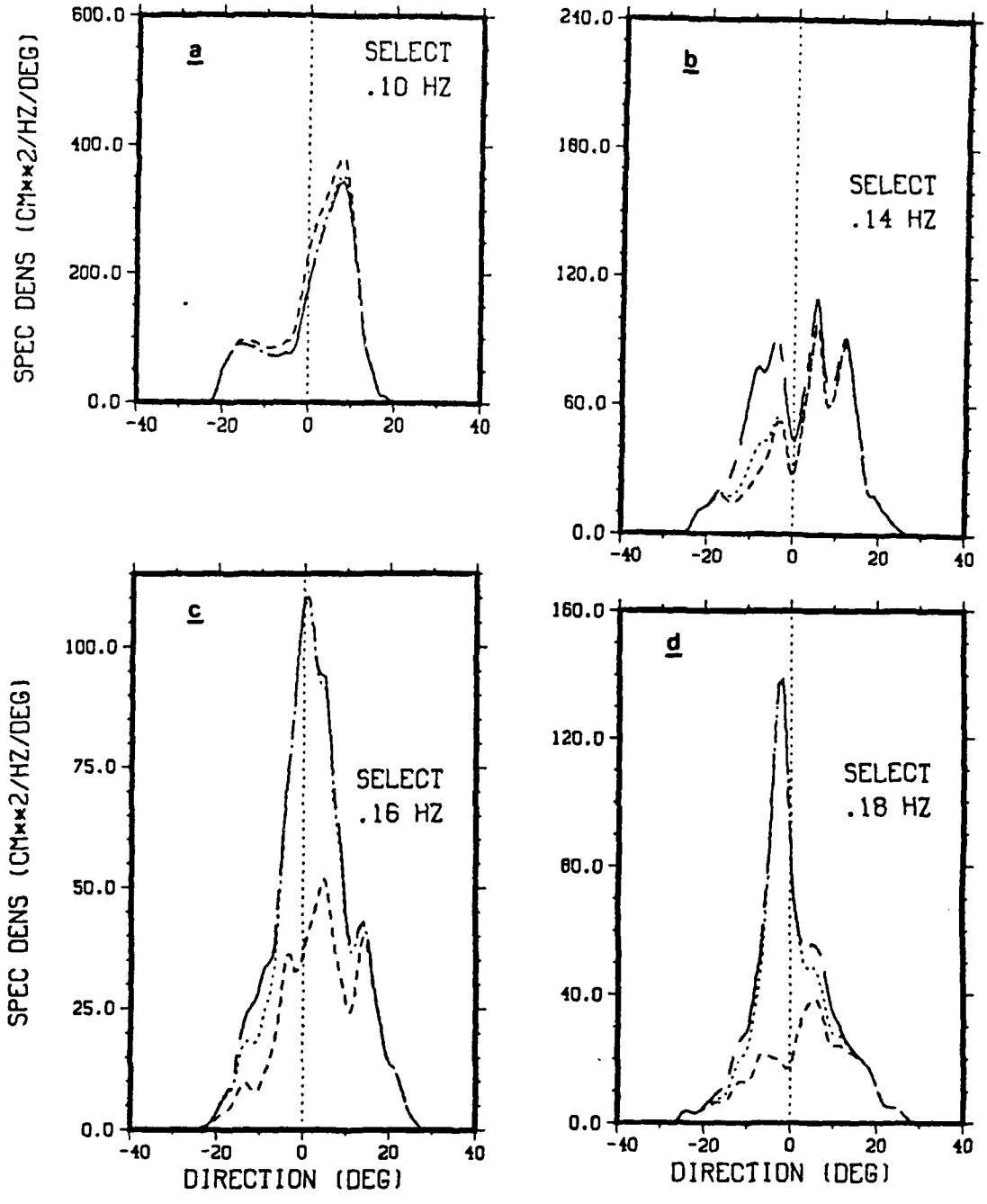

Figure B.5 WST Model Predictions of the Directional Spectra at 4 Meter Depth Using as Input the Digitized Form of Only the Seven Selected Frequency Bands of FGE90 (Dot Line) and the Evolution Predicted for the SDS (Chaindash Line) are Shown to be Similar, Except for the Frequency Band .14 Hz That Shows a Final Result Closer to the Linearly Predicted Evolution (Dash Line) of SDS.

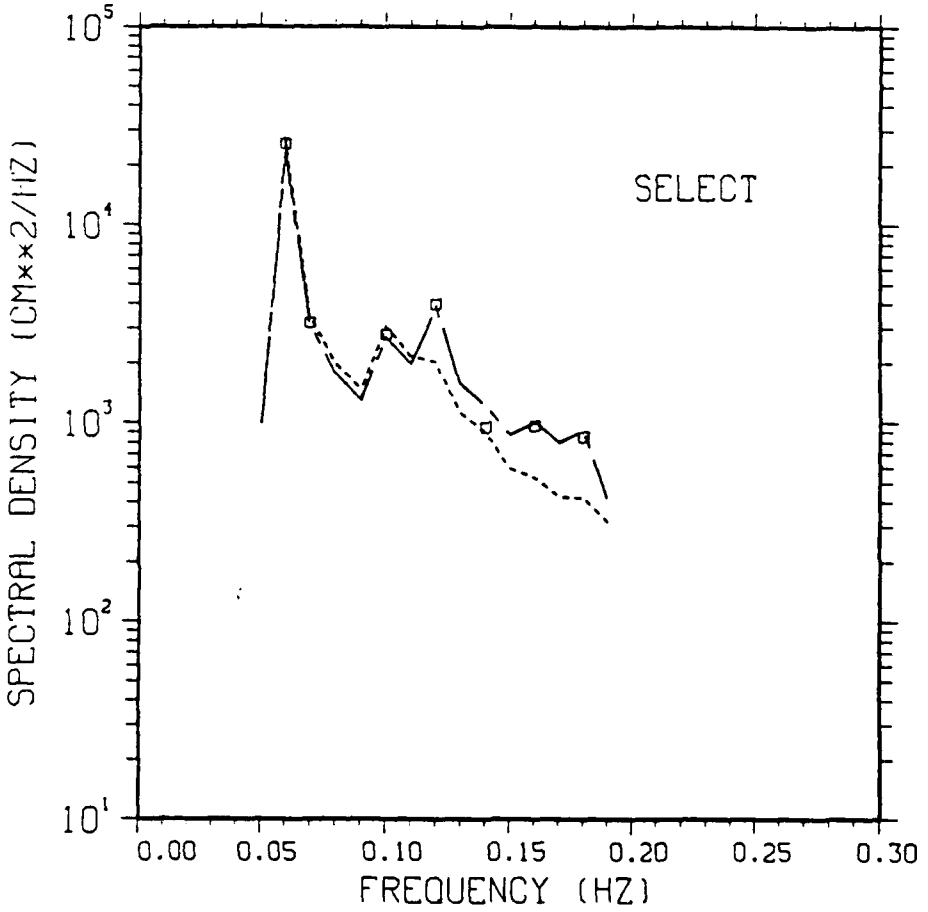

Figure B.6 The Nonlinear Predictions of the Frequency Spectra at 4 Meter Depth Using the WST Model Initialized with the Digitized Form of Only the Seven Selected Frequencies of FGE90 (Squares) are in Close Agreement with the WST Model Results for the Nonlinearly Evolved SDS (Chaindash Line), Except at .14 Hz Which Has a Final State Closer to the Linearly Predicted Evolution of SDS (Dash Line).

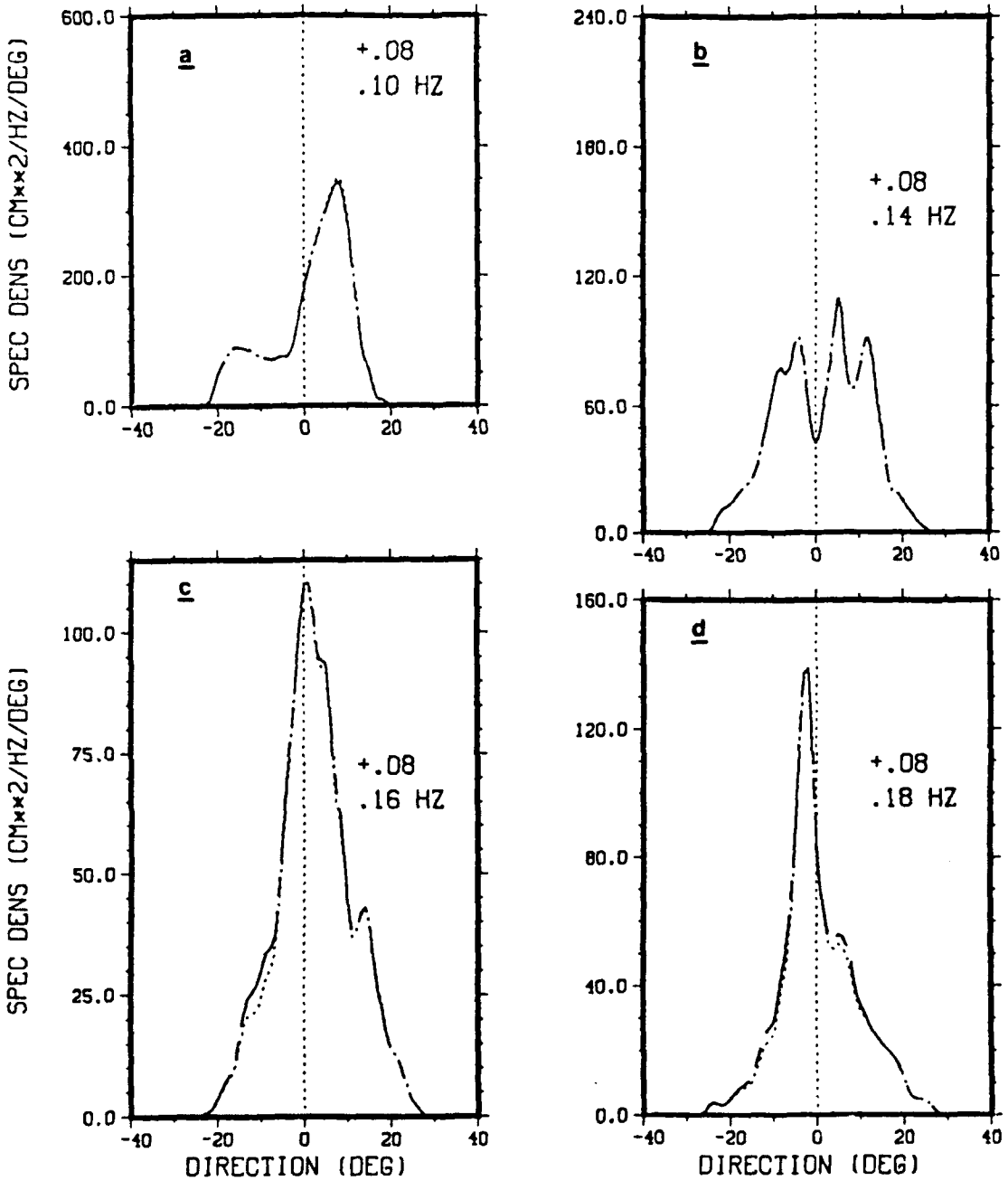

Figure B.7 The WST Model Predicted Nonlinear Evolution Using SDS (Chaindash Line) and Using the Data Set Made Up by Adding to the Digitized Form of the Seven Selected Frequency Bands of FGE90 the Interpolated Frequency Band .08 Hz (Dot Line) are in Close Agreement.

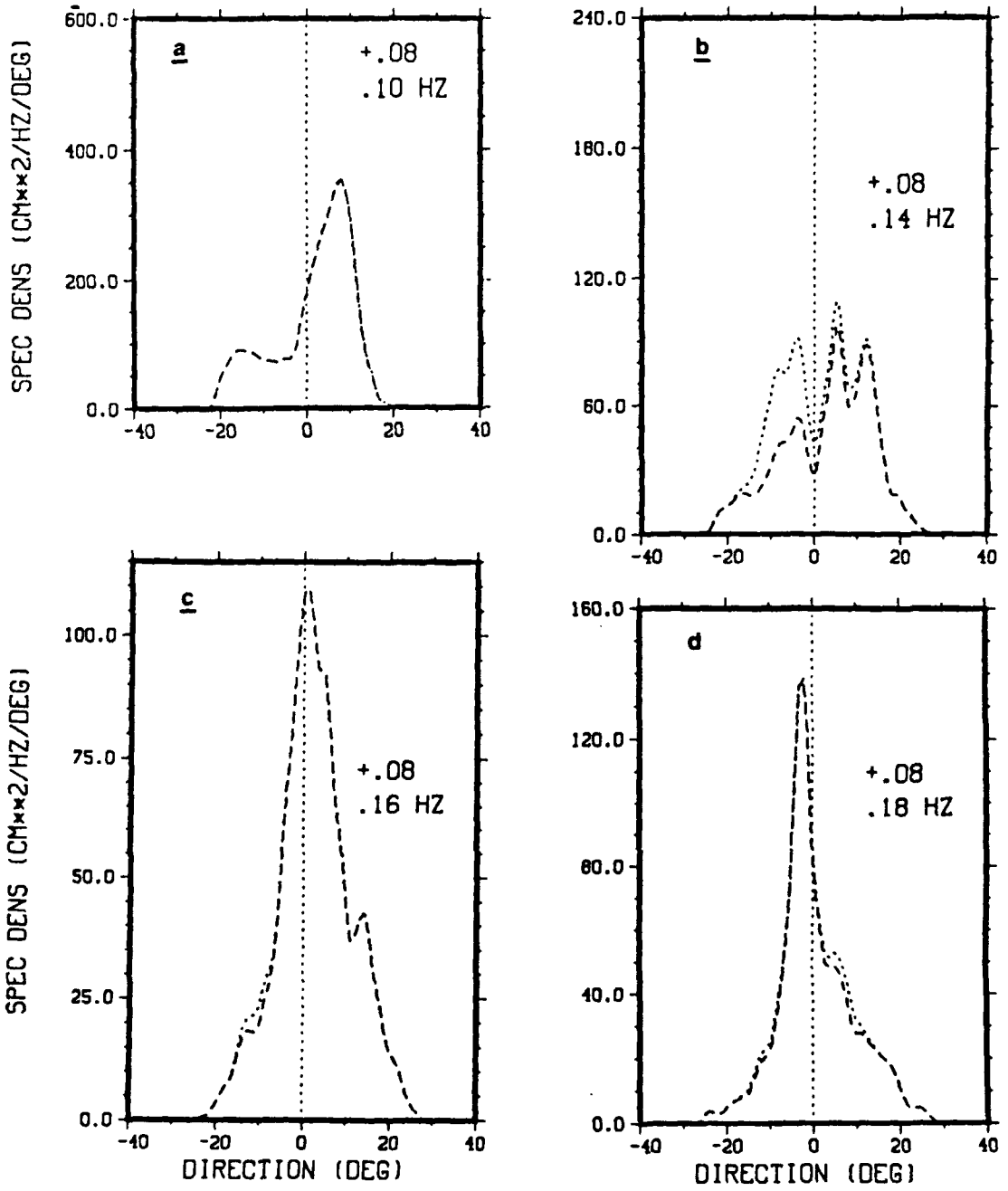

Figure B.8 The Main Contribution of the Interpolated Frequency Band .08 Hz is to the Nonlinear Evolution of .14 Hz Frequency, as Can be Concluded by Comparing the WST Model Nonlinear Predictions of Directional Spectra at 4 Meter Depth When Initialized with the Digitized Form of Only the Seven Selected Frequency Bands of FGE90 (Dash Line) and When the Input was the Previous Data Set Added of the Interpolated .08 Hz Frequency Band (Dot Line).

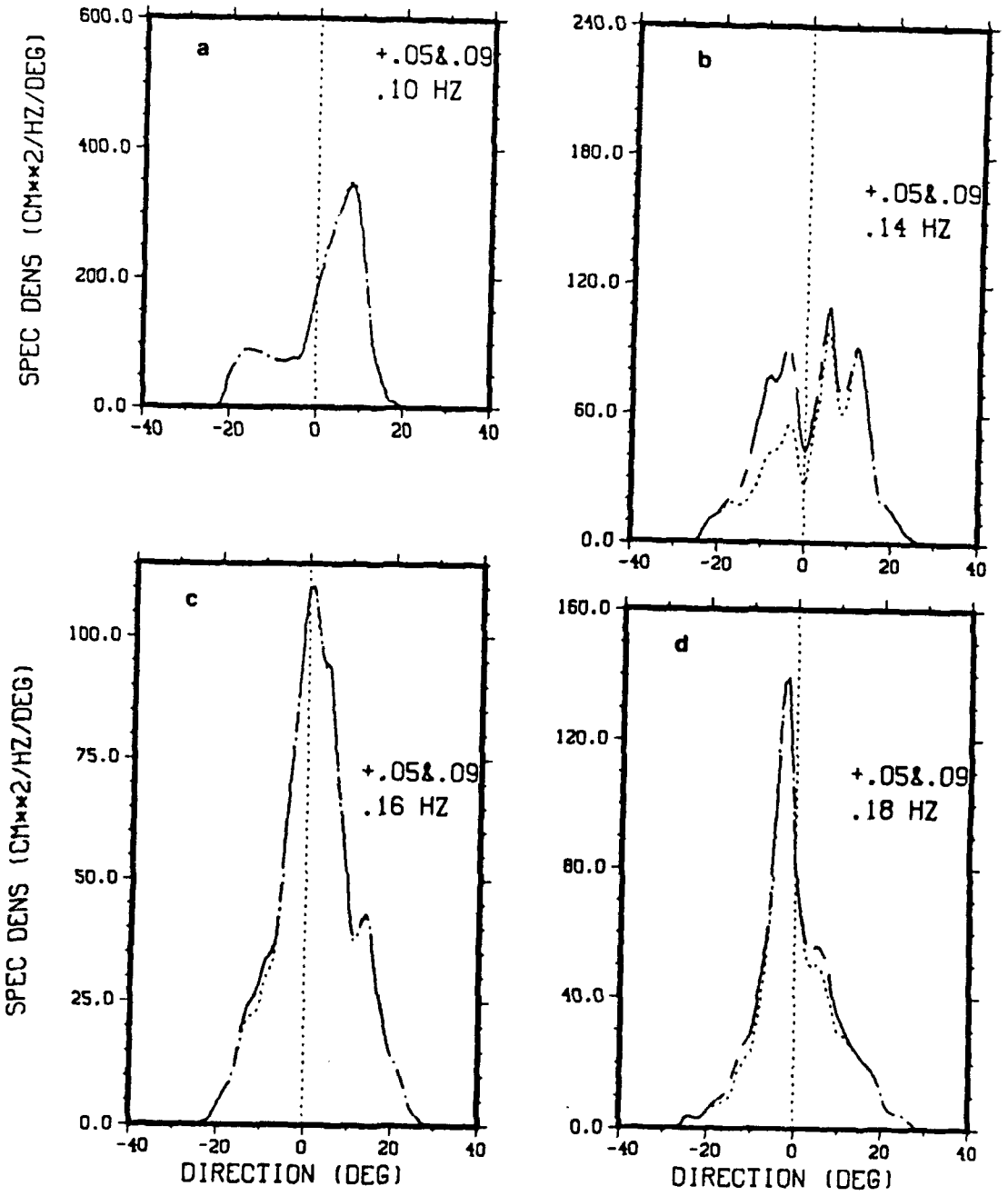

Figure B.9 The WST Model Predicted Nonlinear Evolution at 4 Meter Depth of the SDS (Chaindash Line) and of the Data Set Made Up by Adding to the Digitized Form of the Seven Selected Frequencies of FGE90 the Interpolated Frequencies .05 and .09 Hz (Dot Line) Have a Significant Difference at .14 Hz.

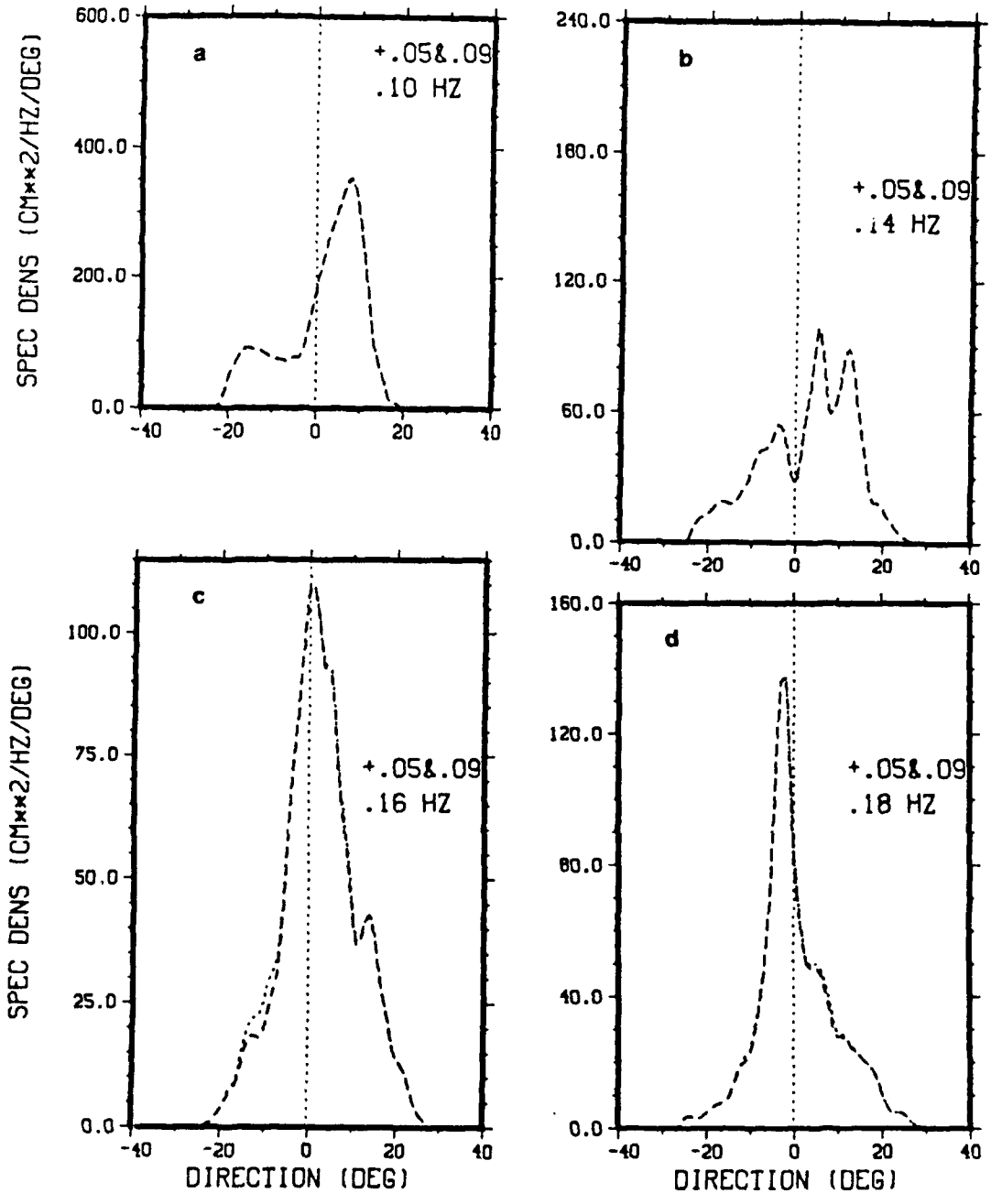

Figure B.10 Shown are the WST Model Predictions of the Nonlinear Evolutions of the Data Set Constituted Only by the Digitized Selected Frequencies of FGE90 (Dash Line), and of the Data Set Obtained by Adding to the Previous One the Interpolated Frequency Bands of .05 and .09 Hz. There is No Major Contribution of the Interpolated Bands .05 and .09 Hz to .14 Hz, But Only a Small Contribution to the Bands .16 and .18 Hz.

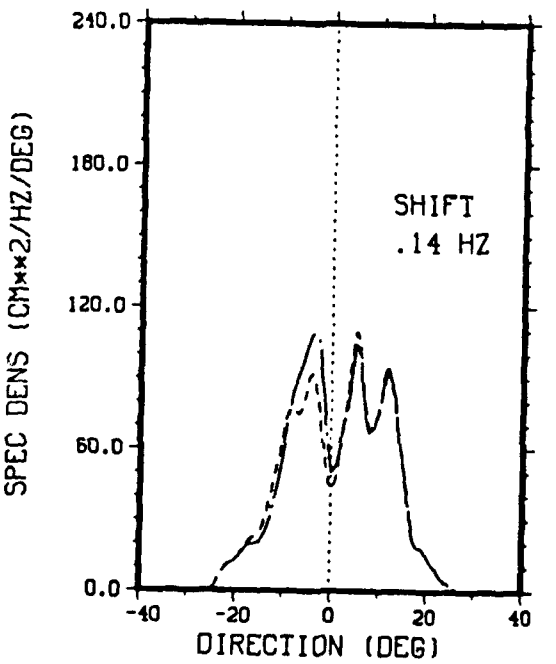

Figure B.11 Shifting the Interpolated Frequency Band of .08 Hz in the SDS 4 Degrees to the South, and Using the Resulting Data Set to Initialize the WST Nonlinear Model, the Predicted Nonlinear Evolution of .14 Hz Directional (Chaindash Line) is Significantly Different from the Evolution Obtained with the SDS.

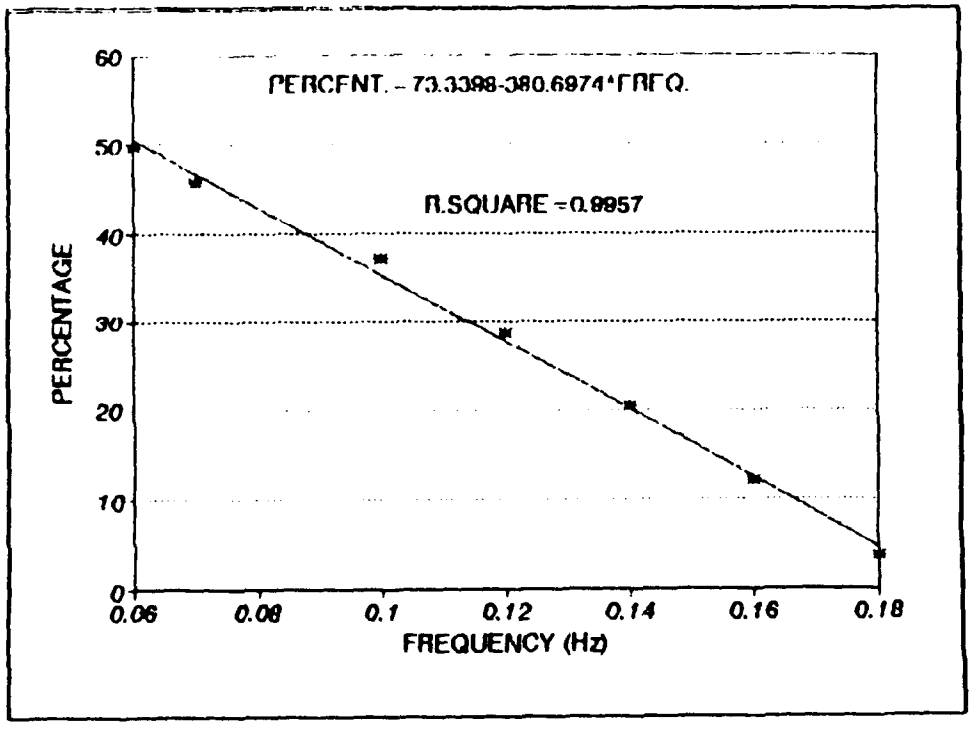

Figure B.12 The Percent Amplification of the Total Energy of the Selected Frequency Bands by Combining Effects of Shoaling and Refraction (Asterisks) Has an Almost Linear Dependence on Frequency. The Line Represents the Linear Least Squares Fit of the Percent Increase of Energy of the Selected Frequency Bands.

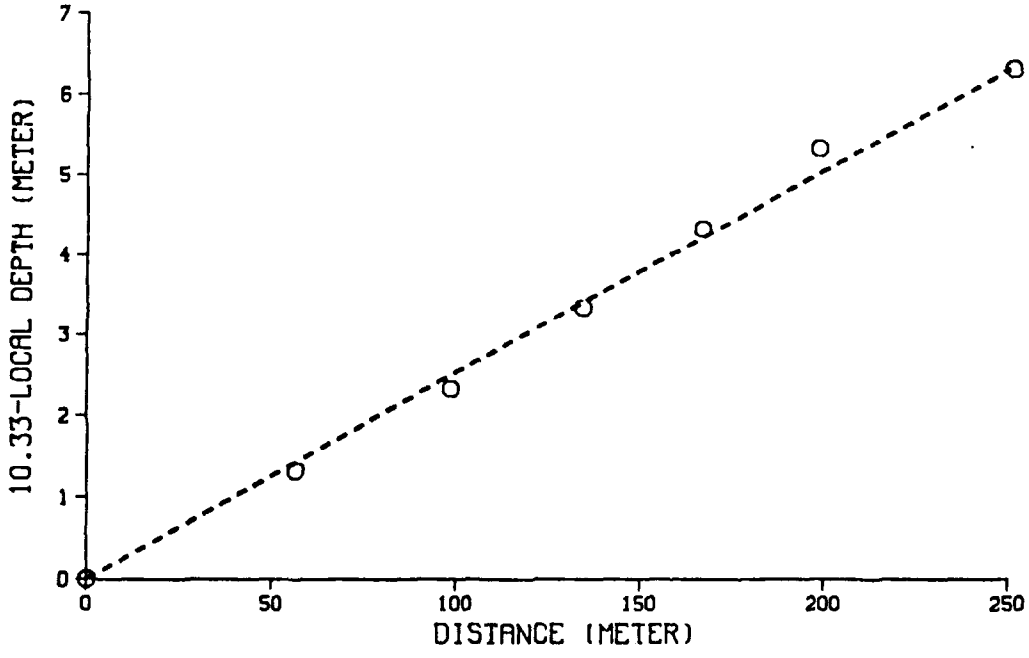

Figure B.13 To Test the Sensitivity to Changing the Spacing Between Bathymetrics of the Experiment Site, the Average Spacing was Calculated from the Distance Between Two Consecutive Points of Seven Discretization Lines (Plot (a)). The Resulting Bathymetry (BT2) (Circles in Plot (b)) is Not Significantly Different from the Planar Bathymetry of FGE90 (Dash Line).

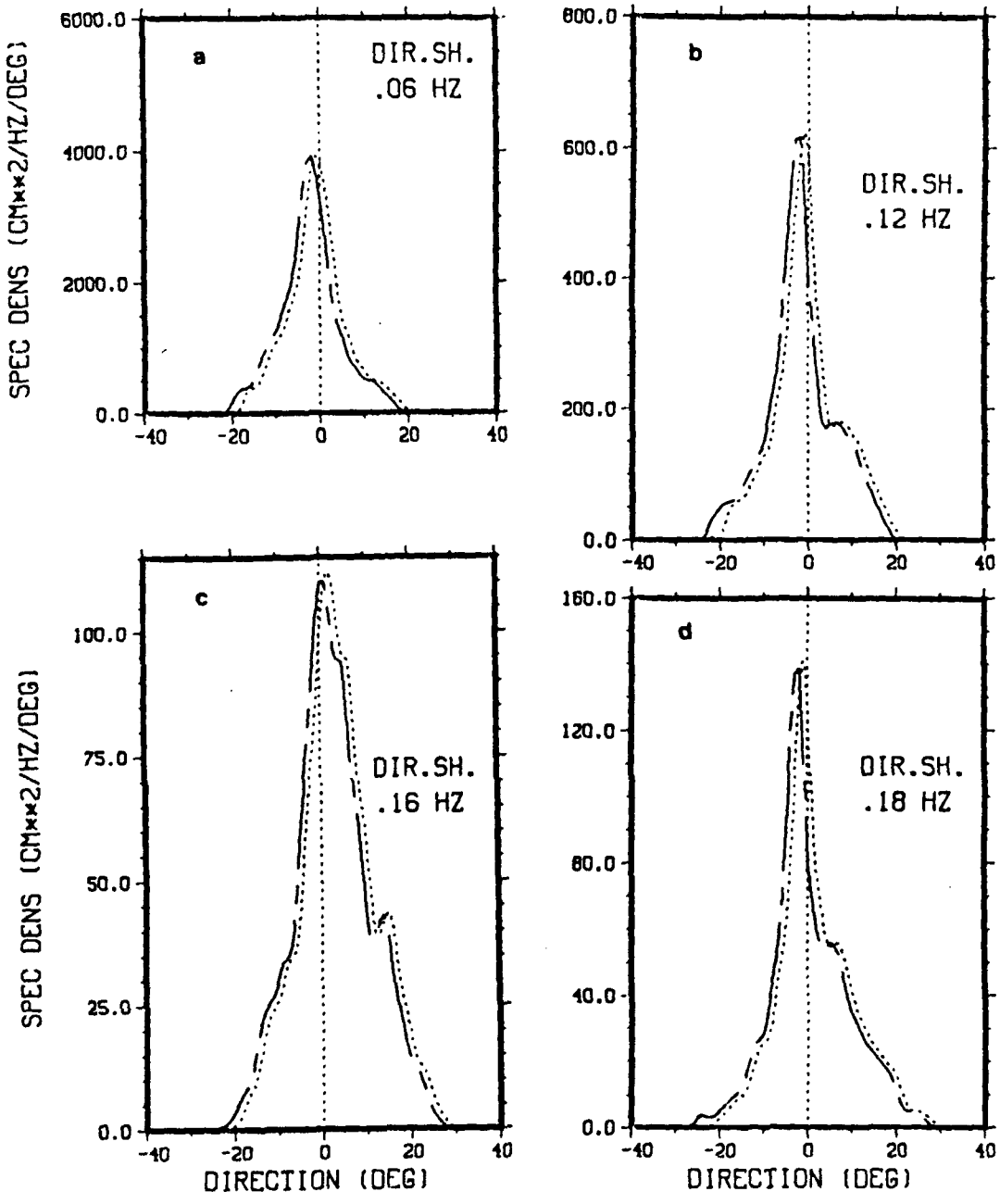

Figure B.14 The Nonlinear Evolution of the SDS Predicted by the WST Model for the Original Bathymetry of FGE90 (Chaindash Line) Shows Different Orientation of the Peaks of Energy and Smaller Energy at the Peaks, Relatively to the Predictiors Obtained by Rotating the Beach Normal 4 Degrees to the South (Dash Line).

LIST OF REFERENCES

Benney, D.J., and Saffman, P.G., 1966, "Nonlinear Interactions of Random Waves in a Dispersive Medium," Proceedings of the Royal Society, London, A289, p. 301.

Collins, J.I., 1972, "Predictions of Shallow Water Spectra," Journal of Geophysical Research, Vol. 77, pp. 2693-2707.

Dobson, R.S., 1967, "Some Applications of a Digital Computer to Hydraulic Engineering Problems," Technical Report 80, Department of Civil Engineering, Stanford University, Stanford, California.

Elgar, S., and Guza, R.T., 1985, "Observations of Bispectra of Shoaling Surface Gravity Waves," Journal of Fluid Mechanics, Vol. 161, pp. 425-448.

Elgar, S., Guza, R.T., Freilich, M.H., and Briggs, M.J., 1991, "Laboratory Simulations of Directionally Spread Shoaling Waves," Accepted for publication in Journal of Waterways, Post Coastal Ocean D.V., ASCE.

Freilich, M.H., and Guza, R.T., 1984, "Nonlinear Effects on Shoaling Surface Gravity Waves," Phil. Transactions of the Royal Society, London, A311, pp. 1-41.

Freilich, M.H., Guza, R.T., and Elgar, G.L., 1990, "Observations of Nonlinear Effects in Directional Spectra of Shoaling Gravity Waves," Journal of Geophysical Research, Vol. 95, pp. 9645-9656.

Hasselman, K., Munk, W., and MacDonald, G., 1963, "Bispectra of Ocean Waves," In Time Series Analysis (Ed. M. Rosenblatt), Wiley Publishers, pp. 125-139.

Haubrich, R.A., 1965, "Earth Noises, 5 to 500 Millicycles Per Second, 1" Journal of Geophysical Research, Vol. 70, pp. 1415-1427.

Izumiya, T., and Horikawa, K., 1987, "On the Transformation of Directional Waves Under Combined Refraction and Direction," Coastal Engineering in Japan, Vol. 30, No. 1, pp. 49-65.

Kim, Y.C., and Powers, E.J., 1979, "Digital Bispectral Analysis and Its Application to Nonlinear Wave Interactions," IEEE Transactions on Plasma Science, Vol. 1, pp. 120-131.

Le Mehaute, B., and Wang, J.D., 1982, "Wave Spectrum Changes on Sloped Beach," Journal of Waterways, Port Coastal Ocean Div., ASCE, Vol. 108, pp. 33-47.

Liu, P.L.F., Yoon, S.B., and Kirby, J.T., 1985, "Nonlinear Refraction-diffraction in Shallow Water," Journal of Fluid Mechanics, Vol. 153, pp. 185-209.

Longuet-Higgins, M.S., 1957, "On the Transformation of a Continuous Spectrum by Refraction," Proceedings of the Cambridge Philosophical Society, Vol. 53, No. 4, pp. 226-229.

McComas, C.H., and Briscow, M.G., 1980, "Bispectra of Internal Waves," Journal of Fluid Mechanics, Vol. 97, pp. 205-213.

Newell, A.C., and Aucoin, P.J., 1971, "Semidispersive Wave Systems," Journal of Fluid Mechanics, Vol. 49, No. 3, pp. 593-609.

Oltman-Shay, J., and Guza, R.T., 1984, "A Data-adaptive Ocean Wave Directional Spectrum Estimator for Pitch and Roll Type Measurements," Journal of Physical Oceanography, Vol. 14, pp. 1800-1810.

Pawka, S.S., 1982, Wave Directional Characteristics on a Partially Sheltered Coast, Ph.D. Dissertation, University of California at San Diego, La Jolla.

Pawka, S.S., 1983, "Island Shadows in Wave Directional Spectra," Journal of Geophysical Research, Vol. 88, pp. 2579-2591.

Pawka, S.S., Inman, D.L., and Guza, R.T., 1984, "Island Sheltering of Surface Gravity Waves: Model and Experiment," Continental Shelf Resources, Vol. 3, pp. 35-53.

Radder, A.C., 1979, "On the Parabolic Equation Method for Water Wave Propagation," Journal of Fluid Mechanics, Vol. 95, pp. 159-176.

Sobey, R.J., and Youg, I.R., 1986, "Hurricane Wind Waves--A Discrete Spectral Model," Journal of Waterways, Post Coastal Ocean Eng. Am. Soc. Civ. Eng., Vol. 112, No. 3, pp. 370-389.

Soward, A.M., 1975, "Random Waves and Dynamo Action," Journal of Fluid Mechanics, Vol. 69, p. 145.

WAMDI Group, 1928, "The WAM Model--A Third Generation Ocean Wave Prediction Model," Journal of Geophysical Research, Vol. 18, pp. 1775-1810.

Weber, S.L., 1988, "The Energy Balance of Finite Depth Gravity Waves," Journal of Geophysical Research, Vol. 93, No. C4, pp. 3601-3607.

Young, I.R., 1988, "A Shallow Water Spectral Wave Model," Journal of Geophysical Research, Vol. 93, No. C5, pp. 5113-5129.

Zakharov, V.A., 1968, "Stability of Periodic Waves of Finite Amplitude on the Surface of a Deep Fluid," Zh. Prikl. Mekh. Tekh. Fiz., Vol. 9, p. 86.

INITIAL DISTRIBUTION LIST

		No. Copies
1.	Defense Technical Information Center Cameron Station Alexandria, Virginia 22304-6145	2
2.	Library, Code 052 Naval Postgraduate School Monterey, California 93943-5002	2
3.	Chairman, Code OC/Co Department of Oceanography Naval Postgraduate School Monterey, California 93943-5000	1
4.	Chairman, Code MR/Rd Department of Meteorology Naval Postgraduate School Monterey, California 93943-5000	1
5.	Dr. E.B. Thornton, Code OC/Tm Department of Oceanography Naval Postgraduate School Monterey, California 93943-5000	3
6.	Mr. T.P. Stanton, Code OC/St Department of Oceanography Naval Postgraduate School Monterey, California 93943-5000	2
7.	Dr. A. Larraza, Code PH/La Department of Physics Naval Postgraduate School Monterey, California 93943-5000	2
8.	Dr. Roland W. Garwood, Code OC/Ga Department of Oceanography Naval Postgraduate School Monterey, California 93943-5000	2
9.	Dr. Beny Neta, Code MA/Nd Department of Mathematics Naval Postgraduate School Monterey, California 93943-5000	2

10. Director, Naval Oceanography Division — 1
Naval Observatory
34th and Massachusetts Avenue NW
Washington, D.C. 20390

11. Commanding Officer — 1
Fleet Numerical Oceanography Center
Monterey, California 93943

12 Commanding Officer — 1
Naval Environmental Prediction Research Facility
Monterey, California 93943

13. Naval Ocean Research and Development Activity — 1
NSTL Station
Bay St. Louis, Mississippi 39522

14. Naval Oceanographic Office — 1
Stennis Space Center
Bay St. Louis, Mississippi 39522

15. Office of Naval Research, Code 420 — 1
800 N. Quincy Street
Arlington, Virginia 22217

16. Direccao do Servico de Instrucao e Treino — 1
Marinha Portuguesa
Rua do Arsenal
1100 Lisboa
Portugal

17. Director Geral do Instituto Hidrografico — 2
Instituto Hidrografico
Rua das Trinas, 49
1200 Lisboa
Portugal

18. LT Manuel A.F. Pinto de Abreu — 4
Instituto Hidrografico
Rua das Trinas, 49
1200 Lisboa
Portugal

19. Director of Research Administration, Code 012 — 1
Naval Postgraduate School
Monterey, California 93943-5000